

University of Montana

ScholarWorks at University of Montana

Graduate Student Theses, Dissertations, &
Professional Papers

Graduate School

1994

Validating diurnal and topographic climatology logic of the MT-CLIM model

Joseph Marion Glassy
The University of Montana

Follow this and additional works at: <https://scholarworks.umt.edu/etd>

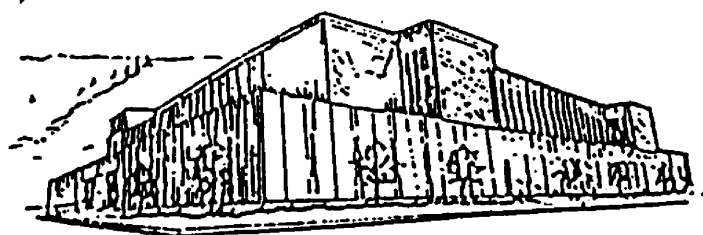
Let us know how access to this document benefits you.

Recommended Citation

Glassy, Joseph Marion, "Validating diurnal and topographic climatology logic of the MT-CLIM model" (1994). *Graduate Student Theses, Dissertations, & Professional Papers*. 7356.
<https://scholarworks.umt.edu/etd/7356>

This Thesis is brought to you for free and open access by the Graduate School at ScholarWorks at University of Montana. It has been accepted for inclusion in Graduate Student Theses, Dissertations, & Professional Papers by an authorized administrator of ScholarWorks at University of Montana. For more information, please contact scholarworks@mso.umt.edu.

Joseph M. Murray



Maureen and Mike MANSFIELD LIBRARY

The University of
Montana

Permission is granted by the author to reproduce this material in its entirety, provided that this material is used for scholarly purposes and is properly cited in published works and reports.

*** Please check "Yes" or "No" and provide signature***

Yes, I grant permission
No, I do not grant permission

Author's Signature Joseph M. Murray

Date: 10/20/1994

**Validating Diurnal and Topographic Climatology Logic
Of The MT-CLIM model**

submitted by

Joseph Marion Glassy

School of Forestry

B.S. University of Montana--Missoula, 1979

Presented in partial fulfillment of the requirements
for the degree of

Masters of Science
University of Montana

1994

Approved by


Chairman, Board of Examiners


Dean, Graduate School

10-24-94
Date

UMI Number: EP38157

All rights reserved

INFORMATION TO ALL USERS

The quality of this reproduction is dependent upon the quality of the copy submitted.

In the unlikely event that the author did not send a complete manuscript and there are missing pages, these will be noted. Also, if material had to be removed, a note will indicate the deletion.



UMI EP38157

Published by ProQuest LLC (2013). Copyright in the Dissertation held by the Author.


Microform Edition © ProQuest LLC.

All rights reserved. This work is protected against
unauthorized copying under Title 17, United States Code



ProQuest LLC.
789 East Eisenhower Parkway
P.O. Box 1346
Ann Arbor, MI 48106 - 1346

Validating Diurnal and Topographic Climatology Logic Of The MT-CLIM model

Director: Steven W. Running 

World-wide interest in potential global climate change continues to motivate the development of a variety of ecosystem models at various spatial scales. Virtually all of these models require meteorological data as part of their parameterization. The MT-CLIM climatology model validated here offers a streamlined approach to providing these estimates. The diurnal component of MT-CLIM treats temporally cyclic parameters (e.g. humidity, incident solar radiation, and diurnal temperature) and the topographic component treats spatially sensitive parameters (e.g. hillslope air temperatures). This study validates key diagnostic variables for both types of logic. The diurnal logic was tested by comparing estimated incident solar and humidity parameters with observed meteorology data collected along a climatic gradient across a 200 km transect in Oregon in 1990. The validity of using night minimum temperatures as a surrogate for dew point temperatures was also tested. The topographic logic was tested through a comparison of modelled air temperatures with remotely sensed, thermal infrared surface temperatures derived from three Daedalus Thematic Mapper Simulator scenes taken in 1990 for a 10.8 km² study area near Sisters, Oregon.

In the diurnal study, I found good agreement between observed and modeled incident solar shortwave radiation (r^2 values ranged from 0.82 to 0.89), and fair agreement between observed and estimated vapor pressure deficits (r^2 values of 0.66 to 0.84). Night minimum temperatures proved to be a fairly useful substitute for dew point temperatures in this study. In the topographic study, after stratifying by canopy closure and relative solar loading, r^2 values of 0.74, 0.89, and 0.97 for the March, June and August samples were obtained using the new air temperature method, with consistently lower correlations using the original method (r^2 of 0.70, 0.52, and 0.66 for the March, June and August samples). Several ideas for related follow-on studies are also suggested.

Table of Contents

Table of Contents	iii
List of Tables	vi
List of Figures	vii
Acknowledgements	ix

Chapter 1

Introduction	1
Literature Cited	5

Chapter 2

Validating Diurnal Climatology Logic of the MT-CLIM Model Across A Climatic Gradient In Oregon	8
Introduction	8
Climatological Data Requirements For Ecological Models	8
Methods	13
Humidity and Vapor Pressure Deficit	16
Incident Solar Radiation	21
Simulations and Analysis	25
Results and Discussion	26
Humidity	26
Incident Solar Radiation	31
Conclusions	32
Literature Cited	35

Chapter 3

Validating Topographic Climatology Logic of the MT-CLIM Model Across A Seasonal	
Gradient	39
Introduction	39
Objectives	42
Background	43
Methods	48
Description of the MT-CLIM Model	50
Description of the MTNTEMP Model	55
MTNTEMP Model Inputs	56
Elevation and Derived Layers	57
Canopy Closure Layer	59
Albedo Layer	61
Relative Solar Loading Layer	62
Derivation of Surface Temperatures from TMS Imagery	64
Description of the new MTNTEMP model air temperature algorithm ..	67
Development of the Canopy (T_c and τ) Temperature Adjustment	
.....	71
Development of the topographic temperature adjustment	76
Analysis Design	77
Pooled Comparisons	81
Across-Category Comparisons	81
Within-Category Comparisons	82
Multiple Regressions	84
Results and Discussion	85
Pooled and Across-Category Partition Results	85
Within-Category Partition Results	91
Multiple Regression Results	93
Conclusions	96
Literature Cited	100

Chapter 4

Conclusions	107
-------------------	-----

Appendices

Appendix 3.1 Statistical Summary of Study Site Variables	112
Appendix 3.2 Example of MT-CLIM Model Input Requirements	114
Appendix 3.3 Inputs Used for MTNTEMP Model Runs	116
Appendix 3.4 Major Differences Between MTNTEMP and MT-CLIM Model Implementations	121
Appendix 3.5 Statistical Summary of the OTTER Project Metolius weather station 1990 daily dataset for 1990	123
Appendix 3.6 Percent Canopy Closure Data Layer	125
Appendix 3.7 Annotated MTNEMP result database table structure listing	126

List of Tables

Chapter 2

Table 2.1: Example of MT-CLIM Model Inputs	11
Table 2.2: OTTER Site Summary	14
Table 2.3: Seasonal Distribution of Day Analyzed By Site	16
Table 2.4: Solar Radiation and VPD Analysis Summary	27

Chapter 3

Table 3.1: Sun-Earth Geometry Parameters Used To Generate Relative Solar Loading Images	63
Table 3.2: Daedalus TMS Channel Characteristics	66
Table 3.3: Comparison of Methods To Assign T_{∞} Coefficients for the three Sample Dates (March 21, June 25, and August 13, 1990)	73
Table 3.4: MTNTEMP Model Run Matrix	78
Table 3.5: Original Method Run Regression Results For Pooled and Across-Category Partitioning	87
Table 3.6: New Method Regression Results from For Pooled and Across-Category Partitioning	88
Table 3.7: Multiple Linear regression models for T_a vs T_s using the new site temperature estimation method	94

List of Figures

Chapter 2	Page
Figure 2.1 Frequencies of days sampled by month for two sample years (1989 and 1990), by OTTER site.	18
Figure 2.2 Diagram of MT-CLIM diurnal logic illustrating the relationship of diurnal minimum and maximum temperature, incoming solar radiation, and the truncated period defining daylight average temperature.	21
Figure 2.3 Comparative plot of vapor pressure deficit (VPD) regression lines for the five sites, illustrating the ranking of the regression slopes across the site gradient.	28
Figure 2.5 Comparative plot of incident solar regression lines for the five sites, illustrating the division of the lines into two basic groups.	29
Figure 2.4 Scatterplot and regression line of the vapor pressure deficit (VPD) model for the Santiam Pass (Oregon) OTTER site using 1989 and 1990 LTER (Long Term Ecological Research) data. This regression model provides a representative example of average humidity performance since data from this site did not require screening.	29
Figure 2.6 Scatterplot and regression line of the incident solar radiation model for the Waring's Woods (Corvallis, Oregon) OTTER site using 1989 and 1990 LTER data.	32
 Chapter 3	
Figure 3.1 OTTER project and study site location.	48
Figure 3.2 Black Butte cinder cone 10.8 km ² study site, rendered from the USGS Bend West 3 arc-second DMA digital elevation model.	49
Figure 3.4 T_{add} adjusted air temperature function, showing planar response surface as a function of radiation ratio and (LAI/MLAI) ratio.	54
Figure 3.3 T_{sub} adjusted air temperature response surface, as a function of the flat-to-sloped radiation ratio and LAI/MLAI.	54
Figure 3.5 March 21 relative solar loading image showing the topographic distribution of the loading across the study area.	62
Figure 3.6 TIR (T_s) high gain thermal channel from the June 25, 1990 Daedalus TMS scene.	64
Figure 3.7 Histogram illustrating the unimodal distribution of the air temperature adjustment ($T_{syn} - T_a$) resulting from the new site temperature algorithm.	70
Figure 3.8 Histogram illustrating the bimodal distribution of the air temperature adjustment ($T_{syn} - T_a$) resulting from the original site air temperature algorithm.	71

Figure 3.9 Example of the T_a output verification raster produced for the August 13 1990 sample using the new site temperature algorithm. 79

Figure 3.10 Defining T_s vs T_a as partition cell-wise averages represents variation in a partition cell as a single value; in this example, 9 pairs of temperatures would be regressed. 81

Figure 3.12 Scatterplot and regression model for {Elevation, Aspect} across-category partition for the June 25 sample using the new site air temperature algorithm. 89

Figure 3.11 Scatterplot and regression model for the {Canopy Closure, Relative Solar Loading} across-category partition for the August, 1990 sample using the new site air temperature algorithm. 89

Figure 3.13 Comparison of the original and new air temperature method regression slopes for the June sample. These lines illustrate the effect of increased temperature amplitude on the sensitivity of the relationship. 90

Figure 3.14 r^2 surface for the within-category regression models using the {Elevation, Aspect class} pairings for the August sample, new air temperature algorithm. 90

Figure 3.15 r^2 surface for the {relative solar load, canopy closure} pairing for the June sample, using the new air temperature method. 91

Figure 3.16 r^2 surface for the {slope, aspect} pairing for the March sample using the new air temperature method. 92

Acknowledgements

I was inspired to work on this research early in my association with Dr. Steve Running, as part of his on-going work in ecosystem modelling. Dr. Joe Coughlan originally encouraged me to meet Steve and ultimately pursue this degree, and I'm grateful to Joe for that turn of fate. I was interested in a problem that combined ecosystem, meteorology, and computer science with my interest in spatial analysis and geostatistics. Little did I know at the time that the simple study we originally envisioned would expand into its current form, take this long to address and still leave so many unanswered questions. I owe my wife, Janet, a great debt of gratitude for her eternal patience in this seemingly interminable endeavor; without her moral support, love, and encouragement it might have taken longer still! I owe Dr. Steve Running a great deal for his encouragement, creativeness, and patience throughout this time, and for the latitude he gave me in exploring new ideas. This thesis is the product of several years of work and could not have been done without the contributions of many generous scientists. In particular I would like to thank Dr. Lars Pierce, my office-mate, friend, and science counselor-at-large, for his consistent interest and helpful advice throughout the duration of this study.

I would like to thank Dr. Ramakrishna Nemani for his spare but insightful critiques of the theoretical problems in the study, Dr. Ray Hunt for his help and continued interest with biophysical issues, Dr. Don Potts for his confidence and sense of humor, and Dr. Ray Ford for his support and for looking the other way as I wrote this model in his

least favorite computer language. This study required many computer resources; Charlie Mcquire and Hal Dorsman were instrumental in keeping these felicitous machines perking along, and I thank them for it. I'd also like to thank the NTSG team for their support throughout.

This research was supported by grant BSR-8919649 from the National Science Foundation, and by grants NAGW-252 and NAGW 1892 of the National Aeronautics and Space Administration, Earth Sciences and Applications Division to Steven W. Running. The Daedalus TMS data was generously provided to me by NASA AMES scientists Mike Spanner and Dave Peterson, digital elevation data was provided for the study site by Gary Angelici of the NASA OTTER project, and image scanning services were generously donated by Rohn Wood. Meteorology data was provided by John Runyon of Oregon State University. As with most studies, there are usually some behind-the-scenes influences who have also contributed to the spirit of the study. I'd like to thank Richard Waring, Barbara Yoder, and Ron Righter for their encouragement early on, and all my Missoula friends (who gave up their high-water canoeing partner these last several years) for their generous moral support.

Chapter 1

Introduction

The renewed interest in potential global climate change world wide has intensified the science communities interest in developing better methods to provide meteorological parameterizations at various spatial scales (Dickenson, 1988; Schimel, 1991). Ecosystem models emphasizing the estimation of net primary productivity (NPP) and related parameters typically require key meteorological variables that include temperature, humidity, radiation loading, and precipitation (Pierce, 1994; Running, 1990; Running et al., 1989). The problems of adequately characterizing meteorology within an ecosystem modelling context involve both the temporal and spatial scales employed (Risser et al., 1988; Running and Coughlan, 1988; Nemani and Running, 1993). Higher resolution (≈ 30 to 90 m) ecosystem analyses have relied on watershed or even smaller scale, point based climatology databases such as the Long Term Ecological Research (LTER) network sites such as Coweeta and H.J. Andrews, National Weather Service (NWS) airport station sites, and USDA Forest Service fire Weather Library (Furman and Brink, 1975). While these weather databases remain useful sources of point based climatology for establishing initial baseline conditions, they generally lack the site and temporal specificity required by newer, multiple scale ecosystem models (Nemani et al., 1993). Point based estimates also typically require special or complex treatments to allow

extrapolation to spatial regions (Isaacs and Srivastava, 1989; Burrough, 1986; Daly et al., 1994). Ecosystem models at the regional, continental or global scales typically address the model problem on an orthogonal grid cell basis, typically simulating conditions on a sequence of spatial adjacent analysis cells ranging in size from 30 m² (stand level), 1 km² (landscape), 50 km² (continental), to 1° by 1° (≈ 100 km²) or larger -- the global scale resolutions common to general circulation model (GCM) approaches (Dickenson et al., 1993). Few of these grid cell raster based analysis approaches represent truly spatially connected designs; for simplicity the majority of these abstract the problem as a large number of contiguous, but essentially independent points.

As attempts are made to accurately represent ecosystem processes at these regional and larger scales, the lack of site specific climatology data at equivalent spatial and temporal scales becomes a serious limitation (Nemani and Running, 1989; Running, 1991; Running and Hunt, 1991). Particularly at larger spatial cell resolutions (above 500 m), a challenge remains in how well current modelling approaches account for sub-grid heterogeneity (Risser et al., 1988; Woodmansee, 1988). Researchers have responded to this need in several ways, with some applying classic geostatistical based approaches (Myers, 1991; Isaacs and Srivastava, 1989; Phillips et al., 1991), some adopting modelling approaches such as MT-CLIM that combine atmospheric physics "first principles" with empirical extrapolation logic (Running et al., 1988), and some favoring statistical dynamical approaches that blend aspects of all of these (Avissar, pers. comm.). A primary advantage in models like MT-CLIM is the relative ease of parameterization

compared to more sophisticated models such as RAMS (Pielke et al., 1992) that treat site energy balances and atmospheric physics much more explicitly. The operational practicality of many of these more explicit models -- a separate concern from their conceptual rigor -- remains an issue for modelers faced with growing responsibilities to scale up in the face of historically unstable budgets.

The basic logic employed within the MT-CLIM model was validated as part of its original development and publication (Running et al., 1987; Hungerford et al., 1989). Since its appearance, the MT-CLIM model has begun to see more widespread use in a number of applications beyond its original scope (Redmond, pers. comm. and Milner, pers. comm). These more recent uses and the potential role MT-CLIM could play in regional and larger scale applications have invited a more thorough examination and validation of the basic assumptions underlying the model.

I address the general issue of validating MT-CLIM logic through two separate studies. The diurnal portion of the model is examined in Chapter 2, where the humidity measure (via vapor pressure deficit dynamics) and solar radiation variables are evaluated. The topographic portion of the model logic is treated in Chapter 3, through an in-depth examination of the site temperature mechanism in the model. The conclusion in Chapter 4 summarizes the results of these two validation studies and suggests some areas in which the basic MT-CLIM logic might be improved in the future. As a comprehensive mountain climatology model, MT-CLIM provides estimates for many more variables than

are explicitly validated in this study. Specifically, minimum and maximum temperature estimates are not addressed here, as the logic used to estimate them is parallel but separate from that used to estimate the site hillslope temperatures. Precipitation patterns over mountainous terrain represent very complex spatial and temporal phenomena. An adequate treatment of precipitation was felt to be beyond the scope of this paper.

Thornton and Running (1994), Daly et al. (1994), and others are currently investigating new, more rigorous methods for estimating precipitation over complex terrain. In the future, some form of this work will hopefully be incorporated into revisions of the MT-CLIM model.

Literature Cited

- Burrough, P.A. 1986. Principles of Geographic Information Systems for Land Resource Assessment. Clarendon Press, Oxford, UK. 194 p.
- Daly, C., R.P. Nielson, and D.L. Phillips. 1994. A statistical-topographic model for mapping climatological precipitation over mountainous terrain. *Journal of Applied Meteorology*, 33(2):140-158.
- Dickenson, R.E. 1988. Atmospheric systems and global change. *In Scales and Global Change: Spatial and Temporal Variability in Biospheric and Geospheric Processes*. T. Rosswall, R.G. Woodmansee, and P.G. Risser, editors. SCOPE-ICSU, Wiley and Sons. 355 p.
- Dickenson, R.E., A. Henderson-Sellers, and P.J. Kennedy. 1993 Biosphere-Atmosphere Transfer Scheme (BATS) Version 1e as Coupled to the NCAR Community Climate Model. NCAR Technical Note NCAR/TN-387+STR. National Center for Atmospheric Research, Boulder, CO. 72 p.
- Furman, R.W. and G.E. Brink. 1975. The National Fire Weather Data Library: what it is and how to use it. Gen. Tech. Rep. RM-19. US Dept. of Agriculture, Forest Service, Rocky Mountain Forest and Range Experiment Station, Ft. Collins, CO. 8 p.
- Hungerford, R.D., Nemani, R.R., Running, S.W., and J.C. Coughlan. 1989. MT-CLIM: a mountain microclimate simulation model. Intermountain Research Station Research Paper INT-414. US Dept. of Agriculture, Forest Service, Ogden, UT. 52 p.
- Isaaks, E.H. and R.M. Srivastava. 1989. An introduction to applied geostatistics. Oxford University Press, Oxford London. 561 p.
- Myers, D.E. 1991. Interpolation and estimation with spatially located data. *Chemometrics and Intelligent Laboratory Systems* 11:209-228.
- Nemani, R.R. and S.W. Running. 1989 Testing a theoretical climate-soil-leaf area hydrologic equilibrium of forests using satellite data and ecosystem simulation. *Agricultural and Forest Meteorology* 44:245-260.
- Nemani, R.R. and S.W. Running. 1993 Developing satellite-derived estimates of surface moisture status. *Journal of Applied Meteorology* 32(3):548-557.

- Nemani, R.R., S.W. Running, L. Band, D. Peterson. 1993. Regional hydro ecological simulation system: an illustration of the integration of ecosystem models in a GIS. In *GIS and Environmental Modeling*, ed. M. Goodchild, B. Banks, and L. Steyert, Oxford Press, London UK. 488 p.
- Phillips, D.L., J. Dolph, and D. Marks. 1991. A comparison of geostatistical procedures for spatial analysis of precipitation in mountainous terrain. US EPA report, Environmental Research Laboratory, Corvallis, OR. 38 p.
- Pielke, R.A., and W.R. Cotton, R.L. Walko, C.J. Tremback, W.A. Lyons, L.D. Grasso, M.E. Nicholls, M.D. Moran, D.A. Wesley, T.J. Lee, and J.H. Copeland. 1992. A comprehensive meteorological modeling system - RAMS. *Meteorol. Atmos. Phys.* 49:69-91.
- Pierce, L.L. 1994. Scaling ecosystem models from watersheds to regions: tradeoffs between model complexity and accuracy. PhD dissertation, School of Forestry, University of Montana, Missoula, MT. 146 p.
- Risser, P.G., and T. Rosswall, R.G. Woodmansee. 1988. Spatial and temporal variability of biospheric and geospheric processes: a summary. *In: Scales and Global Change: Spatial and Temporal Variability in Biospheric and Geospheric Processes*. Thomas Rosswall, R.G. Woodmansee, and P.G. Risser. (Ed.) SCOPE-ICSU, Wiley and Sons. 355 p.
- Running, S. W., R.R. Nemani, and R.D. Hungerford. 1987. Extrapolation of synoptic meteorological data in mountainous terrain and its use for simulating forest evapotranspiration and photosynthesis. *Canadian Journal of Forest Research* 17(6):472-483.
- Running, S. W. and J.C. Coughlan. 1988. FOREST-BGC, a general model of forest ecosystem processes for regional applications. I. Hydrologic balance, canopy gas exchange and primary production processes. *Ecological Modelling* 42:125-154.
- Running, S. W. and R.R. Nemani, D.L. Peterson, L.E. Band, D.F. Potts, L.L. Pierce and M.A. Spanner. 1989. Mapping regional forest evapotranspiration and photosynthesis and coupling satellite data with ecosystem simulation. *Ecology* 70(4):1090-1101.
- Running, S. W. 1990. Estimating Terrestrial Primary Productivity by Combining Remote Sensing and Ecosystem Simulation. IN Remote Sensing of Biosphere Functioning. Springer-Verlag New York. p 65-86.

- Running, S. W. and E. R. Hunt Jr. 1991. Generalization of a forest ecosystem process model for other biomes, BIOME-BGC, and an application for global scale models. 141-156 pp. *In: Scaling Processes Between Leaf and Landscape Levels.* J.R. Ehleringer and C. Field (Ed). 388 p.
- Shimel, D.S., T.G.F. Kittel, and W.J. Parton. 1991. Terrestrial biogeochemical cycles: global interactions with the atmosphere and hydrology. *Tellus* 43AB:188-203
- Thornton, P.E. and S.W. Running. 1994. Generating daily surfaces of temperature and precipitation over complex topography. *In Second Conference of GIS and Environmental Modeling, National Center for Geographic Analysis and Information Analysis, GIS World* (in press).
- Woodmanse, R.G. 1988. Ecosystem processes and global change. *In: Scales and Global Change: Spatial and Temporal Variability in Biospheric and Geospheric Processes.* Thomas Rosswall, R.G. Woodmansee, and P.G. Risser. (Ed.) SCOPE-ICSU, Wiley and Sons. 355 p.

Chapter 2

Validating Diurnal Climatology Logic of the MT-CLIM Model Across A Climatic Gradient In Oregon

Introduction

Climatological Data Requirements For Ecological Models

Climatological data play a critical role in regional and global scale ecosystem applications. In a review of climate information needs for ecological effects models, Peer (1990) describes 19 contemporary models, including biome level, ecosystem process, species dynamics, individual tree, and agricultural models, that all require basic meteorological data. Examples of such applications include hydro-ecology models (Band and Wood, 1988; Band et al., 1991), grassland models such as CENTURY (Parton et al., 1988), and forest and biome ecosystem process models (Ågren et al. 1991; McMurtrie, 1985; Running and Coughlan 1988; Running et al. 1989; Running and Gower, 1991). To exploit current remote sensing and geographical information system (GIS) approaches, many ecosystem models are evolving from one to two dimensional applications (Nemani et al., 1993), encouraging the development of better methods to generate climate surfaces.

These modelling approaches span a large range of spatial and temporal scales, emphasizing the breadth of the climatological data requirement. Climatological parameters required by these models typically include air temperature, solar radiation, some measure of atmospheric humidity, precipitation, and in some cases, wind speed and direction. Meteorology datasets available for ecological models are available in many diverse forms. Project specific on-site data from portable meteorology stations is available, as well as more localized archives such as the USDA Forest Service Remote Automated Weather Stations (RAWS) network (Warren and Vance, 1981; Redmond, 1991). Longer term meteorological data available includes archived historical weather datasets such as the Climatological Data Summaries maintained by the National Oceanic and Atmospheric Administration (NOAA), at the National Climatic Data Center (NCDC), Ashville, North Carolina), derived from U.S. National Weather Service (NWS) stations.

The quality of available meteorological data varies considerably, with problems ranging from missing values to erroneous data collected by poorly calibrated or faulty instruments. An equally serious problem is that in some cases, variables of interest to ecological modelers such as incident solar radiation and humidity are simply not collected at all. The MT-CLIM approach of using 24-h minimum temperature as a surrogate for dew point temperature attempts to address these deficiencies; the ability to further establish the strength and theoretical limitations of this relationship is important in light of the relatively small fraction of established weather stations that collect humidity

measurements of any kind. Running et al. (1987) estimated that the density of primary (NWS) stations recording humidity (as well as solar radiation) in any form was less than 1/100,000 km² throughout the western United States. The challenge for many ecosystem modelers is to match the qualitative and quantitative requirements of their models with the spatial and temporal scales of the various climatological data sources available. NWS Daily Climatological Summaries represent a dependable data source when good on-site weather data cannot be collected and NOAA weather satellite data are too coarse.

However, the only variables routinely archived at both primary and secondary NWS sites are daily maximum and minimum air temperature (taken at 1.4 m above the ground) and precipitation. Dew point temperature measurements are taken, however, at some primary NWS sites usually situated at major airports. Although originally intended to work using NWS station Daily Climatological Summary data, the MT-CLIM model may be driven using any weather station source that provides maximum and minimum temperatures and precipitation.

Primary inputs to MT-CLIM include base station latitude, base station elevation, and site elevation, aspect, slope, albedo, atmospheric transmissivity, base and site precipitation isohyets, and temperature lapse rates (Table 2.1).

Table 2.1: Example of MT-CLIM Model Inputs	
Cascade Head, Site 1	
NASA OTTER PROJECT MTCLIM Validation	
CASC89.MTC	Input data file (temperatures in deg C)
CASC89.CLM	Output data file
S	English (Temps: F and PPT: inches, or SI (CM) Units, [E,S])
N	Dew point temperature supplied [Y or N]
I	Number of PPT stations [1 or 2]; if 2 then use 2 isohyets below
N	Use threshold radiation [Y or N]
T	Total or Average radiation [T or A]
Y	Use Yearday (Julian) in place of month & day [Y or N]
208	N. days, Integer variable, all the rest are single precision real values.
44.05	Latitude, in decimal degrees.
49.0	Site elevation (meters for si, or feet for english).
125.0	Site aspect 0 to 360 degrees (0 = north; 180 = south)
10.0	Site slope (Percent)
6.3	Site lai (all sided)
2.0	Site isohyet (precipitation)
2.0	Base isohyet station 1
0.0	Base isohyet station 2 (optional) see number of ppt stations
1.0	Site east horizon (degrees)
1.0	Site west horizon (degrees)
0.16	Site albedo (.2 = 20%)
0.60	Tran cf (Sea level atmospheric transmissivity)
0.45	Temp cf (Temperature correction for sine approx)
6.377	Environmental Lapse rate (Degrees cooling / 1000 m or ft)
7.288	Lapse rate for maximum temperature (Degrees / 1000 m or ft)
3.644	Lapse rate for minimum temperature (Degrees / 1000 m or ft)
2.730	Dew lapse rate (Degrees / 1000 m or ft)

Standard MT-CLIM outputs include daily microclimate values for air temperature (site temperature, maximum and minimum temperature, in °C), incident solar radiation (0.4 to 2.5 μm , in $\text{kJ}/\text{m}^2/\text{day}$), relative humidity, and precipitation (mm) in mountainous terrain. In response to the paucity of site specific climatology data required for ecological process models, Running et al. (1987) devised a mountain microclimate simulator, the MT-CLIM model.

MT-CLIM evolved from several earlier research models, H2OTRANS and DAYTRANS (Running, 1984) which evaluated the ecosystem level significance of stomatal control mechanisms (transpiration and water stress) at hourly and daily timesteps, respectively. MT-CLIM is composed of two types of climatology logic, the topographic climatology that spatially extrapolates meteorological conditions into complex terrain, and the diurnal climatology that derives additional meteorological information from the input data (Hungerford et al., 1989). In the topographic section of MT-CLIM daily data from primary NWS weather stations is extrapolated to nearby sites, adjusting for the differences in aspect, elevation, slope, and vegetation type between the site of interest and one or two base weather stations.

A key assumption in the development of the MT-CLIM logic, and one that distinguishes it from other meteorological models, is the concept of *operational environment* whereby important environmental variables are defined on the basis of plant physiology rather than only meteorologically (Mason and Lagenheim, 1957; Waring and

Schlesinger, 1985; Waring et al., 1972). For example, day length can be defined in the MT-CLIM model in terms of the period when the light compensation point (70 W/m^2) for conifer needles is exceeded -- the point at which conifer stomatal opening, transpiration, and positive net photosynthesis begins. In irregular or complex topography, this definition of day length may be 20% shorter than the full period from sunrise to sunset (Running et al., 1987). This threshold may be adjusted for other species as well.

The diurnal climatology in MT-CLIM generates two particularly problematic climatological parameters required by ecosystem process models -- incident solar radiation (Running et al., 1987), and a humidity measure useful from a plant physiology standpoint (Grantz, 1990). For this study, our objectives are to test key assumptions in the MT-CLIM model diurnal climatology logic by comparing incident solar radiation and relative humidities measured at five Oregon Transect Terrestrial Ecosystems Research (OTTER) sites against MT-CLIM estimations of these parameters.

Methods

This study was conducted as part of the NASA Oregon Transect Ecological Research (OTTER) project (Peterson and Waring, 1993). The OTTER project includes six primary sites along a 200 km east-west transect through central Oregon at 44 degrees North latitude, with elevations ranging from sea level to 1500 m. A timely opportunity to further validate basic assumptions in the MT-CLIM model was presented since each of

the OTTER sites (except the Juniper site) were equipped with a portable weather station (Campbell Scientific, Logan, Utah). Incident solar radiation was recorded at each OTTER site meteorology station using a Licor LI220S pyranometer, sensitive to radiation at 400-2500 nm wavelengths. Relative humidity was recorded using a PCRC-55 Humidity sensor from Phys-chemical Research Corp. At each site during 1989 and 1990 hourly measurements of 13 meteorological variables were collected, including minimum and maximum temperature, relative humidity, and incident solar radiation; the daily dataset we used was prepared from this hourly dataset.

Site Name	Met. Station Elevation (meters)	Met. Station Location	Physiographic Province	Mean Leaf Area Index (LAI)
Cascade Head	49	44° 3'0" N, 123° 57'30" W	Western coast range	6.4
Corvallis	60	44° 36'0" N, 123° 16'0" W	Interior valley	5.3
Scio	335	44° 40'30" N, 122° 36'40" W	Low elev. west cascades	8.6
Santiam Pass	1500	44° 25'20" N, 121° 50'20" W	High Cascades summit	2.8
Metolius	1027	44° 25'0" N, 121° 40'0" W	Eastern high Cascades	2.0

In this dataset, daylight is defined as the full period from sunrise to sunset. Key site parameters for the five OTTER sites used in this study are presented in Table 2.2. Only sites with meteorology stations were used for this study; the eastern most site

(Juniper) relied on the meteorology station at the Metolius site. For a more complete description of OTTER site characteristics, refer to Runyon et al. (1993) and Goward et al. (1993).

The observed data for this study was obtained from the Forest Science Data Base (FSDB) maintained by Oregon State University as part of the Long Term Ecological Research (LTER) data holdings. Daily observation data from 1989 and 1990 were extracted from the daily meteorological dataset. Our goal was to assemble as close to a full annual data sequence as possible, both to ensure an adequate sample size and to reveal any trends in the data that might have been phenologically driven. Several date ranges of observed data were excluded for 4 of the 5 sites (all sites but Santiam Pass) due to known calibration problems with the RH sensors. Table 2.3 contains a description of the date ranges and total number of days used in this analysis. Daylight is defined within the LTER database as the time from sunrise to sunset, and so the model was set to match this definition of day length. The site variables used were 24 hour minimum and maximum air temperature ($^{\circ}\text{C}$), daylight average relative humidity (%), total incident solar radiation ($\text{kJ}/\text{m}^2/\text{day}$), and precipitation (mm/day).

Table 2.3: Seasonal Distribution of Day Analyzed By Site			
Site	1989 Days	1990 Days	Total Days
Cascade Head	Jun 07 - Dec 31	Jan 1 - May 31	359
Corvallis	May 28 - Dec 31	Jan 1 - Mar 31	308
Scio	May 28 - Dec 31	Jan 1 - Mar 31	308
Santiam Pass	Jun 26 - Nov 05	May 9 - Nov 25	334
Metolius	Jun 05 - Dec 31	Jan 1 - Mar 31	299

Humidity and Vapor Pressure Deficit

There are several common ways of expressing humidity, including vapor density, relative humidity (RH), and vapor pressure deficit (VPD). Vapor density is simply the mass of water vapor in a unit volume of air, and is also known as absolute humidity (Oke, 1987). The most commonly collected humidity measure, relative humidity, is defined as the actual moisture content of a parcel of air as a percentage of that contained in the same volume of saturated air at the same temperature (Barry and Chorley, 1987). Dew point temperature, another index of humidity, is the temperature at which saturation occurs if air is cooled at constant pressure without addition or removal of vapor (Barry and Chorley, 1987). The relative humidity varies inversely with temperature during the day, tending to be lower in the early afternoon and higher at night. When the RH is 100%, the air temperature and dew point temperature are equal. Vapor pressure is a measure of the partial pressure exerted by water vapor molecules in the air (Oke, 1987). The VPD of an air parcel is the difference between the saturation vapor pressure and the actual vapor

pressure. In an ecological context, VPD may be the most useful measure of humidity, as it represents a measure of the *drying power* of air, playing an important part in determining the relative rates of transpiration in plants (Monteith and Unsworth, 1990).

To test the MT-CLIM diurnal humidity logic, VPD was chosen as a humidity measure as opposed to relative humidity (RH) since plants physiologically respond more readily to fluctuations in VPD than to changes in RH (Grantz, 1990). Ecological process variables dependent on VPD include evapotranspiration (ET), stomatal conductance and photosynthesis (PSN) dynamics, and plant water relations. VPD also plays a key role in stomatal conductances (Gates, 1980; Jarvis and Morison 1981) and in plant water flow resistances (Hunt et al., 1991). Running et al. (1987) reported an R^2 coefficient of 0.85 for the relationship between dew point temperature and 24- hour minimum temperature for three stands in the Lubrecht Experimental Forest in Western Montana; in the same study, he also reported R^2 coefficients for relative humidity algorithms of 0.59, 0.43, and 0.60 for 3 western Montana drainages.

Measuring humidity dependably over time has always been a challenge to meteorologists, due to the calibration, reliability, and longevity problems humidity

instruments are subject to. When a given set of meteorological data are obtained, it is helpful to know the type of humidity sensing instrument used; unfortunately, this information is not always available in the dataset documentation. In general, laboratory quality dew point hygrometers are more accurate (Oke, 1987). Unfortunately their expense, power requirements, and the necessity for periodic calibration tends to limit their use to primary NWS weather stations. The less expensive humidity instruments are based on chemical or electrical sensors where the humidity is measured on the basis of changes in chemical substrate or electrical properties due to moisture absorption; these types tend to be the most prone to degradation problems. In the OTTER study, for example, within several months of initial installation the digital RH sensors at all sites except the Santiam site exhibited a

premature signal degradation, seriously compromising the data's usefulness (Goward et al., 1993). The degradation problem was diagnosed in terms of RH trends at the affected sites increasingly

departing from expected diurnal recovery levels. Field conditions

apparently caused some physical loss of the RH sensor substrate over time, resulting in a systematic reduction in sensitivity and signal gain. This problem necessitated additional

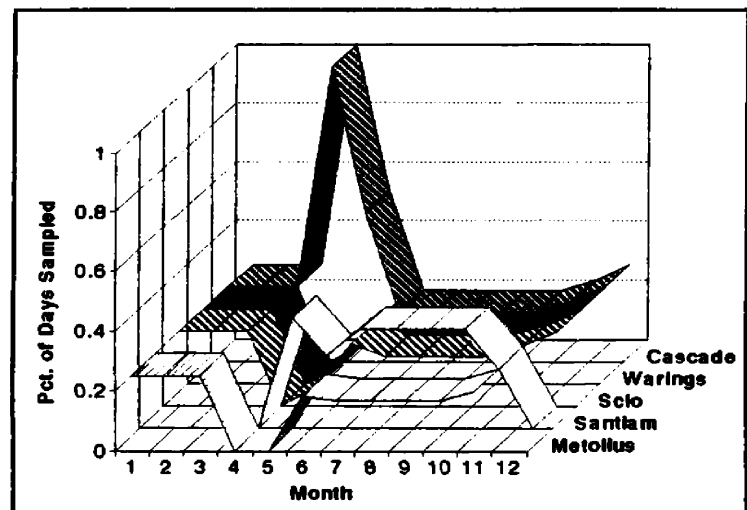


Figure 2.1 Frequencies of days sampled by month for two sample years (1989 and 1990), by OTTER site.

screening and verification of the measured relative humidity data from all sites but the Santiam Pass site.

For this analysis, we used daylight average relative humidity; only contiguously sequenced days with no missing values for temperature, radiation, or precipitation qualified for inclusion in the analysis dataset. We specifically excluded observations where the day fell within a time period where the RH sensor for the site was known to have degraded. Adequate samples sizes were thus obtained by using qualifying data from both 1989 and 1990 (Figure 2.1); as a result of these exclusions, contiguous 365 day sequences for each site were not possible.

The MT-CLIM model estimates site relative humidity and vapor pressure deficits using a scheme whereby dew point temperature is used in Murray's (1967) formulation:

$$esd = 6.1078 \cdot e^{\left[\frac{17.269 \cdot T_{Site}}{237.3 + T_{Site}} \right]} \quad (2.1)$$

where esd is saturated vapor pressure, in (kPa), T_{Site} is average daylight site temperature, in °C, and

$$es = 6.1078 \cdot e^{\left[\frac{17.269 \cdot T_{Dew}}{237.3 + T_{Dew}} \right]} \quad (2.2)$$

where e_s is ambient vapor pressure, in kPa, T_{Dew} is dew point temperature, in °C, and

$$RH_{Site} = \left[\frac{e_s}{e_{sd}} \right] \cdot 100 \quad (2.3)$$

where RH_{Site} is the daylight average site relative humidity, in percent. Two forms of these equations were used to produce the "observed" VPD vs. the "estimated" VPD, differing only in the way that ambient vapor pressure (e_s) was computed. To produce the "observed" VPD, saturated vapor pressure (e_{sd}) was computed exactly as shown in equation (1) and the site ambient vapor pressure was computed using a simple algebraic transform of the RH equation (2.3):

$$e_s = \frac{RH_{Obs}}{100} \cdot e_{sd} \quad (2.4)$$

where RH_{Obs} is the measured daylight average RH (%) at the base station. Vapor pressure deficit is defined simply as the difference between saturated and ambient vapor pressures, $VPD = e_{sd} - e_s$ (Oke, 1987; Monteith and Unsworth, 1990). To compute the "estimated" VPD for each site, ambient vapor pressure (e_s) was computed using equation (2), substituting the night minimum temperature for dew point temperature. Saturated vapor pressure (e_{sd}) was computed for the "estimated" VPD in the usual way as in equation (1).

Incident Solar Radiation

The method MT-CLIM uses for computing solar radiation on the site is adapted from the methods of Bristow and Campbell (1984) and is driven solely by diurnal temperature amplitude, freeing it from the requirement of historically questionable cloud cover estimates. Our hypothesis that diurnal air temperature amplitude relates directly to incident solar radiation loading assumes a horizontally stable atmosphere over the region of interest, with no significant advective exchange (Figure 2.2) To the extent that stable conditions dominate, the model should perform fairly well. One implication of this diurnal temperature approach is that the performance of our model in estimating solar radiation is critically dependent on the

many ways in which air masses may be horizontally modified; an air mass may be heated from below either by passing from a cold to a warm surface or by solar heating of the ground over which the air is located (Barry and Chorley, 1987). When significant horizontal air movement does occur, the differing temperatures and energy exchange properties of these masses

can disproportionately control air temperatures and thus mask or override the more direct

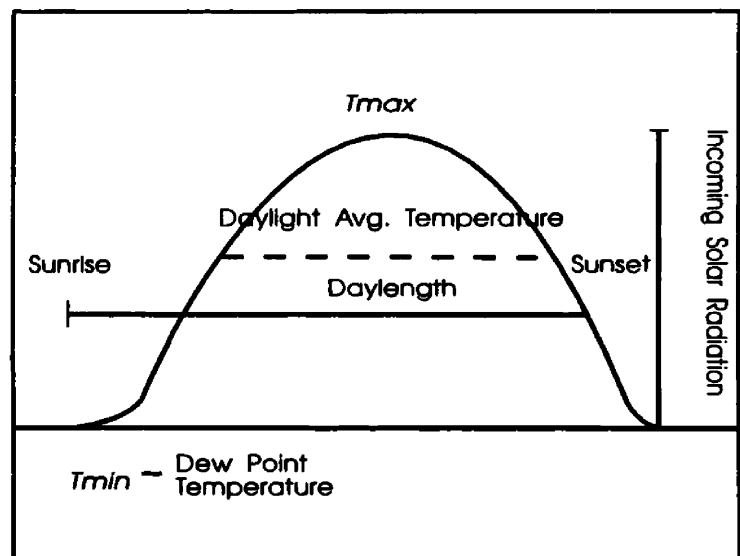


Figure 2.2 Diagram of MT-CLIM diurnal logic illustrating the relationship of diurnal minimum and maximum temperature, incoming solar radiation, and the truncated period defining daylight average temperature.

influence of solar radiation, weakening the models performance. Topographically driven phenomena such as cold air drainages, frost pockets, and physiographic formations that generate or amplify local winds can exert a similar effect. Synoptic scale frontal systems, local temperature inversions, and extremely mesic environments where latent heat exchange dampens the diurnal temperature amplitude present additional meteorological phenomena that the Bristow and Campbell (1984) based approach cannot accommodate well.

The daily 24 hour average incident solar radiation values measured at each of the five OTTER sites were compared directly against the MT-CLIM estimated values, using the total incident solar radiation (24 hour) as the observed data. Incident solar radiation at each site was computed in MT-CLIM using the algorithms documented in Running et al. (1987) requiring only observed daily minimum and maximum temperatures. Clear sky transmissivity is first computed, assuming a value of 0.60 for mean sea level, increasing by 0.008m^{-1} with elevation. Final atmospheric transmissivity is then computed as a function of diurnal temperature amplitude, following the method of Bristow and Campbell (1984). The logic behind this relationship is that the total transmittance for a given day includes both direct and diffuse components incident on a horizontal surface, and therefore integrates the atmospheric attenuation coefficients implicitly (Bristow and Campbell, 1984). Next, a potential radiation model adapted from Garnier and Ohmura (1968) and Swift (1976) is used to calculate direct and diffuse solar radiation, adjusting for slope and aspect and truncating the direct beam solar irradiance by the east and west

horizon of the site. The final estimate of incoming solar radiation to the site is then computed as the above-atmosphere radiation reduced by the atmospheric transmittance. The diurnal temperature range, ΔT , is calculated by the equation:

$$\Delta T_j = T_{maxj} - \frac{[T_{minj} + T_{(minj+1)}]}{2} \quad (2.5)$$

where J is the julian day index (1..365), T_{maxj} is the daily maximum temperature ($^{\circ}\text{C}$), T_{minj} is the daily minimum temperature ($^{\circ}\text{C}$), and ΔT_j is range in daily temperature extremes. The relationship between diurnal temperature amplitude and atmospheric transmittance is calculated using the Bristow and Campbell (1984) formulation:

$$T_t = A \cdot [1 - e^{(-B\Delta T^C)}] \quad (2.6)$$

where T_t is the daily total transmittance, ΔT is the daily range of air temperature, and A is the maximum clear sky transmittance, B (-0.0030), and C (2.4) are empirical constants that determine how soon T_t is achieved as ΔT increases. The B and C constants represent the partitioning of energy characteristic of the modelled site. Although these have historically been fixed at the above values for all sites, future revisions of MT-CLIM should incorporate a better strategy for determining the seasonal site characteristics driving this relationship. The equation used to compute potential incoming radiation is:

$$Q_s = I_{s_s} + D_s \quad (2.7)$$

where Q_s is the total incoming radiation on a slope (kJ/m^2) at the earth's surface, I_{s_s} is the direct beam radiation on a slope at the earth's surface, and D_s is the diffuse radiation at the surface; the direct beam radiation I_{s_s} at the surface is calculated by:

$$I_{s_s} = \cos \phi \left(R_o N \cdot T_t^{(AM)} \right) \quad (2.8)$$

where R_o is the solar constant (kW/m^2) above the atmosphere as a monthly average, N is the time interval for calculation in seconds, T_t is the daily total transmittance from equation (6); and AM is the optical air mass, calculated using the equation:

$$AM = \left[\frac{1.0}{\cos \Theta} \right] + 1.0 \cdot 10^{-7} \quad (2.9)$$

where $\cos \Theta$ is the cosine of the zenith angle (see Running et al., 1987 for more details).

Simulations and Analysis

Two sets of MT-CLIM simulations were run to generate observed and predicted values using versions of MT-CLIM in which the humidity algorithms were modified as discussed above. The observed solar radiation values (as 24 hour averages) used were the original values measured at each of the 5 sites with the LI220S pyranometer mounted on portable weather stations. The first set of simulations produced the observed VPD values for each of the 5 sites, and the second set of simulations produced the estimated VPD values and estimated incident solar radiation values for each of the 5 sites.

Several statistics were used to evaluate algorithm performance, including the R^2 coefficient of determination, the beta and y-intercept linear regression coefficients, and the root mean square error, RMSE. The RMSE provides an indication of curve fit accuracy, with observed values close to estimated values resulting in a lower RMSE. The RMSE is a conservative error measure that tends to penalize large individual errors heavily (Reicosky et al, 1989). Standard two-tailed hypothesis tests of the model beta (B_1) coefficients ($H_0: B_1 = 0$, $H_a: B_1 \text{ not equal } 0$) and y-intercepts (using the same two-tailed tests) were employed to further investigate the strength of the fitted models. Lastly, F statistic and T statistic probability values were calculated to evaluate the overall quality of the linear regression models. All statistics were computed using the SPSS/PC+ statistical software package (Norusis, 1988).

Results and Discussion

Humidity

R^2 coefficients of determination for the observed vs. predicted VPD models ranged from 0.66 to 0.84, with F statistics significant at the 0.001 probability level, with three of the five sites R^2 coefficients above 0.80. This suggests that the VPD approach yields acceptable results overall, particularly in light of a pooled site VPD R^2 of 0.72. An examination of Normal P-P plots indicated no serious departures from normality, and plots of casewise standardized residuals vs. fitted values indicated no obvious patterns in error trends. There was a slight clustering trend in R^2 coefficients with the wetter, more productive sites (Cascade Head and Scio) having the lower correlations (0.66 and 0.68 respectively) and the other sites' R^2 values ranging from 0.80 to 0.83 (Table 2.4). The distribution of point values for most sites was slightly skewed, due in part to a slightly asymmetric sampling distribution seasonally (Figure 2.1). Regression model slopes for the VPD models ranged from a low slope of 0.72 at the mid elevation, productive Scio site to a high slope of 1.5 at the cool, moist Cascade Head site (Figure 2.3). VPD regression y-intercepts ranged from 0.13 to 0.31 kPa, which in conjunction with the positive slopes contributed to a slight trend towards overprediction.

The Santiam Pass VPD regression model, where observed data did not require screening, may represent a useful average case of MT-CLIM's humidity performance; the regression slope for this site was 1.001 with a y-intercept of 0.31 kPa (Figure 2.4).

Table 2.4: Solar Radiation and VPD Analysis Summary

Incident Solar Radiation (kJ/m ²) Relationships					
Site	R ²	Std. Error Y'	RSME	Regression Model	N
Cascade Head	0.83	2878.5	3267.5	$y = 0.792(x) - 657.4$	359
Corvallis	0.89	3033.9	997.9	$y = 1.054(x) - 1499.8$	308
Scio	0.88	2736.5	4498.3	$y = 0.806(x) - 1763.8$	308
Santiam Pass	0.84	3881.4	1619.4	$y = 1.048(x) - 2302.1$	334
Metolius	0.84	4134.6	1667.5	$y = 1.010(x) - 1804.8$	299
All Sites Pooled	0.85	3691.9	2733.0	$y = 0.959(x) - 1678.6$	1608
Vapor Pressure Deficit (VPD, in kPa) Relationships					
Cascade Head	0.68	0.192	0.38	$y = 1.537(x) + 0.2706$	359
Corvallis	0.82	0.242	0.43	$y = 1.293(x) + 0.2953$	308
Scio	0.66	0.205	0.11	$y = 0.727(x) + 0.1345$	308
Santiam Pass	0.84	0.213	0.33	$y = 1.001(x) + 0.3143$	334
Metolius	0.81	0.236	0.38	$y = 1.409(x) + 0.1671$	299
All Sites Pooled	0.72	0.269	0.36	$y = 1.104(x) + 0.2634$	1608
<p>R² is the coefficient of determination for the least-squares model fits. N is the number of data points RMSE is the root mean squared error SEE Y' is Standard error of the estimate (for fitted Y values) T statistic significant at ≤ 0.001 for all model beta coefficients and Y-intercepts F statistic significant at ≤ 0.001 for all regression models.</p>					

In general, MT-CLIM somewhat overpredicted VPD across all sites except Scio. In this study where the emphasis was on testing the diurnal logic of MT-CLIM, the "base station" site characteristics were identical to the "extrapolated" sites; corrections for changes in aspect, elevation, or slope were therefore not

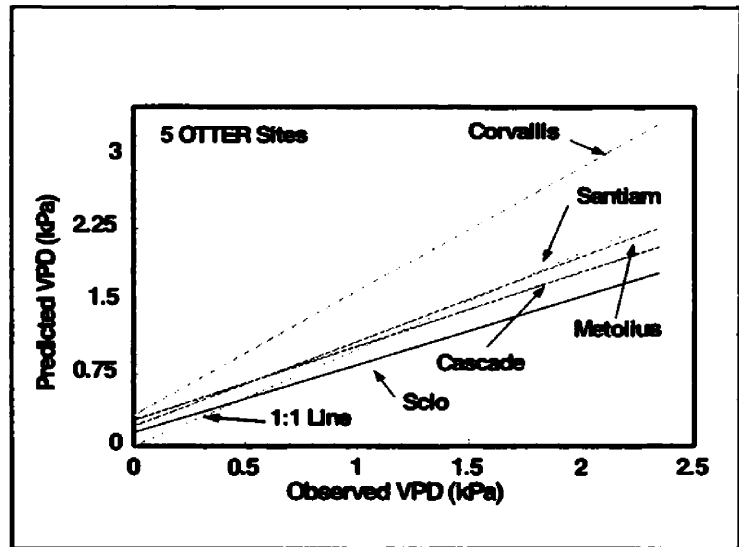


Figure 2.3 Comparative plot of vapor pressure deficit (VPD) regression lines for the five sites, illustrating the ranking of the regression slopes across the site gradient.

required. When the extrapolated site does markedly differ in aspect, elevation and slope from the base station site, it is possible for the MT-CLIM model to slightly over or under estimate air temperatures at the target site, due to the way the algorithms extrapolate the base station daily T_{\max} and T_{\min} temperatures to the new site characteristics. Such errors in estimated air temperature, if present, would naturally affect the VPD estimates.

For process models depending on these humidity estimates, this would likely result in somewhat higher transpiration rates and altered soil water dynamics. Limited availability of dependable humidity or dew point temperature data for ecosystem research applications appears to justify further efforts to strengthen the MT-CLIM approach. Better correction logic, however, still needs to be developed to accommodate the meteorological conditions described earlier that MT-CLIM currently doesn't handle well. As a wider geographic test of the basic relationship between dew point temperature and

24 hour minimum temperature, we fitted linear regression models for daily weather data from six NWS sites across the continental US equipped with higher quality dew point hygrometers. An annual sequence of 365 days for 1984 was used for each of the following sites: Fairbanks, Alaska, Seattle, Washington, Knoxville, Tennessee, Madison, Wisconsin, Tucson, Arizona, and Jacksonville Florida. R^2 values for these regression models ranged from 0.83 to 0.96, with the exception of the drier Tucson site, whose R^2 was 0.55. Model slopes ranged from 0.80 to 1.02, and y intercepts ranged from -6.95 to 1.05°C . While acknowledging the climatological limitations of these relationships in drier environments, we believe these correlations suggest the basic soundness of the dew point--minimum temperature relationship. Particularly in more arid environments with lower absolute

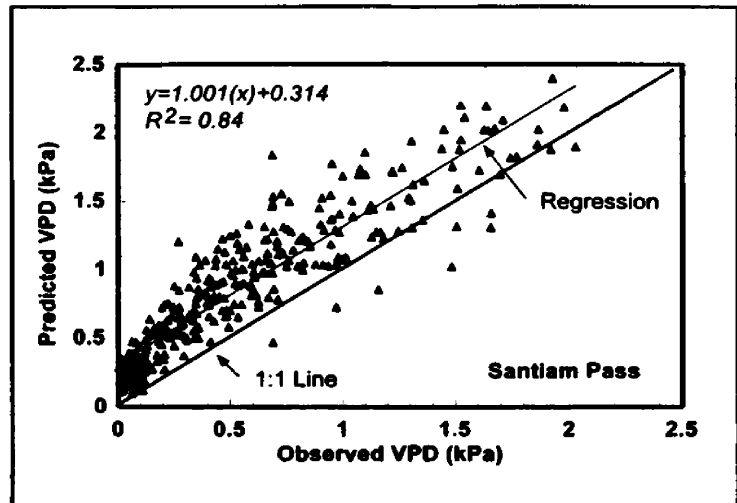


Figure 2.4 Scatterplot and regression line of the vapor pressure deficit (VPD) model for the Santiam Pass (Oregon) OTTER site using 1989 and 1990 LTER (Long Term Ecological Research) data. This regression model provides a representative example of average humidity performance since data from this site did not require screening.

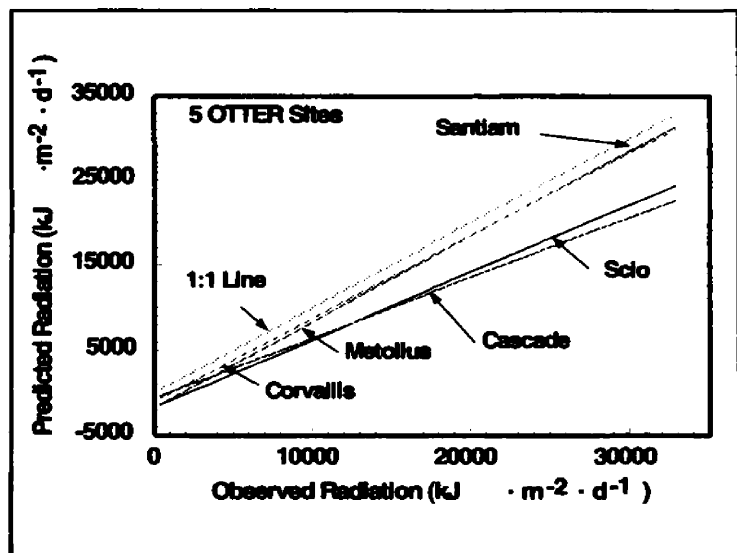


Figure 2.5 Comparative plot of incident solar regression lines for the five sites, illustrating the division of the lines into two basic groups.

humidities, lower LAI levels, and greater clear sky re-radiation, the dew point temperature may often be lower than the reported 24 hour minimum temperature, and thus may never be reached (Lee 1978; Monteith and Unsworth, 1990). A positive correlation between dew point and daily minimum temperature also depends in part on dew point remaining fairly constant throughout the day; significant changes in air mass moisture from advective exchange are expected to alter this basic relationship. We generally feel, however, that the correlation between dew point temperature and 24 hour minimum temperature is strong enough on average to be of use in many ecological modelling applications, particularly since RH sensors are so undependable. The dew point temperature--24 hour minimum temperature correlation we observed may be particularly useful for studies employing larger spatial and temporal scales, where the higher variance in diurnal humidity and temperatures may be smoothed out at larger scales.

Incident Solar Radiation

Correlations between predicted and observed incident solar radiation were generally consistent and high, ranging from 0.83 to 0.89 (Table 2.4), with F statistics significant at the 0.001 level for all regression models. Regression slope T statistics testing the two-tailed null hypotheses, H_0 , that the beta coefficient equals 0 and that the y-intercepts equals 0 were all significant at the 0.001 level, indicating the null hypotheses should be rejected. The regression model beta coefficients for the sites tended to split into two groups, with Cascade Head and Scio beta coefficients at 0.79 and 0.80 respectively, and Metolius, Santiam Pass and Corvallis beta coefficients ranging from 1.01 to 1.05 (Figure 2.5). This division did not seem to occur on a clear environmental gradient, and could therefore relate to local advection conditions, inversions, or random error from sampling noise.

Model y-intercept values were all negative, ranging from -657 kJ/m^2 at the Cascade Head site to -2352 kJ/m^2 for Santiam Pass; the y-intercept two-tailed T statistical significance for all radiation regression models was 0.01 or better. This statistic tests the H_0 that the y-intercept equals 0, vs. a H_a that the y-intercept is not equal to 0. The scatterplot and regression line fitted for the incident solar regression (Corvallis site, Figure 2.6) shows a dense point cluster around the lower radiation range (ca 1000-4000 $\text{kJ/m}^2/\text{day}$) with a fairly balanced cluster for higher values; again, the slight pattern here

could be due to the presence of advection effects on sampled days. RMSE values for the incident solar relationships ranged from 997.0 kJ to 4498.0 kJ, with no apparent trend following the west-east transect gradient.

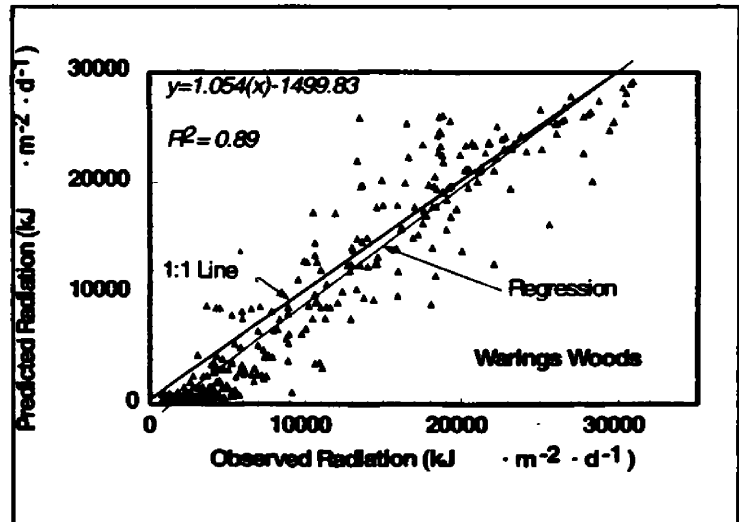


Figure 2.6 Scatterplot and regression line of the incident solar radiation model for the Waring's Woods (Corvallis, Oregon) OTTER site using 1989 and 1990 LTER data.

Normal P-P plots for the radiation data showed no serious departures from normality, and casewise plots of standardized radiation model residuals vs. fitted values indicated no obvious patterns in error trends. As a check on how regression VPD and solar radiation residuals might covary, plots of VPD residuals vs. incident solar residuals were examined, both by site and by pooling data for all sites; no trends were observed for either type of plot. Overall, the consistent strength of the incident solar relationships suggests this method may be sufficiently robust under a typical range of meteorological conditions (Ryan, pers. comm; Barron, pers. comm).

Conclusions

The comparisons made here between observed and estimated radiation and humidity suggest that MT-CLIM can provide the climatology acceptable inputs for many

hydrologic and ecosystem models. This approach may prove particularly useful for coarser spatial scale applications where absolute precision at higher spatial resolutions may not be as important as an adequate characterization of incident solar radiation, diurnal temperature variations, and humidity dynamics over larger regions. The problems with humidity instruments and the current lack of incident solar radiation data archived daily at NWS weather stations further supports the value of this approach. Two projects in the International Geosphere-Biosphere Program have identified the need for a "weather generator" that takes standard climatological data and estimates additional meteorological variables needed by ecological research. The GCTE (Global Change and Terrestrial Ecosystems), and the BAHC (Biospheric Aspects of the Hydrologic Cycle) projects are collaborating on developing these weather generator tools to improve both the temporal and spatial utility of climate datasets for ecological studies. We think that MT-CLIM may be a useful precursor model for this new work.

Aside from problems relating to the quality of input data, a revision of MT-CLIM should attempt to redress current limitations in the model extrapolation logic. Areas needing improvement include a provision for adjusting between sites with significantly different air mass moisture properties (e.g. low coastal vs. dry inland sites), and a better way to generally address horizontal advection influences. Addressing estimation error due to cold air drainage influences and other topographically driven phenomena would probably require more radical changes, extending the model from a 1D point model to a 2D spatially connected model. The term *spatially connected* as used here implies that the

modelled point may be influenced, at the very least, by selected landscape characteristics of neighboring areas. If a more spatially connected approach was pursued, a more explicit treatment of the topography directly influencing to the modelled site could then be taken into account. The question of landscape scale becomes a critical one here, as a treatment of micro-topography effects would likely differ from drainage-level or even mesoscale topographic influences. An additional but related challenge involves how valley and katabatic diurnal wind patterns might be treated in the model, if at all. Relative to the current more simplistic MT-CLIM logic, such approaches would likely involve some conscious tradeoffs in model complexity and parameterization.

The VPD relationships observed in this study, particularly for the Cascade Head and Scio sites were not as conclusive as we would have liked, probably due to a combination of meteorological conditions not handled well in MT-CLIM as well as the selection of observed days (Figure 2.1 and Table 2.3). Nonetheless, they may be sufficiently useful for larger scale modelling efforts for the reasons indicated above for solar radiation. Quality and maintenance of humidity sensors routinely used in the field were also important issues this study confronted, suggesting that it may be more advantageous to extrapolate from more distant but arguably higher quality NWS primary weather stations using dew point hygrometers than to rely on less expensive and more problematic electro-chemical based RH instruments with shorter operational lifespans.

Literature Cited

- Ågren, G.I., R.E. McMurtrie, W.J. Parton, J. Pastor, and H.H. Shugart. 1991. State of the art models of production-decomposition linkages in conifer and grassland ecosystems. *Ecological Applications* 1(2):118-138.
- Band, L.E. and E.F. Wood. 1988. Strategies for large scale, distributed hydrologic simulation. *Journal of Applied Mathematics and Computation* 27:23-37.
- Band, L.E., D.L. Peterson, S.R. Running, J. Coughlan, R. Lammers, J. Dungan, and R.R. Nemani. 1991. Forest ecosystem processes at the watershed scale: basic for distributed simulation. *Ecological Modelling*, 56:171-196.
- Barry, R.G. and R.J. Chorley. 1987. *Atmosphere, Weather and Climate*. Routledge, London, England. 460 p.
- Bristow, K.L. and G.S. Campbell, 1984. On the relationship between incoming solar radiation and daily maximum and minimum temperature. *Agricultural Forest Meteorology* 31:159-166.
- Gates, D.M. 1980. *Biophysical Ecology*. Springer-Verlag, New York, NY. 461 p.
- Garnier, B.J. and A. Ohmura. 1968. A method of calculating the direct shortwave radiation income on slopes. *Journal of Applied Meteorology* 7(5):796-800.
- Goward, S.N., R.H. Waring, D.G Dye, and J. Yang. 1994. Ecological Remote Sensing At OTTER: satellite macroscale observations. *Ecological Applications* 4(2):322-343.
- Grantz, D.A. 1990. Plant response to atmospheric humidity. *Plant Cell and Environment* 13:667-679.
- Hungerford, R.D., Nemani, R.R; Running, S.W., Coughlan, J.C. 1989. MTCLIM: a mountain microclimate simulation model. Research Paper INT-414. Ogden, UT: U.S. Department of Agriculture, Forest Service, Intermountain Research Station. 52 p.
- Hunt, E.R., Jr., S.W. Running, C.A. Federer. 1991. Extrapolating plant water flowresistances and capacitances to regional scales. *Agricultural Forest Meteorology* 54:169-195.

- Jarvis, P.G. and J.I.L. Morison. 1981. The control of transpiration and photosynthesis by the stomata. In: *Stomatal Physiology*, (eds P.G. Jarvis and T.A. Mansfield), Cambridge University Press. Cambridge, England. pp. 247-278.
- Lee, R. 1978. *Forest Microclimatology*. Columbia University Press, New York, NY. 275 p.
- Mason H.L. and Langenheim, J.H. 1957. Language analysis and the concept of environment. *Ecology* 38:325-339.
- McMurtrie, R.E. 1985. Forest productivity in relation to carbon partitioning and nutrient cycling: a mathematical model. In *Attributes of Trees as Crop Plants*. Eds. M.G.R. Cannell and J.E. Jackson. Institute of Terrestrial Ecology, Abbots Ripton, Huntingdon, England. pp. 194-207.
- Monteith, J.L, and Unsworth, M.H. 1990. *Principles of environmental physics*. Edward Arnold, London, England. 291p.
- Murray, F.W. 1967. On the computation of saturation vapor pressure. *Journal of Applied Meteorology* 6:203-204.
- Nemani, R.R., S.W. Running, L. Band, D. Peterson. 1993. Regional hydro ecological simulation system: an illustration of the integration of ecosystem models in a GIS. *in Integrating GIS and Environmental Modelling* pp. 296-304. editors M. Goodchild, B. Banks, and L. Steyert, Oxford London. 488 p.
- Norusis, Marija J. 1988. *SPSS/PC+ V3.0 Update Manual*. SPSS Inc., Chicago, IL 60611. 116 p.
- Oke, T.R. 1987. *Boundary layer climates*. 2nd edition, Routledge, New York, NY. 435 p.
- Parton, W.J., J.W.B. Stewart, and C.V. Cole. 1988. Dynamics of C, N, P, and S in grassland soils: a model. *Biogeochemistry* 5:109-131.
- Peer, R.L. 1990. An overview of climate information needs for ecological effects models. Contract No. 68-02-4288. Atmospheric Sciences Modelling Division, Air Resources Laboratory, National Oceanic and Atmospheric Administration, Research Triangle Park, NC. 27711. 52 p.
- Peterson, D.L. and R.H. Waring. 1994. Overview of the Oregon transect research project. *Ecological Applications* 4(2):211-237.

- Reicosky, D.C., L.J. Winkelman, J.M. Baker, and D.G. Baker. 1989. Accuracy of hourly air temperatures calculated from daily minima and maxima. *Agricultural Forest Meteorology* 46:193-209.
- Running, S.W. 1984. Documentation and preliminary validation of H2OTRANS and DAYTRANS, two models for predicting transpiration and water stress in western coniferous forests. USDA Forest Service Research Paper RM-252 Rocky Mountain Forest and Range Experiment Station, Fort Collins, CO. 45 p.
- Running, S.W., R.R. Nemani, R.D. Hungerford. 1987. Extrapolation of synoptic meteorological data in mountainous terrain and its use for simulating forest evapotranspiration and photosynthesis. *Canadian Journal of Forest Research* 17(6):472-483.
- Running, S.W. and J.C. Coughlan. 1988. FOREST-BGC, a general model of forest ecosystem processes for regional applications. I. Hydrologic balance, canopy gas exchange and primary production processes. *Ecological Modelling* 42:125-154.
- Running, S.W. and R.R. Nemani, D.L. Peterson, L.E. Band, D.F. Potts, L.L. Pierce and M.A. Spanner. 1989. Mapping regional forest evapotranspiration and photosynthesis and coupling satellite data with ecosystem simulation. *Ecology* 70(4):1090-1101.
- Running, S.W. and S.T. Gower. 1991. FOREST-BGC, a general model of forest ecosystem processes for regional applications. II. Dynamic carbon allocation and nitrogen budgets. *Tree Physiology* 9:147:160.
- Runyon, J., R.H. Waring, S.N. Goward, and J.M. Welles. 1994. Environmental limits on above-ground production: observations from the Oregon Transect. *Ecological Applications* 4(2):226-237.
- Swift, L.W. Jr. 1976. Algorithm for solar radiation on mountain slopes. *Water Resources Research* 12(1):108-112.
- Waring, R.H., K.L. Reed, W.H. Emmingham. 1972. An environmental grid for classifying coniferous forest ecosystems. *in* proceedings: Research on Coniferous Forest Ecosystems-A Symposium. Bellingham, WA March 23-24, 1972. Pacific Northwest Forest and Range Experiment Station, Forest Service, U.S. Department of Agriculture, Portland, Oregon, USA. pp. 1-26:13-26.
- Waring, R.H. and W.H. Schlesinger. 1985. *Forest Ecosystems*. Academic Press, Inc. San Diego. 340 p.

Warren J.R. and D.L. Vance. 1981. Remote automatic weather station for resource and fire management agencies. USDA Forest Service General Technical Report INT-116, Intermountain Research Station, Ogden, Utah. 11 p.

Chapter 3

Validating Topographic Climatology Logic of the MT-CLIM Model Across A Seasonal Gradient

Introduction

Ecological simulation modelling represents an increasingly useful approach for estimating landscape carbon and water budgets at various spatial scales (Peterson and Waring, 1994; Running, 1990; Band et al. 1991). Accurate characterizations of site hillslope temperature are critically linked to the usefulness of these models (Schimel et al., 1991; Barry, 1987; Nemani et al., 1993), due to the key role temperature plays in partitioning a sites energy balance (Heilman and Brittin, 1989; Nemani and Running, 1985). To the extent that climate defines the composition and geographical distribution of biomes, climatological data also represents a key requirement of global scale land classification schemes (Pierce, 1994; Running, 1993; Woodmansee, 1988). As a generalized variable, environmental temperature plays a key role in a diverse array of ecosystem dynamics, driving plant biochemical responses (Fitter and Hay, 1987), photosynthesis rates (Gates, 1980), as well as the pattern and timing of plant development (Good, 1974), carbon balance (Running and Nemani, 1991; Running and Gower, 1991) and humidity and evapotranspiration dynamics (Running et al. 1989; Running, 1991; Grantz, 1990).

The limited availability of adequate quality meteorological data continues to motivate the development of numerical meteorology codes such as MT-CLIM that provide the needed climatological variables (Running et al., 1987; Hungerford et al., 1989). The NASA Earth Observing System (EOS) distributed information system (EOSDIS) currently plans to distribute a global climatology dataset at 1° by 1° (≈ 100 km) scale; this is too coarse a resolution for regional or even mesoscale studies. Meteorological variables required as inputs to climatology models typically include a measure of site temperature, humidity, precipitation, and incident shortwave radiation. Validating climatology models is best facilitated by observed data sets that closely match the model logic's temporal and spatial scales. Various point data sets are generally available from the National Weather Service (NWS), National Oceanic Atmospheric Agency (NOAA), or commercial providers, yet few are available in spatially gridded form at stand level scales, let alone for mesoscale or regional scale work. While such data are occasionally available in the context of narrowly focused studies, investigators most often rely on point based climatology datasets that are limited both in the variables included and in their spatial coverage. Agricultural crop meteorology studies have employed tower micro-meteorology techniques to derive high resolution meteorological descriptions (Heilman and Kanemasu, 1976; Kustas et al. 1989; Verma et al. 1989). For these studies, full energy balances are typically calculated using Bowen ratio (Fritschen and Qian, 1992), aerodynamic (Monteith and Unsworth, 1990), or eddy correlation (Moncrieff et al. 1992). These methods are generally considered too expensive and

impractical for multiple scale ecology studies, in addition to imposing serious logistical constraints on investigators. The increased emphasis on regional and global scale ecosystem research has thus encouraged various remote sensing based approaches, to which models like MT-CLIM play a complementary role.

The MT-CLIM authors provided a preliminary validation in an examination of three sites in Western Montana -- Ambrose Creek, Ninemile, and Schwartz Creek (Running et al., 1987). The topographic analysis of the original study was restricted to a north vs. south slope comparison, where observed vs. predicted seasonal average air temperature, relative humidity, and incoming shortwave radiation were compared. Regressions of predicted vs. observed air temperature yielded r^2 values of 0.88, 0.88 and 0.90 for the Ambrose, Ninemile, and Shwartz Creek sites respectively. The original study emphasized the temporal portion of the logic, however, since a daily data set was modeled for an annual period at only three points (N= 204, 146, and 202 days respectively for the three sites). This study emphasizes a more detailed topographic treatment, and examines the models seasonal performance for three samples throughout the 1990 year; March 21, June 25, and August 13. The seasonal aspect of this study was undertaken to reveal possible subtleties in the hillslope temperature relationships due to sun-angle differences.

Objectives

This validation of MT-CLIM topographic logic addresses the following question: "how well do MT-CLIM estimated hillslope temperatures (T_a) compare with surface temperatures (T_s) derived from thermal infrared data (TIR, $\approx 8-14\mu\text{m}$ wavelength) across diverse topographic and canopy closure gradients?" Critical controls on T_a and T_s temperature patterns include both physiographic (elevation, aspect, slope) and biophysical (canopy properties, primarily canopy cover fraction) factors (Moran et al., 1989; Huband and Monteith, 1985). The comparison of surface temperature with air temperature trends in this study are therefore made in the context of these gradients.

An immediate complication with this type of comparison involves differences in the basic dimensionality inherent in the two measures. T_s derived from the Daedalus Thematic Mapper Simulator (TMS) instrument represents an instantaneous quantity integrated over a considerable spatial extent. Conversely, MT-CLIM estimated T_a represents a time-averaged signal, governed by somewhat different physics over essentially a single point in space. As such, these two measures represent somewhat asymmetric concepts with different statistical variance structures; averages (i.e. T_a) by definition encapsulate population variation, whereas a set of spatially distributed (T_s) values represent individual random variates. While this conceptual inconsistency cannot be readily mitigated, awareness of the biophysical implications of each should help clarify an interpretation of differences between them.

In addition to more thoroughly evaluating the original MT-CLIM algorithm for estimating site hillslope temperatures, a secondary objective of this study was to try to develop a site temperature algorithm better suited to spatial modeling applications. Tests across the topographic gradients described above for the three TMS scene sample dates (March 21, June 25, and August 13) for a new site temperature algorithm are reported.

Background

Any comparison of surface temperature with air temperature should be predicated by a discussion of the important characteristics that distinguish the two quantities. Heat is defined as the total kinetic energy of the atoms or molecules composing a substance, whereas temperature is the average kinetic energy of a substance's atoms or molecules (Moran and Morgan, 1989). As a form of mechanical energy at a submicroscopic scale, heat may be interpreted as a kinetic energy translation within a body, or bodies in contact, as a radiative, conductive, or convective energy transfer process (Lee, 1978). Surface temperature is defined as the true kinetic temperature measured at a given surface (Oke, 1987). It integrates several complex energy fluxes, including incident, reflected and absorbed solar fluxes (W m^{-2}), as well as moisture energy exchanges between the soil, vegetation, and atmosphere. Surface temperature is therefore modified by physiographic and biophysical site attributes such as slope, aspect, and elevation, as well as by the radiative properties of the site's canopy and soil. Heat energy may be transferred via convection, conduction or radiation, and is biophysically partitioned between two

controls: sensible heat and latent heat. Sensible heat refers to the energy transfer associated with a measurable temperature change; latent heat refers to energy transfer associated with a phase change (latent heat of vaporization, latent heat of fusion), in the absence of a temperature change. An example of latent heat exchange is the energy state transformation that occurs whenever free water changes from a liquid to a gaseous state, or from a gas to a liquid or solid state. Through this partitioning, surface temperature is intimately tied to a sites overall radiation and water energy balance.

All radiant energy from the sun must be absorbed (a), transmitted (t), or reflected (r). An expression of this law of energy conservation defines the energy partitioning as $a+r+t=1$. A black body is defined as a perfect absorber and emitter (Monteith and Unsworth, 1990); for a theoretical blackbody, $a=1$, and so $r=t=0$ (Campbell, 1977). The concept of instantaneous surface temperature may also be considered in terms of the continuity equation (Oke, 1987) which describes the net conservation of energy, in W/m^2 at the earth's surface:

$$R_n - H - G - \lambda E_t - \rho = 0 \quad (3.1)$$

where R_n is the net radiation including solar and thermal wavelengths, H is the sensible heat exchange with the atmosphere, G is heat transfer due to conduction, where downward flow is a loss (heat storage, with a temporal lag) and upward flow is considered a gain to the earth's surface, λ is the latent heat of vaporization (J/g), E_t is the

rate of evapotranspiration ($\text{g m}^{-2}\text{s}^{-1}$), the product of λ and E_t ($\text{g h}_2\text{O}$) is the rate of evapotranspiration (W/m^2), and ρ represents the sum of complex chemical energy conversions involved in photosynthesis and respiration (Hewlett, 1982). R_n is also commonly expressed as $[S(1-a)-L_n]$, where S is the incoming short-wave radiation, a is the fractional albedo of the surface, and L_n is the net outgoing long-wave radiation; collectively this is the sum of all incoming short and long wave radiation from the sun and sky, less reflected short wave radiation and emitted long wave radiation (Barry and Chorley, 1992). Surface temperature is related to the long wave irradiance emitted and reflected by a grey body at a given temperature by the general equation:

$$R = \epsilon \cdot \sigma \cdot T_s^4 + (1 - \epsilon) \cdot B_s^* \quad (3.2)$$

where R is the long wave (thermal) irradiance emitted and reflected, ϵ is the emissivity of the surface (typically ≈ 0.97), σ the Stefan-Boltzmann constant ($5.67 \cdot 10^{-8} \text{ W m}^{-2} \text{ K}^{-4}$), B_s^* is a measure of long-wave irradiance received by the surface from its surroundings (in W m^{-2}), and T_s is the surface temperature on site, $^{\circ}\text{C}$.

Air temperature, T_a , represents the average instantaneous temperature of an air mass at screen height (≈ 1.4 meters). Air temperature typically cycles on a diurnal basis, and is coupled to (but lags behind) the daily radiation flux. Air temperature is controlled not only by the on-site net radiation loading and energy partitioning between sensible and latent heat, but also by diurnal wind patterns and relative air mass stability. Sensor view

angles (McGuire et al. 1989) and canopy structural properties (roughness length, buoyancy, and fetch) also attenuate the temperature signal (Oke, 1987; Monteith and Unsworth, 1990). A number of approaches in modelling hourly air temperatures have been suggested; Reicosky et al. (1988) reviewed several methods for estimating hourly air temperatures from daily minima and maxima, including the method of Parton and Logan (1981) used in MT-CLIM. Reicosky (1988) emphasized methods used to estimate air temperature within crop growth models and found that all the methods reviewed worked best on clear days, with more limited success on cloudier days. Reicosky et al. (1988) found that the Parton and Logan (1981) method calculated a higher temperature earlier in the daylight hours. In estimating daily average air temperature, MT-CLIM makes a number of assumptions, including basic vertical stability in the air mass, moderately good vertical mixing throughout the canopy, and no significant horizontal advection.

From this brief background, the complex interactions between surface temperature and air temperature dynamics are more easily envisioned. In the context of Bowen ratios, air temperature tracks sensible heat more closely, so T_a more closely approximates the energy budget and T_s whenever the sensible heat flux dominates the ratio. T_a and T_s are more coupled on sites with generally higher canopy densities, higher cloud cover conditions, and better ventilation (e.g. generally taller trees, smaller leaves, and higher windspeeds) -- whenever environmental conditions collectively act to dampen the diurnal net radiative flux and surface temperature amplitude (Oke, 1987). Conversely, T_a and T_s tend to increasingly diverge on sites where conditions depart from those described above

-- with more heterogeneous structural features. In a study involving vegetation regeneration of coal mining sites, Lee (1978) reports differences between mean air and surface temperatures varying from 1.9 °C for light colored, natural surfaces to 16.3 °C for dark toned, natural surfaces. Linacre (1992) cites an example at Pune, India where the ground surface maximum and minimum temperatures differed by 34 °C, whereas at 1.5 m, the difference was only 22 °C. These examples illustrate the large potential differences between T_a and T_s for a given site at one point in time, and in T_s diurnally. Goward et al. (1994) and Nemani and Running (1989) also show the direct role that canopy fraction (via NDVI in these studies) plays in the coupling of T_s and air temperature; the results of both studies suggest that T_s approximates T_a on sites with higher NDVI indices, and departs the most from T_a on sparsely vegetated sites.

Direct quantitative comparisons of surface temperatures to air temperatures are therefore problematic at best due to a number of potentially compensatory factors: the typically unknown absorbed solar fraction, the role of atmospheric and surface properties controlling reflectivity, as well as the natural differences in heat capacity between air at 1.4 m ($0.0002 \text{ J m}^{-3} \text{ K}^{-1}$ at 10°C) and the typically larger heat capacities of a diverse array of ground surfaces. Acknowledging these constraints should therefore temper our expectations on how well T_a and T_s might correlate.

Methods

This study adopted a remote sensing orientation through its participation in the National the Aeronautics and Space Administration (NASA) Oregon Transect Ecological Research (OTTER) project. The primary OTTER project objective was to study ecosystem function in coniferous forests using computer modeling, experimental and theoretical remote sensing, and ecological field and laboratory experiments (Peterson and Waring, 1994). The project included a coordinated, multiple-aircraft field campaign, and included six primary sites along a 200 km east-west transect through central Oregon at 44° north latitude, with elevations ranging from sea level to 1500 m. (Figure 3.1).

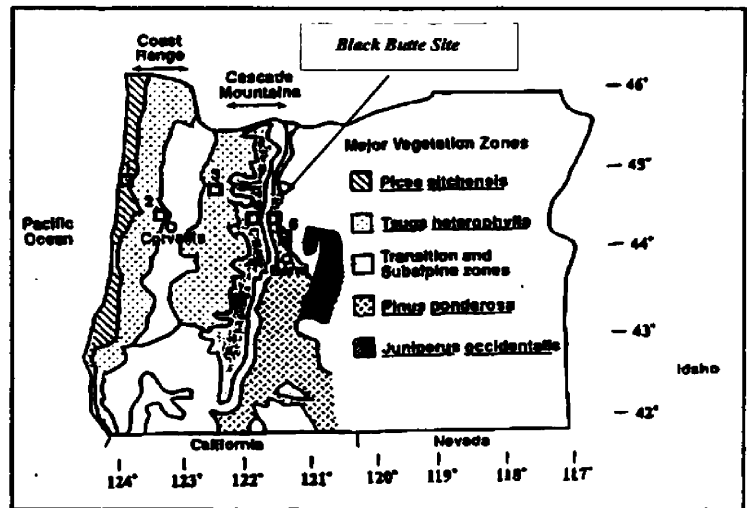


Figure 3.1 OTTER project and study site location.

Among the remote sensing platforms carrying thermal sensors deployed in the OTTER study were C-130 aircraft based NS001 and ER-2 aircraft based Daedalus Thematic Mapper Simulator (TMS) sensors. When spatially distributed surface temperature datasets are required, deriving these measures from Daedalus thermal infrared (TIR) channels (8-14 μ m wavelength) can sometimes represent a more practical alternative than an intensive field sampling program. The major tradeoffs in using TMS data seem to be the indirect physical relationship of T_s to T_a , and the sometimes

considerable preprocessing effort required to calibrate and correct the remotely sensed imagery for research applications. The site air temperature variable T_a estimated by MT-CLIM was selected as the most practical topographic validation parameter, since topographic trends in air temperature could be compared with the highly resolved (≈ 25 m), spatially distributed TIR datasets. The Daedalus TMS scenes taken during the OTTER project were also temporally well distributed over the 1990 year, allowing a seasonal evaluation.

The topographic validation area defined in this study is located ≈ 1.5 km from the Metolius OTTER

site near Sisters, Oregon just east of the crest of the Oregon Cascade Range near Santiam Pass. The study area comprises a 10.8 km² area

centered on Black Butte, a symmetric

shaped volcanic cinder cone (Figure 3.2). This site was chosen for its inclusion of a full range of topographic attributes, as well as for its proximity to the OTTER Metolius

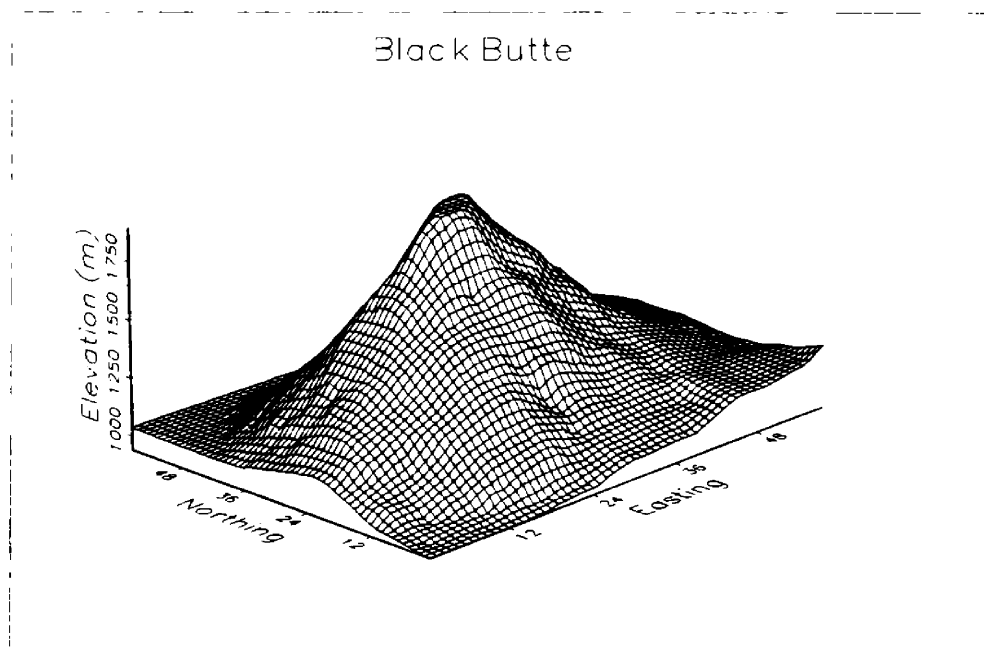


Figure 3.2 Black Butte cinder cone 10.8 km² study site, rendered from the USGS Bend West 3 arc-second DMA digital elevation model.

weather station located several kilometers from the base of the butte. Since Black Buttes shape is nearly symmetric, all aspects were represented, and a suitable elevation relief was present, extending from a base of 940 m to the top at 1892 m. A more detailed statistical summary of study site attributes appears in Appendix 3.1 .

Forest vegetation types present on Black Butte range from Ponderosa pine (*Pinus ponderosa*) dominated stands on the drier aspects and lower elevations, to mixed stands of varying densities of Douglas Fir [*Pseudotsuga menziesii* (Mirbel) Franco] at the middle elevations, to alpine fir [*Abies lasiocarpa*] communities at the upper reaches of Black Butte. The climate at Black Butte, although in a transition zone at the interface of the east slope of the Cascades and the drier, warmer Oregon steppe is considered more continental than maritime.

Description of the MT-CLIM Model

The MT-CLIM model evolved from the H20TRANS and DAYTRANS (Running, 1984) models, which evaluated the ecosystem level significance of stomatal control mechanisms (transpiration and water stress) at hourly and daily time steps respectively. MT-CLIM began as a point based model used to extrapolate key base station weather data parameters to nearby adjacent hillslopes. One of its primary advantages is that it is driven by more easily obtained climatology variables: daily average maximum and minimum temperature ($^{\circ}\text{C}$), relative humidity (%) and precipitation (mm). If available, dew point

temperatures may be used to directly parameterize the humidity algorithm; otherwise, night minimum temperature may be used as a surrogate for the dew point temperatures routinely taken only at primary NWS sites. Glassy and Running (1994) examined the dew point temperature/night minimum temperature equivalence across the five OTTER project sites. They found that night minimum temperature served reasonably well as a substitute for dew point temperatures subject to certain acknowledged limitations. Parameters estimated by MT-CLIM include minimum and maximum air temperature ($^{\circ}\text{C}$), relative humidity (%), incident solar radiation (W m^{-2}), and precipitation (mm). Refer to Appendix 3.2 for a complete listing of the inputs MT-CLIM requires.

This topographic study did not independently model or analyze daily minimum and maximum temperatures, since the observed variable (T_s) used in this study was most comparable to site air temperatures estimated by MT-CLIM. Incident solar, relative humidity and precipitation trends were also not examined in this study, due to the lack of a sufficiently dense, spatially distributed observed dataset. Estimating spatial precipitation patterns with any accuracy is a significant and separate challenge currently being pursued by a number of investigators (Daly et al., 1994; Phillips et al. 1991; Thornton and Running, 1994).

MT-CLIM estimates daylight average air temperature using an assumption that the diurnal temperature trace approximately follows a sine form (Parton and Logan,

1981), with the maximum and minimum points provided by base weather station records (Running et al., 1987).

$$T_{avg} = TEMPCF \cdot (T_{max} - T_{min}) + T_{mean} \quad (3.3)$$

where T_{avg} is the weighted average daily temperature, T_{mean} is arithmetic mean $(T_{max} - T_{min})/2$ for the day, and TEMPCF is the coefficient (typically 0.45) used to adjust daylight average temperature (Running et al., 1987; Hungerford et al., 1989). This daylight average synoptic temperature is then corrected using an environmental lapse rate, resulting in a daily average air temperature measure for the site. Lapse rates used to parameterize the model runs in this study were estimated from observed temperature differences between the Santiam Pass (1460 m elevation) and Metolius (1027 m elevation) weather stations; a rate of 6° cooling per 1 km rise was used.

The site daily average air temperature is then corrected for slopes receiving different amounts of radiation loading, using a scale factor calculated as the ratio of sloped to flat absorbed solar radiation (Equations 3.4, 3.5). As a result, north slope temperatures are dampened, and south slope temperatures are given a boost. The LAI adjustment attempts to account for the way that sensible vs. latent heat energy is partitioned at the site. The original MT-CLIM site temperature algorithm was tailored to produce site temperatures that supported reasonable snow-melt dynamics within ecosystem process models (Nemani, pers. comm.). A T_{add} factor is added to the daily

average, environmental lapse-rate adjusted air temperature whenever the sites absorbed radiation load exceeds the radiation load for a hypothetical, flat slope equivalent at the same elevation (e.g. whenever the radiation ratio is ≥ 1.0):

$$T_{add} = R_{fs} \cdot (1.0 - (LAI/MLAI)) \quad (3.4)$$

where T_{add} is the factor in °C, added to the daily average synoptic temperature to produce the adjusted T_a estimate, R_{fs} is the ratio of flat to sloped absorbed radiation, LAI is the sites estimated leaf area index (LAI), and MLAI is the theoretical maximum leaf area index. Conversely, a T_{sub} factor is subtracted from the daily average air temperature whenever the ratio of flat to sloped radiation is less than 1.0:

$$T_{sub} = (1.0/R_{fs}) * (1.0 + (LAI/MLAI)) \quad (3.5)$$

here T_{sub} is the factor in °C subtracted from the lapse rate adjusted synoptic temperature to derive the estimate of T_a , R_{fs} is the ratio of flat slope absorbed radiation to the actual slopes radiation, LAI is the site leaf area index and MLAI is the theoretical maximum leaf area index for the site. Selection of one of these two correction subfunctions (T_{add} or T_{sub}) is determined solely by the absorbed radiation ratio calculated for the site. The expression used to set the air temperature is:

$$T_a = [T_{syn} - (\Gamma \cdot \Delta Elev)] + (T_{add} \text{ ..or.. } T_{sub}) \quad (3.6)$$

where T_{syn} is the synoptic air temperature ($^{\circ}\text{C}$), Γ is the environmental lapse rate ($^{\circ}\text{C}$ cooling per 1000 m rise), ΔElev

is the elevation difference

between the base weather station

the and site elevation/1000 (m),

and T_a is the final adjusted air

temperature ($^{\circ}\text{C}$). The T_{add} factor

is applied when the radiation ratio

is ≥ 1.0 , and the T_{sub} factor is

applied when the radiation ratio is

< 1.0 . The T_{add} and T_{sub} functions

each produce quite different functional responses. The T_{sub} adjustment function

generates a negative exponential response surface (Figure 3.3). The T_{add} adjustment

function produces a monotonically

increasing planer response surface

with increases in the R_r and

(LAI/Maximum LAI) ratios

(Figure 3.4). In the original MT-

CLIM code, there are no bounds

placed on either the T_{sub} or T_{add}

function values; the steeply rising

portion of the T_{sub} response surface

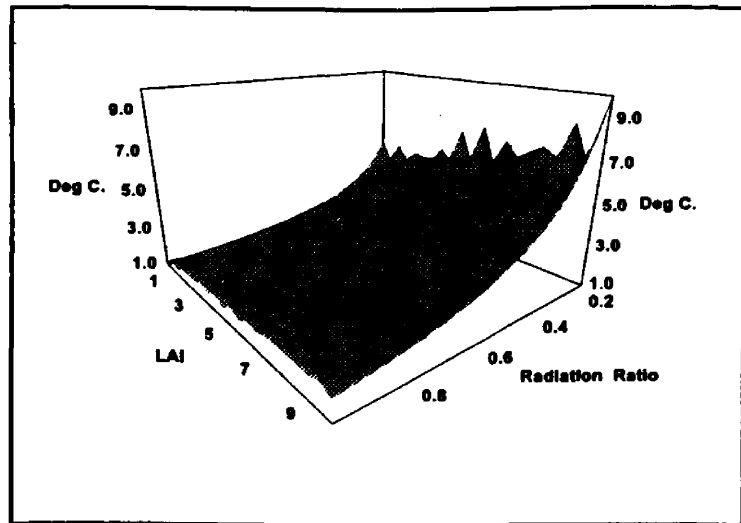


Figure 3.3 T_{sub} adjusted air temperature response surface, as a function of the flat-to-sloped radiation ratio and LAI/MLAI.

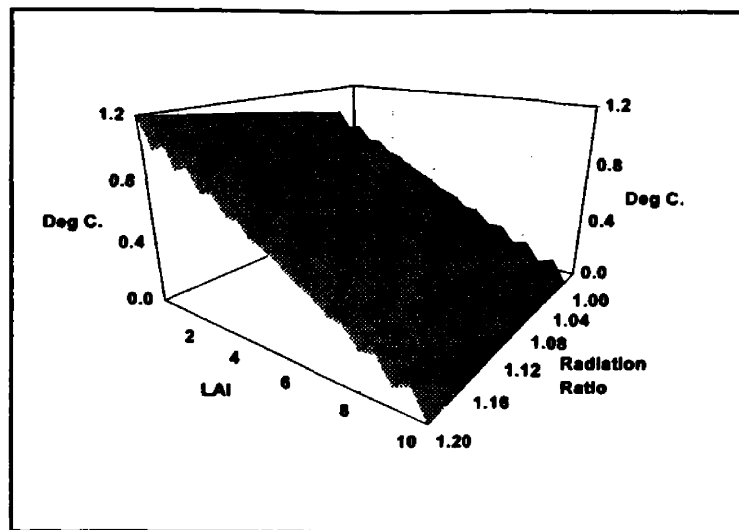


Figure 3.4 T_{add} adjusted air temperature function, showing planar response surface as a function of radiation ratio and (LAI/MLAI) ratio.

in Figure 3.3 indicates that artificially high temperature correction factors could inadvertently be applied with radiation ratios below ≈ 0.30 . The data from this study indicates the radiation ratios typically cluster about 1.0. Note that with average LAI/MLAI (0.4 to 0.6) and radiation ratios (≈ 1.0), the actual adjustment added or subtracted from the lapse rate adjusted air temperature is often only about 2-4 degrees, with the T_{sub} function somewhat more sensitive than the T_{add} function.

Description of the MTNTEMP Model

The original MT-CLIM model is defined strictly as a point based model and was therefore not well suited to the spatial and remote sensing orientation of this study. Consequently, a variant of MT-CLIM called MTNTEMP was developed to better address some of this studies characteristics. By point based, I refer to both the model's conceptual basis and to the way inputs are specified and introduced to the model. In a point based model, each "point" (or site) represents an independent entity that is modelled in isolation from all other points. Spatially connected models, on the other hand, explicitly treat the problem spatially by defining outputs for a given point as necessarily influenced by the values at neighboring points (Tomlin, 1990). Under this definition, MTNTEMP is still considered a point based model, though it does incorporate some attributes of spatially connected models such as reading and writing multiple raster data structures. The MTNTEMP model is written on top of (and is heavily dependent on) a larger science model application programming interface (API) currently in development¹. The

on the Sisters, Oregon 15" USGS topographic quadrangle, registering these points to the Universal Trans Mercator (UTM) rectilinear map projection with a false color composite image {digital channels 4,5,3} using ERDAS version 7.5 image processing software. The ARC/INFO GIS *project* command was used to translate the DMA registered in the geodetic projection to the rectilinear UTM (Zone 10) map projection. The NAD 27 datum and Clark 1866 spheroid were used as the geodetic reference. Gridded aspect and slope layers were derived from the digital elevation data layer using the ARC/INFO GIS GRID function *slope* and *aspect*. The elevation layer was coded in decimal meters ($890 \text{ m} \leq e \leq 1890 \text{ m}$), the aspect layer was coded in decimal degrees, $\{1 \leq a \leq 360\}$, and the slope layer was expressed as percent slope $\{1 \leq s \leq 100\}$.

To use the elevation, aspect and slope variables as grouping variables for partitioning the variation of T_s vs T_a , categorical proxy variables were developed using a linear contrast stretch (Lillesand and Kiefer, 1987) to level slice them into 6, 8, and 4 equal-width classes respectively. Partitioning the scene-wise variation of T_s and T_a into broader environmental classes enabled a more focused comparison of temperatures at pixels sharing underlying physiographic properties. Appendix 3.1 provides a statistical summary of these key study site variables. Random variates analyzed with parametric statistical methods should possess a linear rather than periodic scale; consequently, the aspect values originally in decimal degrees were transformed using a conversion function ($a' = \cos(a_r) + 1.0$) forcing all transformed aspect values positive (where a_r is aspect in radians, and a' is the transformed aspect, bounded by the range $\{0.0 \leq a' \leq 2.0\}$).

meteorology algorithms in the MTNTEMP model closely follow those in the original MT-CLIM model, with the exceptions of the new site temperature algorithm and the other minor changes documented in this paper. Appendix 3.3 lists the full input script files used to parameterize the model runs for this paper, and Appendix 3.4 details the major differences between MT-CLIM and the MTNTEMP model implementation.

MTNTEMP Model Inputs

The spatial nature of this study required a number of two dimensional data layers: elevation, slope, aspect, canopy closure fraction, albedo, and a relative solar loading raster. These were all spatially co-registered to the 10.8 km² study area. The MT-CLIM / MTNTEMP model logic employ a series of scalar initialization parameters for each "site" modeled, as well as a table of daily average climatological data from at least one weather station covering the temporal period modeled. Daily average climatology variables required by the MT-CLIM model in this table are: 24 hour daily average minimum and maximum temperatures (°C), and total daily precipitation (mm). The original MT-CLIM requires the following physiographic variables to be expressed as single values: elevation, aspect, slope, albedo, canopy closure, and relative solar loading. In this application, each of these vary spatially enough to warrant their definition as separate 2D data layers. A spatial resolution of 93.7 m was chosen for this study primarily to match the resolution of

¹ A complete description of the science model framework and API underlying the MTNTEMP implementation is beyond the scope of this paper. Technical documentation for this software is in preparation.

the elevation layer -- a 3 arc-second Defense Mapping Agency (DMA) digital elevation model. A variety of undesirable geostatistical artifacts appear in rasters derived from the DMA (e.g. slope, aspect, and relative solar loading) if the DMA is first resampled up to match the 20.3 m resolution of the Daedalus TMS data. To avoid these artifacts (i.e. lattice pattern noise) the 20.3 m Daedalus TMS scenes were each resampled to the DMA's 93 m original resolution using a bilinear convolution algorithm (via the *resample()* function) in the ARC/INFO GRID GIS. This resampling approach is more geostatistically defensible, although it did slightly smooth the original 20.3 m TMS scenes.

Due to the limited spatial extent of the study area (10.8 km²), a single nearby weather station was chosen -- the OTTER project Metolius weather station. Appendix 3.5 includes a statistical summary of the Metolius weather station data for 1990. Model runs for each of the three sample days (March 21, June 25, and August 13) evaluated the entire spatial extent of the study area on a (58 x 58) pixel by pixel basis for just these sample days.

Elevation and Derived Layers

Elevation data for the study site was extracted from the Bend West USGS 3 arc-second Defense Mapping Agency (DMA) digital elevation product. Georegistration of the Daedalus TMS imagery to the DMA was done using 15 ground control points located

Canopy Closure Layer

A site's collective canopy properties represent an important control on the energy balance and thus on the surface moisture and temperature regimes (Nemani et al., 1993). A number of studies have examined the relationships of remotely sensed spectra to various aspects of canopy structure. While some have concentrated on establishing associations between stand species composition and age structure (Leprieur et al., 1988), others have included an analysis of basal area (Peterson et al., 1986; Peterson et al. 1987), cover type (Dottavio and Williams, 1982), canopy closure (Butera, 1986) and soil thermal properties (Huete and Jackson, 1988). Several of these studies concluded that canopy closure fraction (percent of vertically projected coverage) may be directly or indirectly inferred from various Thematic Mapper channel combinations (Butera, 1986; Peterson et al., 1986) with reasonable precision. Butera (1986) found that TMS bands 1,5, and 7 proved most significant in relating forest percent canopy closure to spectral response. The investigators differed considerably on which bands or band conveyed the most information about stand structure, but most included the bands identified by Butera (1986).

Using this basic logic, a canopy closure (percent canopy fraction) classification image for the Black Butte study site was subjectively developed on the basis of a number of different TMS instrument bands. This classification was prepared using a supervised

maximum likelihood classification procedure (*maxlike*) contained in the ERDAS version 7.5 image processing software package. A discrete rather than continuous classification was developed because this approach met the general precision requirements of the application while approximately balancing the 93 m precision of the other data layers.

The goal of the classification was to divide a ratio level canopy closure variable, bounded by the range $\{0.0 \leq c \leq 100.0\}$ into one of five discrete classes of equal width, matching the USDA Forest Service traditional 5-class canopy closure classes (Pfister et al., 1977). Several different band combinations were evaluated for defining the canopy closure classification², including: Bands 4,5,3 from the August sample date, August Band 5 alone, Bands 4,5,3 from the June 25 sample date, and June Band 5. Color infrared (IR) photography ($\approx 1:62000$ scale) covering the study area was used to subjectively evaluate the quality of each trial classification. Ideally, field verification plots would be used to verify the classification but due to logistical problems this could not be done in this study. The resulting canopy closure class mid-points were: Class 1=0.01, Class 2=0.15, Class 3=0.38 Class 4=0.63, and Class 5 = 0.85. All visible and IR bands were terrain corrected using the trigonometric methods detailed in Smith et al. (1980). The classification based on the August TMS band 5 (1.55 - 1.75 μm) was judged as representing canopy closure best for this study area. Appendix 3.6 illustrates the canopy closure data layer used for all model runs.

² Note that the channel ID numbers used here refer to the subset of TMS channels retained from the original set of 12 as defined in Table 3.2.

Albedo Layer

An albedo data layer was developed by subjectively matching literature albedo values (Oke, 1987; Barry and Chorley 1992; Linacre, 1992) visually to the study site using color IR photography and the canopy cover classification mask layer described above. Albedo was defined as a spatial variable to avoid the potential bias resulting from the use of a single average albedo for the entire study area. Openings and scree patches were scaled to the higher albedos (0.40), while the densest canopies were given the lower albedos (0.11). While admittedly a coarse albedo classification, I felt it adequately balanced the precision of the other environmental gradient variables (slope, canopy closure, and elevation all resolved at 90 m). To investigate the relative sensitivity of (T_a) model output to changes in albedo, an informal sensitivity analysis was conducted. Seven trials were run with a baseline value of 0.15, and alternative albedo levels set increased and decreased by 5, 10, and 15 percent. The MTNTEMP model appeared to be only moderately sensitive to the range of albedo values felt to be present on the Black Butte study site ($\approx 0.11 - 0.40$).

Relative Solar Loading Layer

The term *relative solar loading* refers to the spatial partitioning of incident solar radiation on a site at a given pixel relative to its peers. It is calculated solely on the basis of the sites latitude, time of day and year, and the slope geometry (aspect and slope) derived from the digital elevation model. No microsite biophysical attributes are accounted for in this measure. A relative solar loading raster was prepared for each Daedalus TMS scene day -- March 21, June 25, and August 13 (Figure 3.5).

The method used to generate the relative solar loading images is the same as the method commonly used in GIS software to produce *shaded relief maps* ; it is based on light ray-tracing theory

(Burrough, 1986) The digital elevation model landscape is represented as if it were composed of a material of uniform reflectance illuminated from a user defined position in 3D space (Aronoff,

1989). Rather than positioning the illumination source -- in this case the sun-- at the "standard cartographic position" of 45° above the horizon in the northwest, the actual

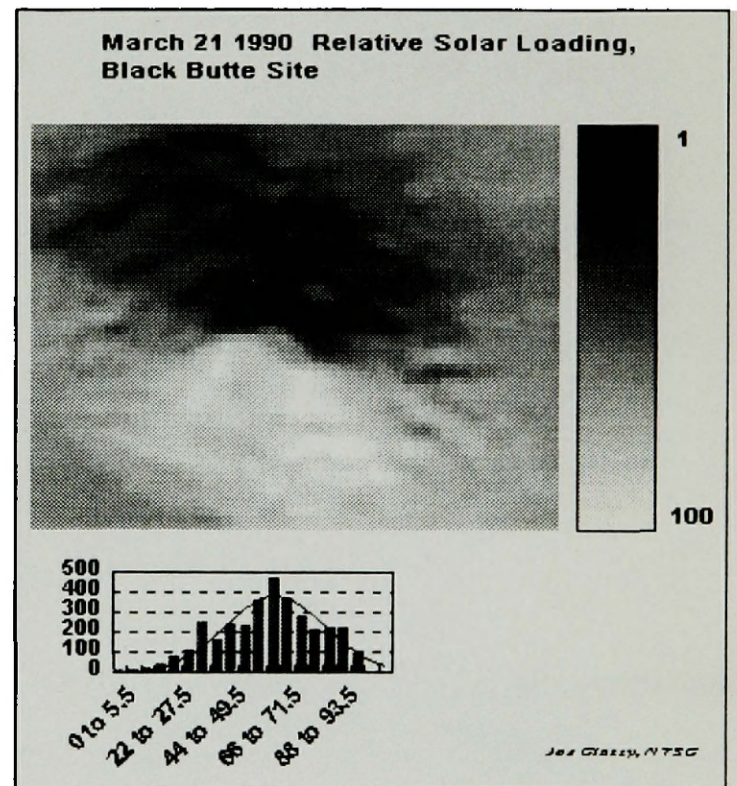


Figure 3.5 March 21 relative solar loading image showing the topographic distribution of the loading across the study area.

solar elevations and azimuths at the time of the three TMS sample dates (March, June, and August) were used. Solar zenith (90° - solar elevation angle) and azimuth angles (Table 3.1) corresponding to the study sample date were calculated using standard sun-earth geometry algorithms (Oke, 1987; Monteith and Unsworth, 1990).

The ARC/INFO GIS GRID function *hillshade* was used to produce the actual relative solar loading rasters. The result for each flight day was a byte encoded raster $\{0 \leq S_s \leq 255$, where S_s is the relative solar loading score} whose pixel values represented the hillslope solar loading "score" relative to the other pixels for that time and location. These scores were then stretched using a linear contrast algorithm to a numeric range of $\{1 \leq S_s \leq 100\}$. The resulting scores served as standardized weighting coefficients in the new site temperature estimation algorithm described later in this paper. Since both the flat-slope and sloped relative solar loading rasters were stored as byte encoded data products, the MTNTEMP software internally divided the values in the range $\{0 \leq S_s \leq 100\}$ by 100 to scale them to the final desired range, $\{0.0 \leq S_s \leq 1.0\}$.

Table 3.1: Sun-Earth Geometry Parameters Used To Generate Relative Solar Loading Images

Sample Date	Solar Elevation	Zenith Angle	Solar Azimuth	Flat Slope Score $0.0 < f < 1.0$
March 21	45°	45°	181°	0.640
June 25	59°	31°	123°	0.744
August 13	60°	30°	169°	0.742

Note: the *flat slope* scores shown above represent the incident solar radiation loading at a sites flat slope equivalent position.

Derivation of Surface Temperatures from TMS Imagery

The Daedalus TMS instrument, mounted on a NASA ER-2 high altitude aircraft provided the remote sensing imagery from which surface temperatures were derived (Figure 3.6). The normal operating altitude of the ER-2 jet aircraft is ≈ 20 km mean sea level (MSL) which generally results in a stable, distortion free signal. The TMS instrument is a 12 channel multispectral scanner supporting 8 bit radiometry with a spatial resolution of ≈ 25 m at nadir (Table 3.2). A total of

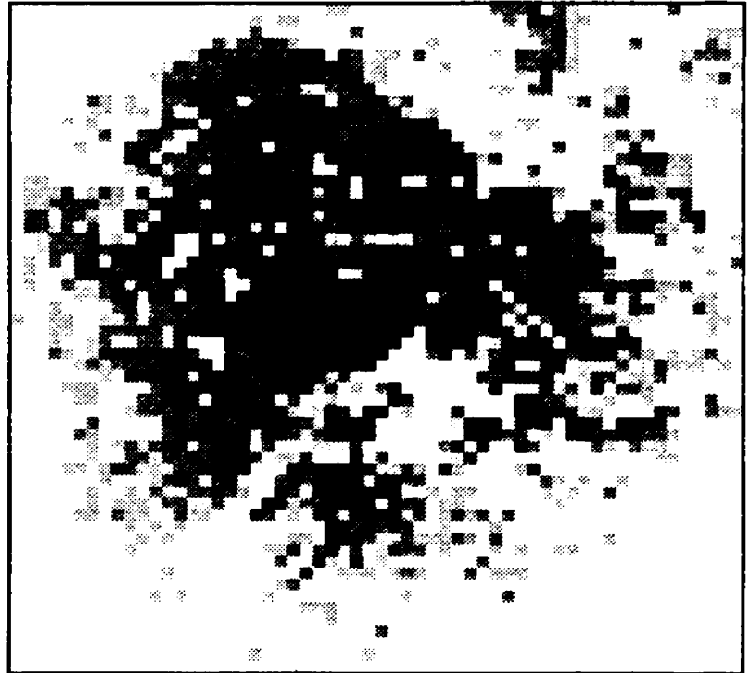


Figure 3.6 TIR (T_1) high gain thermal channel from the June 25, 1990 Daedalus TMS scene.

four Daedalus TMS scenes flown throughout 1990 were originally selected for this study: March 21, June 25, August 13, and October 19. Actual flight altitudes were 19,500 m, resulting in a measured actual pixel size of 20.31 m. The October 19 scene was subsequently disqualified after discovering corrupted at-sensor calibration data in the scene's line headers. Overflight times taken from the mission flight summary reports (at the center of the imaging swaths) were 12:18:00, 10:16:00, and 11:46:00 PST for the March, June and August scenes, respectively. The TMS instrument on the Daedalus package carries two separate thermal sensors, a low gain and a high gain unit, both

sensitive to wavelengths ranging from 8.5-14.0 μm . The low gain channel is useful if the high gain channel exhibits marked signs of saturation -- a right skewed distribution. Examination of histograms from both channels indicated no saturation in the high gain, so the high gain channel was selected to represent the surface temperature TIR signal. Only a subset of the original TMS channels were retained throughout the analysis, corresponding to those found on the satellite borne TM instrument (Table 3.2, rightmost column) For the remainder of this discussion, high gain TMS channel 12 is referred to as the TIR channel.

Thermal infrared (TIR) studies using the Daedalus TMS and similar instruments (Cooper and Asrar 1989; Price 1985) typically correct the signal for atmospheric attenuation effects (Price, 1983; Slater et al., 1987; Holbo and Luvall, 1989) to account for Rayleigh and Mie optical scattering (Campbell, 1987). Normally, radiosonde profiles from physically adjacent areas are required to supply appropriate atmospheric correction coefficients to a radiative transfer model such as LOWTRAN vers. 6.5 (Pierce and Congalton, 1988; Price 1983); these data are infrequently available for many remote areas, however, due to the expense and logistics of deploying them and maintaining the data. The source nearest to the Black Butte study area for radiosonde data was Salem, Oregon; this Willamette valley source was considered impractical for this study since it is on the west side of the Cascade range and experiences a considerably more maritime climate than does Black Butte. Consequently, the TIR dataset for this study could not be

atmospherically corrected due to the lack of optical depth data at the site for the overflight times.

TMS Channel	TM Equivalent	Wavelength μm	Spectrum	ID for bands retained in this study
2	1	0.45 - 0.52	Blue-green	1
3	2	0.52 - 0.60	green	2
5	3	0.63 - 0.69	red	3
7	4	0.76 - 0.90	near-infrared	4
9	5	1.55 - 1.75	mid infrared	5
10	7	2.08 - 2.35	mid infrared	6
11 lo-gain	6	8.5 - 14.0	far infrared (thermal)	
12 hi-gain	6	8.5 - 14.0	far infrared (thermal)	7

A software utility (TMSUTIL) written in the ANSI C language was developed to radiometrically correct the TIR channel of the Daedalus TMS scenes, converting this to atmospherically uncorrected surface temperatures (T_s) in $^{\circ}\text{C}$. TMSUTIL was used to retrieve the 50 byte header block of data on each image line containing the at-sensor calibration coefficients. These coefficients included two site and time-specific black body reference temperatures in $^{\circ}\text{C}$, and two black body radiance calibration coefficients.

Atmospherically uncorrected surface temperatures were generated by fitting each pixel, $t_{i,j}$, to the scaling equation (Pierce and Congalton, 1988) shown below:

$$t_{i,j} = \left[\frac{(bt_2 - bt_1)}{(br_2 - br_1)} \right] (dn_{i,j} - br_1) + bt_1 \quad (3.7)$$

where $t_{i,j}$ is the calculated temperature of a pixel ($^{\circ}\text{C}$) at row i , column j of the image, bt_1 and bt_2 are the first and second black body reference temperatures ($^{\circ}\text{C}$), respectively, br_1 and br_2 are the first and second black body radiance counts, respectively, and $dn_{i,j}$ is the reflectance data number (DN) for a pixel at row i , column j of the image.

Description of the new MTNTEMP model air temperature algorithm

The new site temperature algorithm described here separately accounts for two kinds of environmental controls on air temperature -- percent canopy closure, and topographic effects. Somewhat similar in overall logic to the original method, it is based on two dimensionless indices that integrate potentially complex microsite interactions. The method trades off some precision for ease of parameterization, and neglects any treatment of katabatic and valley winds, cold air drainage, or advection. Its underlying conceptual basis assumes that the two integrating indices (canopy cover fraction to represent overall canopy influences, and relative solar loading to treat topographic influences) adequately encapsulate the aggregate influences of the underlying phenomena.

At best, this simplistic empirical-statistical approach is only an evolutionary advance relative to the original formulation. Since its application is currently limited to the spatial application of this study, it could probably be improved with more experience and testing under wider conditions.

The new site temperature method works by adjusting a daily average synoptic air temperature on the basis of two separate, algebraically summed temperature factors. The first is a canopy closure influence factor, and the second is a topographic influence factor. The sign of the separate canopy and topography adjustments may be positive or negative so they are able to counteract each other. In northern temperate ecosystems, vegetation on a given site (and thus canopy structure) is only indirectly related to its diurnal radiation loading. As a broad generality, the moisture and edaphic regimes on warmer, drier aspects tend to favor more open canopy, shade intolerant species (e.g. Ponderosa pine communities on this site), versus the typically denser coniferous stands (Douglas fir, grading to Alpine fir and Spruce at the higher elevations) on less exposed and more mesic microsites. This phytosociological heuristic is routinely contradicted in the field, however, due to stand influences that collectively override these "expected" associations (e.g. local fire and pathogen history, local seed dispersal patterns, anthropogenic effects, etc). The original site temperature method based the addition or subtraction adjustment to the synoptic temperature entirely on the sites radiation ratio; the new site temperature formulation described here consciously departs from that logic by adopting a more numerically continuous scaling logic. The algebraic sum mechanism used here allows the

two generalized influences (canopy and topography) to act more independently, and provides for more subtle gradations in the combined influences. The final form of the algorithm is:

$$T_a' = [T_{syn} - (\Gamma \cdot \Delta Elev)] + (T_c + T_t) \quad (3.8)$$

where T_a' is the estimated daily average site air temperature, in °C, T_{syn} is the synoptic daily average (in °C), Γ is the lapse rate °C cooling per 1000 m rise), $\Delta Elev$ is the change in elevation from base weather station to site (m), T_c represents the net gain or loss in temperature (in °C) attributed to the sites percent canopy closure, and T_t represents the net gain or loss in temperature attributed to the sites combined topographic (aspect, slope) attributes. The separate scaling terms, T_c and T_t , in Equation 3.8 emphasize that the net adjustment as an algebraic sum represent two *potentially compensatory* effects. The temperature correction term, T_c , due to canopy closure is defined as:

$$T_c = T_{\infty} \cdot [(1 - GC_{r,c}) - (1 - \tau)] \quad (3.9)$$

where T_{∞} represents a maximum theoretical temperature by which the simple lapse rate adjusted temperature may be expected to vary as a function of the sites combined percent canopy closure and topography (slope, aspect) influence. $GC_{r,c}$ is the percent canopy closure (ground cover) coefficient $\{0.0 \leq GC \leq 1.0\}$ at the site (e.g. pixel at raster address row, column), and τ is an optional, user assigned percent canopy closure value above

which the algorithm actively dampens the synoptic temperature, rather than providing a (weak) positive boost inversely proportional to its magnitude. This term was set at 0.70 for all analyses in this study. To specify no canopy dampening effect, τ may be set to 1.0. The T_t term represents the (signed) temperature influence ($^{\circ}\text{C}$) attributed to differences in topography (aspect, slope) between the site and the base weather station(s):

$$T_t = T_{\infty} \cdot (S_s - S_f) \quad (3.10)$$

where S_s is the sloped relative solar loading score, scaled to the range $\{0.0 \leq S_s \leq 1.0\}$, S_f is the flat slope relative solar loading score $\{0.0 \leq S_f \leq 1.0\}$, and T_{∞} is defined as above. A cursory look at the statistical characteristics and boundary performance of the new algorithm suggests that it produces reasonably well distributed dependent terms over the range of values in the independent term (Figure 3.7).

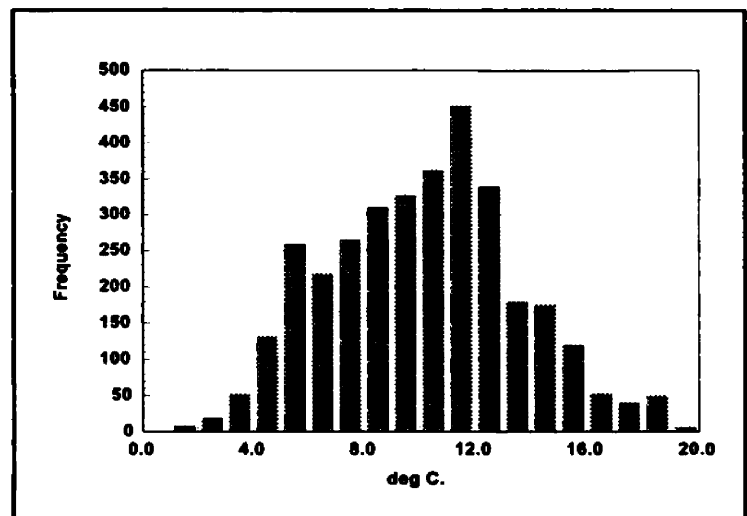


Figure 3.7 Histogram illustrating the unimodal distribution of the air temperature adjustment ($T_{syn} - T_a$) resulting from the new site temperature algorithm.

An important criteria in designing scaling algorithms is that the dependent terms should exhibit statistical properties and a variance structure closely approximating those of the measure modelled. The binary decision logic used in the original site temperature algorithm that adds or subtracts a factor (e.g. T_{add} , T_{sub} in

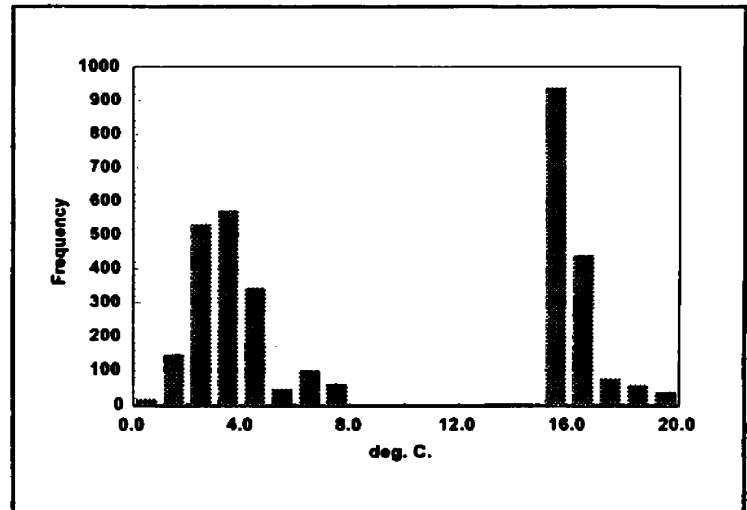


Figure 3.8 Histogram illustrating the bimodal distribution of the air temperature adjustment ($T_{syn} - T_a$) resulting from the original site air temperature algorithm.

Equation 3.6) from the lapse rate adjusted air temperature results in an undesirable bifurcated statistical distribution (Figure 3.8). The degree of bifurcation occurs roughly in proportion to the kurtosis of the adjustment factors distribution. The additional noise added by the correction mechanism is probably not attributable to the underlying phenomena it represents. In contrast, the weighting scheme using in the new site air temperature algorithm produces a more unimodal, continuous response pattern (Figure 3.7) that eliminates the discontinuous, step function "noise" introduced by the original methods bimodal distribution.

Development of the Canopy (T_{∞} and τ) Temperature Adjustments

The T_{∞} temperature scaling factor represents an idealized maximum temperature (in °C) about which the synoptic temperature might be expected to vary due to changes in

percent canopy closure and topographic variables (aspect, slope) relative to the base weather station. Although two T_{∞} factors could have been separately defined for the canopy and topography influences, I choose this more streamlined approach acknowledging that over-precision here would probably be artificial. In practice, the magnitudes of the temperature differentials attributed to canopy and topography influences are controlled by complex, instantaneous energy exchanges on the site that are very difficult to precisely parameterize within time-averaged methods (McNaughton and Jarvis, 1983). To establish an initial "best guess" estimate of T_{∞} for each of the three sample dates, I performed a linear optimization analysis³. The solution criteria (e.g. the objective function) was set such that the coefficient of determination, r^2 , was maximized for a pairwise examination ($N=3364$) of T_a vs remotely sensed T_s for each of three sample days (March 21, June 25, August 13). The solution converged after only a few iterations for each sample (Table 3.3).

The method used to set T_{∞} should eventually be expressed in terms of commonly available climatological parameters (e.g. 24 average T_{\max} , T_{\min}) since it is obviously impractical to perform an optimization analysis with each model run.

³ The linear optimization was performed using the QuattroPRO/Win version 5.0 software package.

Sample Date	"Optimum" T_{∞} Factor, °C	T_{∞} (in °C) using heuristic model.
March 21	6.98	8.41
June 25	10.05	8.56
August 13	12.66	12.70

where:
the "optimum" factor was determined using an empirical, linear optimization method,
and the "heuristic" factor was determined using Equation 3.11..

As an illustration and a simplistic first approximation, I fit a linear function using T_{∞} as the dependent term, and the daily temperature amplitude ($T_{\max} - T_{\min}$) as the independent term for each the three sample dates available to the study. The simple straight line function relating T_{∞} to the daily observed temperature amplitude did agree with the basic trend of the "optimum" T_{∞} value, but it must be emphasized that this crude function should *not* be interpreted as a "regression" equation since the sample size is ridiculously small (the *df* for 3 samples is only 1). The heuristic correction function was:

$$T_{\infty} = -0.47 \cdot (T_{\max} - T_{\min}) + 18.83 \quad (3.11)$$

The applicability and sensitivity of this heuristic for assigning T_{∞} was not tested in this study due to the small (seasonal) sample size. It is reported here only to illustrate

how the "optimum" T_{∞} factors determined here might eventually be related to common available (daily) meteorology variables. Further analysis is obviously needed to refine this approach, where additional controls on T_{∞} beyond daily temperature amplitude could also be evaluated. In the MTNTEMP software, the function used to assign the T_{∞} factor (Equation 3.11) may be overridden at runtime by a site-specific value. The determination of T_{∞} is somewhat complicated by the fact that synoptic air temperature adjustments are based on *relative differences* between base weather station(s) and the site of interest. Linacre (1992) suggests that "...the pattern of (weather) stations should be most dense in the direction of right angles to 'isopleths' of contour, rainfall, temperature..." and further that "...the climate station should be located on level, open ground with a clear horizon, and not be in a hollow or on a steep slope". These criteria theoretically arise from the requirement to establish reliable long term, statistically comparable climatological records.

In practice, field experience indicates that many NWS and USDA Forest Service weather stations are indeed located in canopy openings, meadows, or fields. These stations probably yield temperature readings comparable with more "open" canopy conditions. Though the actual instrument enclosures (i.e. Stevenson screen) must be shaded and include fans to circulate the air in the enclosure (Oke, 1992; Furman and Brink 1975), these valley bottom sites often have weakly defined aspects and slopes. If the base weather station(s) used to parameterize MT-CLIM possesses either weakly defined or unknown topography (e.g. sited on essentially flat, openings), a correction

logic based on *relative* topographic differences rests on somewhat ill-defined premises. I suspect that at least part of the expected error in MT-CLIM temperature estimates originates in this uncertainty. Linacre (1992) goes on to infer that canopy geometry (in particular, percent canopy closure) may represent a more important control on air temperature than traditional topographic gradients per se; this notion is corroborated by a study on surface moisture status (Nemani et al., 1993) and by the author's field experience.

I felt that the lapse rate adjusted temperatures ($T_{syn} - \Gamma \cdot \Delta Elev$) values on average did not represent a symmetric middle "balance point" about which a boost or dampening factor might be evenly distributed, due to the common practice discussed above of locating weather stations in openings and meadows that represent more "open" canopy conditions relative to radiation loading and microsite ventilation. The assumption here is that the siting policy for locating weather stations (even accounting for buffering by the Stevenson screen) could favor slightly "warmer" recorded temperatures than might actually occur. The $(1-\tau)$ term in equation 3.9 is an optional, user assigned percent canopy closure value above which the algorithm actively dampens the synoptic temperature. By definition, weighting functions of the form $w = a(1-x) : \{0.0 \leq x \leq 1.0\}$ return only positive results. Including the $(1-\tau)$ term in this algorithm allows it to return *weighted negative values* ($^{\circ}C$) in proportion to the difference between τ and GC when ground cover (GC) values meet or exceed those of τ . The net effect of this term is to allow increasingly closed canopies to weakly suppress the resulting T_a in proportion to the

amount of closure. Consequently, for all model runs the τ coefficient was assigned a value of 0.70. This has the effect of shifting the in-situ distribution of T_c slightly downward. The τ parameter is set to 1.0 to specify no explicit canopy dampening effect; this is the MTNTEMP software default. I have not yet, however, performed a separate analysis of T_a sensitivity to relative changes in the τ parameter.

Development of the topographic temperature adjustment

The topographic adjustment term, T_t , is defined on the assumption that slope and aspect driven attenuation of air temperature (T_a') can be adequately represented by a single integrating index. This index is the simple difference between the sites (sloped) relative solar loading, scaled $\{0.0 \leq S_s \leq 1.0\}$ and a hypothetical *flat slope* equivalent solar loading score, also scaled $\{0.0 \leq f \leq 1.0\}$. T_t is thus defined by multiplying the T_∞ factor by the difference between the sites sloped (S_s) and flat slope (S_f) relative solar loading scores. The "flat slope" solar loading scores were generated from the same algorithm as the sloped solar loading score, except that a value of "0.0" was input as the site slope, negating any aspect effect. The algebraic difference of the sloped minus the flat-slope equivalent relative solar loading score (Δ), scaled to the range $\{1 \leq \Delta \leq 100\}$ was then assigned as the normalized solar loading score for each pixel. The *difference* between the flat and sloped relative solar loading scores was used rather than just the sloped relative solar loading to better account for the full heterogeneity in the loadings.

Analysis Design

One set of MTNTEMP model runs were defined to evaluate the original MT-CLIM site temperature algorithm for each of three TMS scene sample dates (Table 3.4) and one set for evaluating the new site temperature algorithm for the three samples. Note that since leaf area index (LAI) was not determined for the Black Butte study site, the ratio of canopy closure to maximum canopy closure was substituted as a surrogate for the (LAI/MLAI) term in the original MT-CLIM site temperature T_{add} (Equation 3.4) and T_{sub} (Equation 3.5) adjustment functions. As a point based model, the original MT-CLIM was not equipped to accept input parameters on a distributed spatial basis. MTNTEMP addresses this limitation through its ability to read and write spatial data layers in their native ERDAS v.7.5 or IDRISI 4.1 image formats. Input variables that significantly varied on a spatial basis (albedo, canopy cover, relative solar loading, elevation, aspect, and slope) were therefore maintained as single band, 8 or 16 bit image raster files, eliminating the need to maintain redundant, intermediate generations of the imagery. Each MTNTEMP run was defined on the basis of a unique input data mix that included the standard scalar inputs and the set of 58 x 58 (93.8 m pixel resolution) rasters listed above.

Table 3.4: MTNTEMP Model Run Matrix

"Baseline": used original MT-CLIM site temperature algorithm: $T_a = f(\text{radiation ratio, canopy closure})$		"New Method": used new site temperature algorithm, $T_a = f(\text{canopy closure, relative solar load})$	
Stratification Level	Samples:	Stratification Level	Samples
(none - unstratified)	March, June, August	none - unstratified	March, June, August
Between Class (partition wise averages)	March, June, August	Between Class (partition wise averages)	March, June, August
Within Class	March, June, August	Within Class	March, June, August

Appendix 3.3 lists the full set of inputs used for all model runs. The output from each MTNTEMP model run consisted of a database table (in xBASE⁴ ".dbf" format) with one record per pixel, with each requested output variable in a database field. Appendix 3.7 shows a database table structure list of a typical MTNTEMP output database table. The database output table scheme was adopted primarily due to convenience for subsequent statistical analysis. Each database record included the raster cell row and column index, allowing all spatial variables to be grouped into a single geocoded file. For preliminary trial runs, single band raster images (of T_a and/or T_s) were also output in ERDAS v.7.5 or IDRISI 4.1 GIS formats for visual verification of model results (Figure 3.9).

⁴ The term "XBASE" used here refers to the generic collection of database management software packages conforming to the binary database table format originally developed by the Ashton-Tate Inc. dBASE specification.

The temperature data layers, T_a and T_s , were maintained as continuous, ratio level variables. A number of ratio level variables were chosen as candidate categorical variables on the basis of their

perceived influence on temperature processes: elevation, slope, aspect, relative solar loading, and canopy closure fraction. Each of these variables was level sliced using a standard linear contrast stretch algorithm (Lillesand and Kiefer, 1987). As a categorical variable, aspect was divided into eight (45° arc) classes, slope into 4 classes,

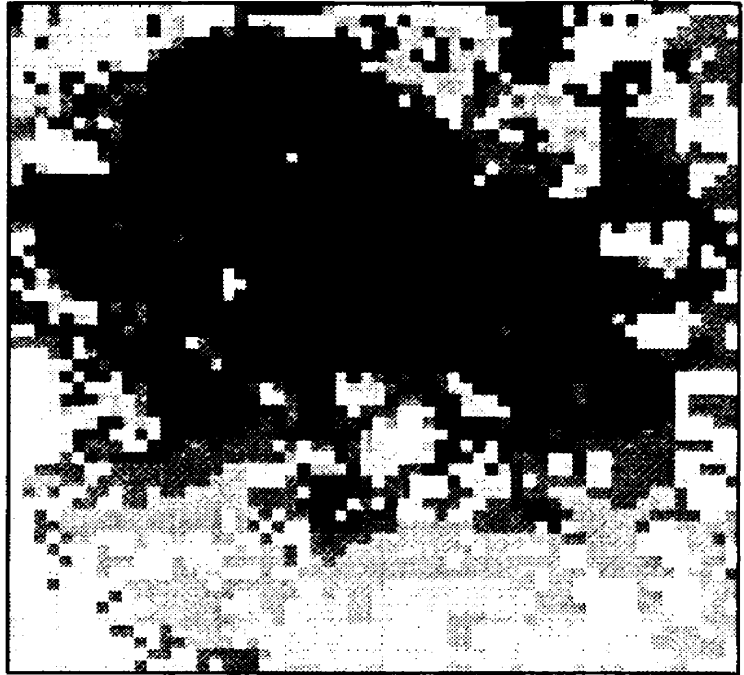


Figure 3.9 Example of the T_a output verification raster produced for the August 13 1990 sample using the new site temperature algorithm.

with canopy closure and relative solar loading each divided into 5 equal width classes. These class breakdowns were then used as discrete indexes for statistical sample partitions.

The justification for partitioning T_a and T_s came after an examination of the distributions and variance structure of individual T_a and T_s values, and unstratified T_a vs. T_s correlation trends ($N=3364$). I felt that if the population was partitioned using categorical variables controlling much of the temperature variation, more relevant comparisons between the T_a and T_s trends could be made. This assumption was tested by

performing a series of one way analysis of variance using SPSS ONEWAY tests (Norusis, 1993), setting the T_s variable as the dependent term and each of several candidate categorical variables (slope, aspect, elevation, canopy closure, relative solar load, and incident shortwave solar radiation) as the independent terms. Using a Scheffe's multiple comparison range test at the $\alpha=0.05$ level, a significant number of these variables thus categorized had significantly different classwise means. This is the same basic experimental design logic used when performing stratified random sampling (Levy and Lemshow, 1991; Ott, 1977).

MTNTEMP model T_a outputs were statistically compared with T_s using several analytical approaches. The primary statistical hypothesis tested was: H_0 "there is no positive correlation between predicted T_a and observed T_s " at the $\alpha=0.05$ significance level, vs. H_a : "there is a positive correlation between T_a and T_s ". The correlation hypothesis is tested via a standard F-statistic at the $\alpha =0.05$ level (Wonnacott and Wonnacott, 1977) and is somewhat analogous to a standard equal-means hypothesis test, $H_0: \mu T_a - \mu T_s = 0$, (e.g. no statistically significant difference exists between mean predicted T_a and mean observed T_s estimates). For further diagnostic purposes, a series of linear regressions of T_a vs. T_s were run, producing model slope, intercept, r^2 , as well as the F-statistic described above (95% confidence level). Statistical analyses were conducted using the SPSS version 5.02 and 6.0 statistical software packages and custom FoxPRO database routines.

Pooled Comparisons

Pooled (e.g. unstratified) regressions of dependent (T_a) vs independent (T_s) variables were calculated by considering all pixels in the (58·58) pixel study area (N=3364) as a single population. The analysis was repeated for the three 1990 sample days (March 21, June 25, and August 13) using both the original MT-CLIM site temperature algorithm (Equation 3.6) and the new MTNTEMP site temperature algorithm (Equation 3.8). The regression model coefficients and error estimates listed above were calculated for each trial. While this type of comparison provided the benefit of illustrating the T_a and T_s trends across the entire study area, the environmental causes of the (considerable) temperature variation across the area were essentially ignored by this pooling.

Across-Category Comparisons

To examine the relationships of T_a vs. T_s across different pairs of environmental gradients, partition cell averages of the T_a and T_s values were regressed

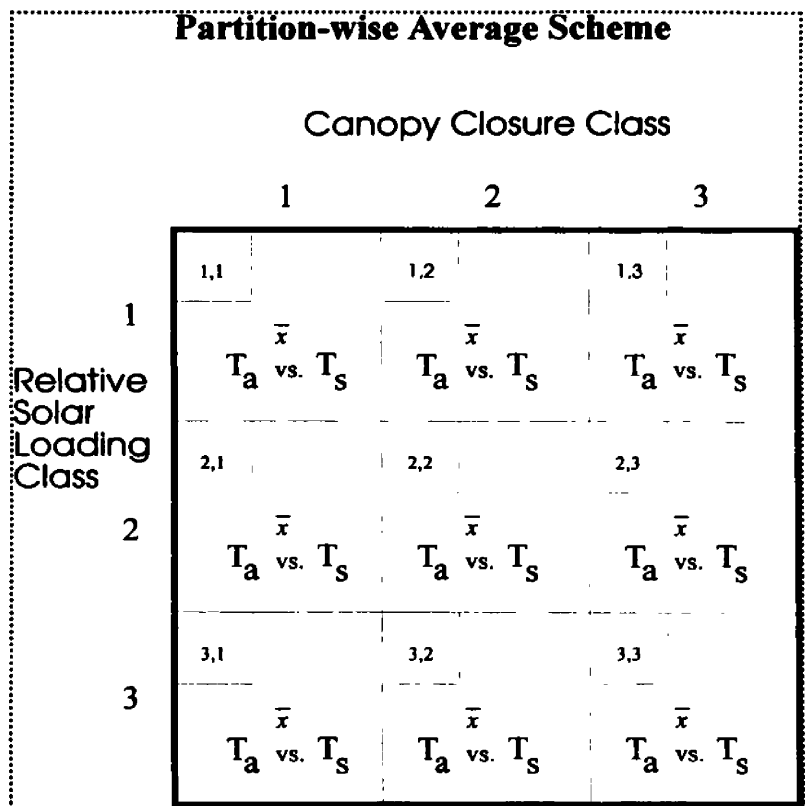


Figure 3.10 Defining T_s vs T_a as partition cell-wise averages represents variation in a partition cell as a single value; in this example, 9 pairs of temperatures would be regressed.

against each other. This sample partition scheme is illustrated here for a hypothetical 3x3 matrix of category pairs (Figure 3.11). The environmental category pairs were chosen on the basis of how they represented continuums in temperature variation. Category variable pairs examined were: {canopy closure class and relative solar loading class}, {elevation class and aspect class}, and {aspect and slope class}. The across-category partition scheme resulted in regressions whose degrees of freedom (*df*) equaled the products of the numbers of classes between the two categories, while there were sufficient numbers of pixels (e.g. ≥ 5) in the given partition cell (e.g. "...Partition on aspect classes (8 levels) and elevation classes (5 levels), to yield a sample size of $N=40$ pairs of T_a vs. T_s ..."). While this approach tended to dramatically reduce the regression sample size, it also provided a helpful look at the T_a vs. T_s trends across broader environmental gradients. Note that in some cases, the *df* shown in the results section below is slightly less than this product; this is due to some partition combinations being excluded due to too small (≤ 5) a sample size.

Within-Category Comparisons

In this stratification scheme, raw T_a vs. T_s values for several category pairings were regressed. The same categorical variable pairings were defined as described above for the across-category comparisons. This analysis approach attempted to address the question: "how well do T_a and T_s correlate *within* more narrowly defined environmental gradients (e.g. "...regress all the T_a vs. T_s . (pixels) sharing membership in aspect class 4

and slope class 3", or, "...regress all T_a vs. T_s . pixels in canopy closure class 5 (85% closed) and relative solar class 5"). This analysis also indirectly tests how well a given pair of grouping variables (e.g. {elevation, aspect} or {canopy closure, relative solar load}) partitions the natural variation in hillslope temperatures. Again, the assumption was that if the categorical variables partitioned the variance well, regression datasets constrained to these sub-populations should yield more actual information about the underlying relationships and spatial trends. Output from this analysis consisted of a series of linear models and error coefficients, one for each unique combination defined by the joint categorical class values. Since a separate model was generated for each unique partition cell (e.g. 40 linear models for the (8) aspect and (5) slope class pairing) this made a classic model-by-model interpretation of the output somewhat cumbersome. These results are consequently reported using 3D "pseudo" surfaces where the model coefficient of determination (r^2) is shown on the Z axis, and the two category class variables form the X and Y axes. These are "pseudo" surfaces because the surfaces were interpolated from a series of discrete independent "points", where each regression model represents one point on the surface. They are thus meant to convey a more qualitative than quantitative illustration of the "best" and "worst" correlations of T_a vs. T_s across the selected environmental gradient space.

Multiple Regressions

The T_a air temperature variable is of course driven by more than just surface temperature. To examine the relative contribution made to the relationship by different environment variables (in ratio level form) several forward-stepwise multiple linear regressions were run using SPSS (Norusis, 1993). Surface temperature (T_s), canopy closure fraction, elevation, percent slope, and transformed aspect (cosine of aspect+1) were set as the independent terms, and T_a was set as the dependent term. The surface temperature (T_s) term was forced into the equation first since I was most interested in the contribution of this term to the model. Again, these models were developed more for their diagnostic value than as traditional descriptive models, to help assess the relative contribution of each independent term in explaining the total variation in the relationship. Model coefficients, significance statistics at the $\alpha=0.05$ confidence level, and r^2 coefficients of determination are reported for these multiple regressions to further test the new method for estimating site temperature.

Results and Discussion

Pooled and Across-Category Partition Results

The topographic validation was performed with two major sets of MTNTEMP model runs: a baseline run using the original MT-CLIM site temperature algorithm, and a "new method" run with the new site air temperature algorithm. These are hereafter referred to as the "original" and "new methods" runs. Linear regressions of T_a vs. T_s for the "original" run with all pixels pooled (e.g. unstratified) were only moderately conclusive (r^2 of 0.60, 0.25 and 0.42 for the March, June, and August samples respectively). This is at least partly a function of sites with very different environmental qualities being pooled into the same analysis population, and due to the diminished temperature amplitude resulting from use of the T_{add} (Equation 3.4) and T_{sub} (Equation 3.5) functions. As discussed earlier in this paper, expressing T_a solely as a function of T_s is a gross over-simplification of the underlying physics; this simplified analysis does however provide a useful view of the relative shifts in the relationships. When partitioned by selected pairs of topographic/canopy variables, the strength of the basic relationships consistently improved (Table 3.5). Linear regressions of T_a vs. T_s for the pooled sample "new methods" resulted in consistently better relationships (r^2 of 0.69, 0.56, and 0.83 for the March, June and August samples respectively) than those obtained using the original air temperature estimation method. Partitioning by topographic and

canopy variables improved the relationships still further (Tables 3.5, 3.6) for both the original and new air temperature methods. F statistics for all regressions were significant at the $\alpha = 0.05$ level or better, and the null hypothesis of equal mean Y' terms (predicted T_a vs. observed T_s) was rejected at the $\alpha = 0.5$ level for all sample dates and both site temperature estimation methods.

Of the three samples, regression models from the June sample consistently reported the weakest relationships between T_a and T_s , regardless of how or if the samples were partitioned along environmental gradients, or whether the original or new method site temperature algorithm was used. This general effect is probably due to the domination of the λE term in the Bowen ratio associated with the lush spring/early summer green up pattern and higher moisture levels on site. Conversely, the August sample regression models were consistently more definitive, also showing improvement from the new site temperature algorithm method vs. the original method. At this point in the season, the higher Bowen ratios associated with warmer, drier conditions resulted in a closer coupling of T_a with the energy budget and thus with T_s . Regression model slopes were generally lower and y intercepts higher for the original method (pooled) regressions, indicating more diffuse relationships in T_a vs. T_s across all sample dates. This was likely due to the relative lower temperature amplitudes resulting from the original methods flatter response characteristics at radiation ratios close to 1.0 (Figures 3.3 and 3.4). Slopes for the across-category partitioned models varied from about 0.23 to 0.52, with the higher slopes associated with the June sample.

Table 3.5: Original Method Run Regression Results For Pooled and Across-Category Partitioning							
Sample	Control Variable 1	Control Variable 2	N	R ²	Model Slope	Y Intercept	Y' Std Error
March	Pooled (Unstratified)		3364	0.609	0.252	6.0316	1.071
	Elevation	Aspect	47	0.769	0.358	4.2229	1.002
	Closure	Rel Solar	17	0.704	0.242	5.5418	0.970
	Aspect	Slope	28	0.861	0.386	4.0045	0.659
June	Pooled (Unstratified)		3364	0.257	0.208	12.070	1.508
	Elevation	Aspect	47	0.457	0.455	5.390	1.573
	Closure	Rel Solar	17	0.525	0.224	10.768	1.029
	Aspect	Slope	28	0.731	0.521	4.321	0.940
August	Pooled (Unstratified)		3364	0.414	0.231	15.891	1.291
	Elevation	Aspect	47	0.549	0.394	10.440	1.360
	Closure	Rel Solar	17	0.666	0.231	15.580	0.939
	Aspect	Slope	28	0.873	0.412	10.490	0.600

Samples: Jun =June 21 TMS flight, Mar =March 25 TMS Flight, Aug =August 13 TMS flight
Control Variable 1 is the first categorical variable.
Control Variable 2 is the second categorical variable.
Y' Std Error is the standard error of the model dependent variable
All regression model slopes and y intercepts were significant at the $\alpha=0.05$ level.

The y intercept of these T_a vs T_s linear models may be generally interpreted as the influence of the numerator term of the Penman-Monteith equation (Monteith and Unsworth, 1990) -- the contribution to the relationship essentially due to atmospheric forcing. Y intercepts varied from 4.2 to 15.0 °C for the original method models, with standard errors for the predicted terms varying closely about 1.0. Higher y intercepts between the T_a and T_s represent differences at lower surface temperatures driven by underlying environmental conditions.

Table 3.6: New Method Regression Results from For Pooled and Across-Category Partitioning							
Samples	Control Variable 1	Control Variable 2	N	R ²	Model Slope	Y Intercept	Y' Std. Error
March	Pooled (unstratified)		3364	0.693	0.372	4.761	1.314
	Elevation	Aspect	47	0.826	0.448	3.526	1.051
	Closure	Rel Solar	17	0.745	0.472	3.525	1.706
	Aspect	Slope	28	0.869	0.561	1.858	0.927
June	Pooled (unstratified)		3364	0.564	0.561	3.194	2.040
	Elevation	Aspect	47	0.829	0.972	-7.161	1.399
	Closure	Rel Solar	17	0.891	0.948	-7.415	1.598
	Aspect	Slope	28	0.880	0.950	-6.384	1.042
August	Pooled (unstratified)		3364	0.827	0.727	0.798	1.558
	Elevation	Aspect	47	0.904	0.904	-4.576	1.119
	Closure	Rel Solar	17	0.970	0.847	-3.388	0.927
	Aspect	Slope	28	0.950	0.922	-4.981	0.804
<p>Samples: Jun =June 21 TMS flight, Mar =March 25 TMS Flight, Aug =August 13 TMS flight Control Variable 1 is the first categorical variable Control Variable 2 is the second categorical variable Y' Std Error is the standard error for the models dependent variable, T_a All regression model slopes and y intercepts were significant at the $\alpha=0.05$ level.</p>							

Partitioning across-categorical variables tended to increase the regression slopes, decrease the y intercepts, and lower the standard error of the predicted terms relative to the pooled analyses. These effects are partly due to the apparent reduction in variance gained by averaging the T_a and T_s pixels on a partition cell-wise basis. Of course, the

intrinsic variance in these models is still present so the reduction is only apparent, masked somewhat through the expression of the raw regression data points as averages. These regression models are useful more in a diagnostic sense than as

prescriptive models, providing a relative comparison between the

original and new methods and between sample dates. The generally improved correlations between T_a and T_s for both the unstratified and stratified analyses suggests that the new dual-weighted canopy closure and relative solar loading scheme could possibly represent the underlying spatial air temperature dynamics somewhat better than the original scheme.

For the "new site air temperature method" regression

models, slopes were generally higher, with lower y intercepts across the board for the new

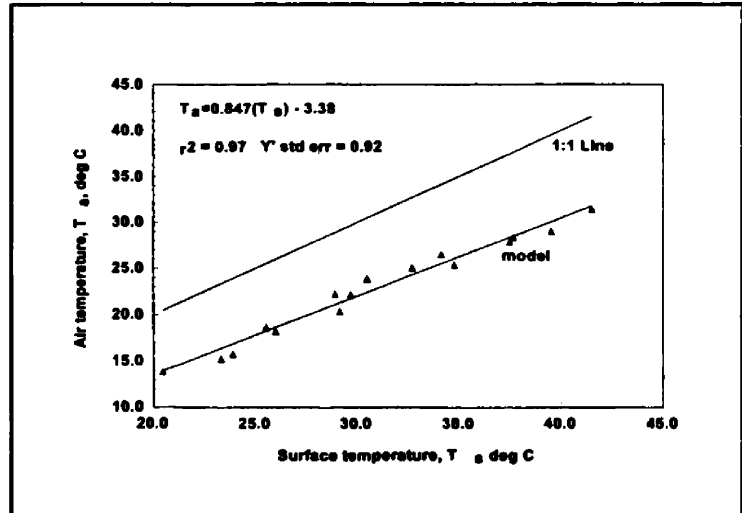


Figure 3.11 Scatterplot and regression model for the {Canopy Closure, Relative Solar Loading} cross-category partition for the August, 1990 sample using the new site air temperature algorithm.

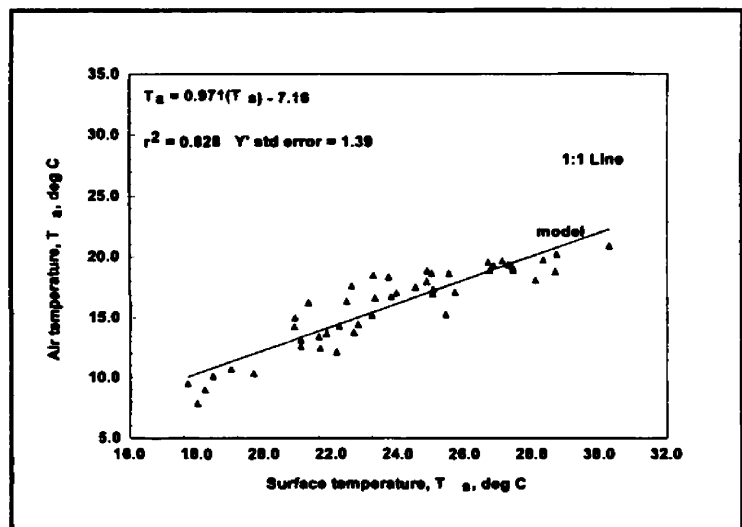


Figure 3.12 Scatterplot and regression model for the {Elevation, Aspect} cross-category partition for the June 25 sample using the new site air temperature algorithm.

site temperature method analyses.

The model for the August 13 sample exemplifies this improvement (Figure 3.11).

Note that both the August 13 and June 25 model slopes are approximately parallel to the 1:1 line, with y intercepts offset by

approximately 16-18°C reflecting different levels of atmospheric forcing (Figure 3.11 and 3.12). The new site air temperature method produced a particularly noticeable improvement in the June sample, in part through a boost in sensitivity associated higher temperature amplitudes (Figure 3.13). Seasonally, both the magnitude and direction of these trends appear consistent given the relative changes in sun angle between the March, June, and August sampled dates (Table 3.1, solar elevation column).

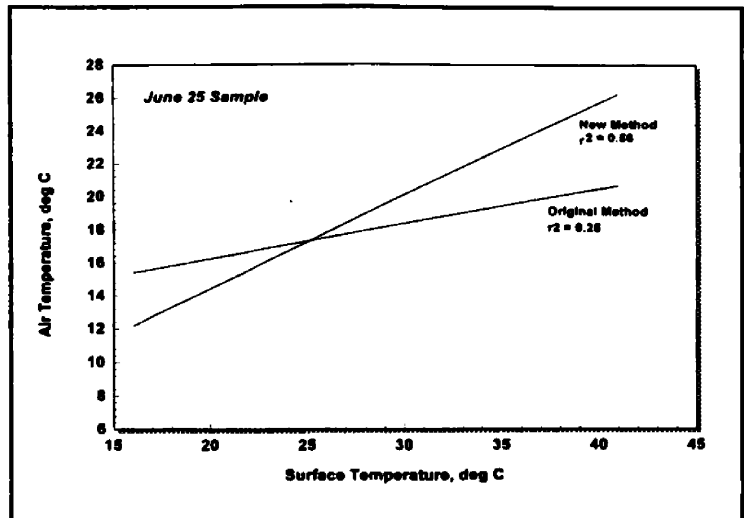


Figure 3.13 Comparison of the original and new air temperature method regression slopes for the June sample. These lines illustrate the effect of increased temperature amplitude on the sensitivity of the relationship.

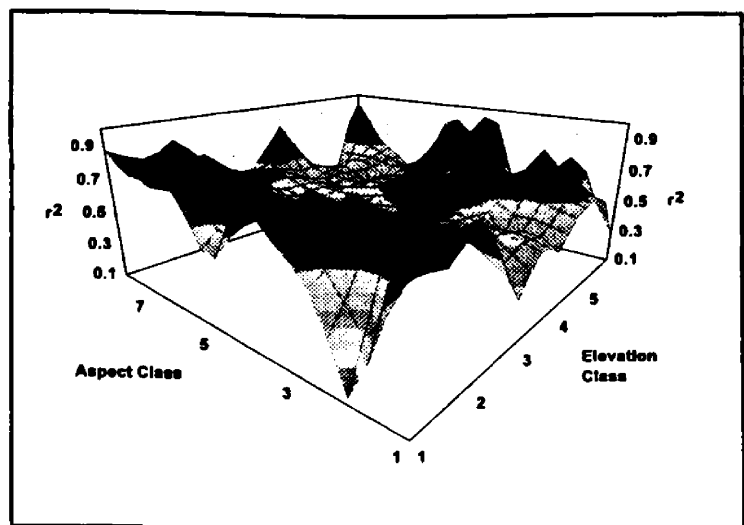


Figure 3.14 r² surface for the within-category regression models using the {Elevation, Aspect class} pairings for the August sample, new air temperature algorithm.

Within-Category Partition Results

The within-category variance in the T_a vs. T_s relationships was examined by running regression models partitioned by different combinations of categorical variables: elevation class (4 levels), canopy closure class (5 levels), slope class (4 levels) and aspect class (8 levels). The {elevation class, aspect

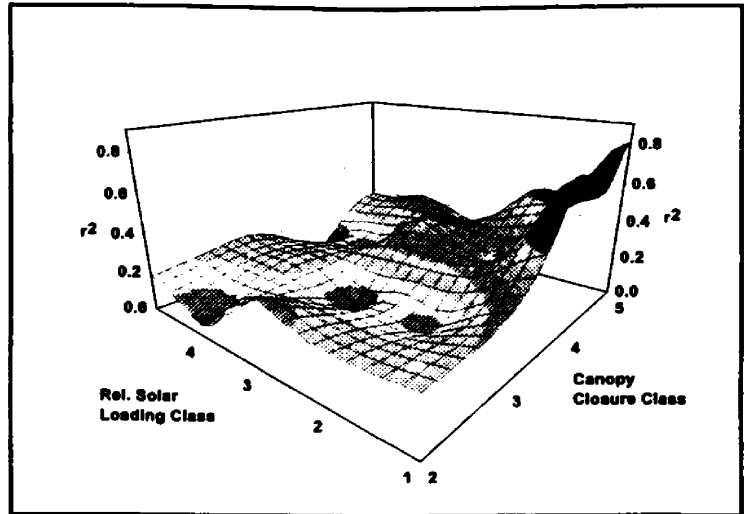


Figure 3.15 r^2 surface for the {relative solar load, canopy closure} pairing for the June sample, using the new air temperature method.

class} pairings yielded generally uneven surfaces for all sample dates for both the "original" and new methods runs, with a general improvement in r^2 values for the "new method" models (Figure 3.14). The overall correlation level of the surface however suggests moderately good agreement. A number of factors may be contributing to the heterogeneity here, including canopy influences not accounted for in this simplistic 2D pairing. Also note that the scaling of the aspect class variable places the two northern most aspect classes at opposite ends of the y axis, resulting in a physical split of this naturally periodic index. With that in mind, the upturned corners of the surface at either end of the aspect scale are more easily interpreted (Figures 3.14 and 3.16).

The {relative solar loading class, canopy closure class} pairing tended to produce somewhat more evenly varying r^2 surfaces with a more definitive overall gradient. Lower r^2 values generally occurred at higher relative solar loadings, and higher r^2 values were more associated with higher canopy closures and

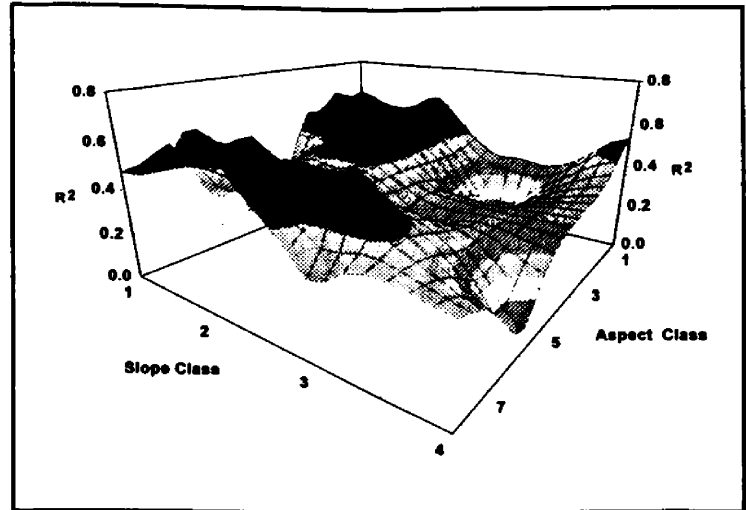


Figure 3.16 r^2 surface for the {slope, aspect} pairing for the March sample using the new air temperature method.

lower relative solar loadings (Figure 3.15). This effect is likely due to better T_a and T_s coupling at the typically moderated temperatures present under more closed canopies.

In the {Slope, Aspect} class pairings, several features appeared for all three samples dates in the r^2 surfaces. Noticeable "pits" or local depressions in the surface seemed to consistently occur around west aspects (aspect class 6, or 202.5 to 247.4°) and the lower slope classes, and minor depressions also occurred in mid slope and aspect class categories (Figure 3.16). In general, the best fits within the {slope, aspect} pairings tended to occur at lower slopes and north facing aspects.

Multiple Regression Results

As an additional verification of the basic T_a vs. T_a relationships across environmental gradients using the new method, multiple linear regressions were fit for each sample date setting T_a as the dependent variable, and ratio level forms of T_s , the canopy closure, elevation, slope, and cosine-transformed aspect as the independent variables. All regression models Y' , slopes, and y intercepts were significant at the $\alpha=0.05$ probability level. The seasonal trends detected in the other analyses are reinforced here as well: the June sample had the least definitive r^2 coefficient (with 0.785), and had a higher standard error of Y' than the other two dates (Table 3.7). Regression coefficients for these models were predominantly negative, indicating an expected inverse response in T_a to increased values in most of the independent variables. The low magnitudes of some of the fitted term coefficients (e.g. elevation in all samples, and transformed aspect in March and August), suggests these contribute only weakly to the model fit. The canopy closure and aspect variables had consistently higher coefficient levels across the seasonal samples, indicating a more direct influence on air temperature. The higher canopy closure variable coefficients in particular reinforce the importance of including this or a proxy parameter in the air temperature algorithm.

Table 3.7: Multiple Linear regression models for T_a vs T_s using the new site temperature estimation method			
Sample	Multiple regression model	R^2	Y' standard error
March	$T_a = (0.061) T_s - (6.678) C - (0.005) E - (1.43) A' - (0.02) S + 22.619$	0.940	0.58
June	$T_a = (0.157) T_s - (7.49) C - (0.002) E - (1.0) A' - (0.123) S + 25.097$	0.785	1.43
August	$T_a = (0.200) T_s - (9.520) C - (0.004) E - (2.289) A' - (0.074) S + 32.454$	0.932	0.97

where:
 T_a = air temperature estimated by MTNTEMP model using new site temperature method
 T_s = surface temperature derived from TIR, in °C
C = percent canopy closure
 A' = transformed aspect in degrees [cosine(aspect)+1], all values forced positive to {0.0 < a' < 2.0}
S = percent slope
E = elevation, in meters.
 R^2 = adjusted multiple linear regression coefficient of determination.

Nemani and Running (1989) and Goward et al. (1994) both found that canopy properties (in this case, NDVI) play a similarly influential role, where the T_s approximated T_a at the highest NDVI values, and T_s departed the most from T_a over bare soil.

Note that although these multiple linear regression models ultimately suggest fairly good correlation between T_a and the independent variables examined, their application beyond this study would require local validation. Gaugh (1982) summarized the application of other multivariate analysis methods to meteorology, including principle components analysis (PCA) as well as direct ordination. These and techniques such as detrended correspondence analysis (DCA) may prove useful in future investigations into

the relationships between spatially important environmental variables and the key diagnostic meteorology variables identified in this study.

Conclusions

In lieu of a much more rigorous modeling approach representing a full energy balance within multiple nested grids such as RAMS (Pielke et al., 1992), the approach taken by MT-CLIM/MTNTEMP appears to meet the broader climatology needs of ecosystem process models. For larger scale (e.g. 500 m, 1 k) ecosystem modelling applications, an array of assumptions must be made about the distribution of topographic variables that the MT-CLIM and MTNTEMP models are presumably sensitive to. The microsite level study described here thus leaves some unanswered questions about how well this model approach would work when such influences are defined more coarsely. Larger scale test datasets taken from a geographically widespread network of remote area weather stations, RAWS, (Warren and Vance, 1981) could play a key role in investigating these scale questions.

The strength of the relationship between T_a and the TIR based T_s appears to be at least partially based on there being sufficient amplitude in the diurnal temperature signal. This amplitude (e.g. measurability) in turn is linked to sufficient spatial heterogeneity in a sites surface properties and energy balance dynamics. The June TMS dataset had the most damped temperature amplitude of the three samples and resulted in regression models that did not match the MTNTEMP model results nearly as well as the other two dates. The early spring green-up conditions of June probably contributed to this. The regression model slopes for all sample dates were consistently lower than the 1:1 line,

reflecting the atmospheric forcing influence between T_a and T_s discussed earlier. These slope trends agreed with those found by Nemani and Running (1989) who examined T_s vs. a normalized difference vegetation index (NDVI) on a seasonal basis and found that T_s dropped with increases in NDVI. Goward et al. (1994) found similar patterns, stating that extrapolation of NDVI to an "infinitely thick" canopy provides an estimate of foliar temperature generally comparable to air temperature. Regressions for the August sample reflected improved correlations between T_a and T_s where the drier conditions resulted in increased temperature amplitudes. The (more conclusive) regressions from the March sample were more similar to those from the August sample than the June sample, probably due to the fact that cooler soil temperatures in March prevented the vegetation canopy from transpiring at June levels.

Appropriate caution must be taken in interpreting the statistical relationships between T_a and T_s since these are only indirectly physically related. In denser stands with higher aerodynamic roughness, we observe a generally closer coupling of T_a with T_s , as the majority of scatter plots (Figure 3.12, Figure 3.13) indicate at lower ranges of T_s . In general, the new site temperature algorithm for adjusting synoptic air temperature introduced in this paper produced better correlations of T_a and T_s across the environmental gradients of elevation, aspect and slope than did the original MT-CLIM algorithm (Equation 3.3).

In general, partitioning the spatial study site by various environmental gradients universally improved the basic agreement in topographic trend between the observed T_s and the estimated T_a . This is due at least in part to the effect of minimizing within-class variance relative to between-class variance. The breadth and consistency of the trends evident from this study do suggest some robustness in the underlying relationships, particularly in light of the consistency of these results between sample dates, and between pooled vs. stratified samples. To the extent that the topographic heterogeneity at Black Butte approximates typical "real world" conditions, the results obtained here might apply to a broader range of site conditions. The performance of the new site temperature estimation algorithm on a wider range of sites should be examined however, to further establish its applicability. In particular, examination of model performance on sites with a greater overall elevation relief and a more diverse mix of micro-topography (including minor swales, hanging valleys, etc) would be useful. The heuristic method used to determine T_{∞} for a given run (Equation 3.11) could be further explored as a practical way to implement the new site temperature estimation algorithm reported here. More work also needs to be done to independently validate the precipitation variable not addressed in this study.

This study probably did suffer somewhat from the lack of atmospherically corrected Daedalus TMS imagery; in the future, an improved experimental design should include vertical atmospheric profiles, either from radiosondes or a better elevation-distributed observed temperature dataset. More rigorous atmospheric corrections,

however, would likely have altered the magnitude of the observed T_s but not the basic correlation patterns found here.

A suggested follow-on to this study might be to establish a stratified random sample of field plots on a mountain slope with diverse topography, where the following variables would be collected at each plot: a) several replicates of T_s measurements obtained using a hand held radiometer, b) aspect, slope, elevation, and canopy closure measurements, and c) precise spatial location determined via a hand-held global positioning system (GPS). A series of MTNTEMP model runs would then be parameterized, one to match each field plot taken, to establish model T_a estimates associated with the T_s at each field plot. A potential advantage of this type of study is that although the T_s signal would require routine calibration, it would probably not require the same type of atmospheric correction as would a remotely sensed signal, and the logistics of when the samples were taken (time of day, time of year, environmental gradients) could be more closely controlled. This ground based study design could be extended to larger scales through an analysis based on a geographically widespread RAWS network, or could also be coordinated with a denser set of remotely sensed thermal imagery. If the sample error rates were kept sufficiently low (e.g. through sufficient sampling density, etc), such a study could help fine tune the MT-CLIM approach and further contribute to the development of meteorology models useful in ecosystem research.

Literature Cited

- Aronoff, S. 1989. Geographic Information Systems: a management prospective. WDL Publications, Ottawa, Canada. 294 p.
- Band, L.E., D.L. Peterson, S.R. Running, J. Coughlan, R. Lammers, J. Dungan, and R.R. Nemani. 1991. Forest ecosystem processes at the watershed scale: basis for distributed simulation. *Ecological Modelling*, 56:171-196.
- Barry, R.G. 1987. Mountain climatology: status and prospects. *Ecological Bulletins* 38:38-46.
- Barry, R.G. and R.J. Chorley. 1987. *Atmosphere, Weather and Climate*. Routledge, London, England. 460 p.
- Burrough, P.A. 1986. *Principles of Geographic Information Systems for Land Resource Assessment*. Clarendon Press, Oxford, UK. 194 p.
- Butera, M. K. 1986. A correlation and regression analysis of percent canopy closure versus TMS spectral response for selected forest sites in the San Juan National Forest, Colorado. *IEEE Transactions on Geoscience and Remote Sensing* GE-24(1):122-129.
- Campbell, G.A. 1977. *An Introduction to Environmental Biophysics*. Springer Verlag, New York, New York USA. 159 p.
- Campbell, J.B. 1987. *Introduction to Remote Sensing*. Guilford Press, London UK. 551 p.
- Cooper, D.I. and G. Asrar. 1989. Evaluating atmospheric correction models for retrieving surface temperatures from the AVHRR over a tallgrass prairie. *Remote Sensing of Environment* 27: 93-102.
- Daly, C., R.P. Nielson, and D.L. Phillips. 1994. A statistical-topographic model for mapping climatological precipitation over mountainous terrain. *Journal of Applied Meteorology*, 33(2):140-158.
- Dottavio C.L. and D.L. Williams. 1982. Mapping a southern pine plantation with satellite and aircraft scanner data: a comparison of present and future landsat sensors. *J. Appl. Photogrammetric Engineering*, 8(1):58-62.

- Fitter, A.H. and R.K.M. Hay. 1987. Environmental physiology of plants. Second edition. Academic Press, London, UK. 421. p.
- Fritschen, L.J. and P. Qian. 1992. Variation in energy balance components from six sites in a native prairie for three years. *Journal of Geophysical Research* 97(D17):18,651-18,661.
- Furman, R.W. and Brink, G.E. 1975. The National Fire Weather Data Library; what it is and how to use it. Gen. Tech. Rep. RM-19. Ft Collins, CO: U.S. Dept of Ag., Forest Service, Rocky Mountain Forest and Range Experiment Station. 8 p.
- Gates, D. M. 1980. Biophysical ecology. Springer-Verlag, New York, N.Y. 461 p.
- Gaugh, H.G. Jr. 1984. Multivariate analysis in community ecology. Cambridge University Press, New York, New York. 298 p.
- Glassy, J.M. and S.W. Running. 1994. Validating diurnal climatology logic of the MT-CLIM model across a climatic gradient in Oregon. *Ecological Applications* 4(2):248-257.
- Grantz, D.A. 1990. Plant response to atmospheric humidity. *Plant Cell and Environment* 13:667-679.
- Good, R. 1974. The Geography of Flowering Plants. Longman Group Limited, London, England. 557 p.
- Goward, S.N., R.H. Waring, D.G Dye, and J. Yang. 1994. Ecological Remote Sensing At OTTER: satellite macroscale observations. *Ecological Applications* 4(2):322-343.
- Heilman, J.L. and E.T. Kanemasu. 1976. An evaluation of a resistance form of the energy balance to estimate evapotranspiration. *Agronomy Journal*, 68:607-611.
- Heilman, J.L., and Brittin, C.L. 1989. Fetch requirements for bowen ratio measurements of latent and sensible heat fluxes. *Agricultural and Forest Meteorology*, 44:261-273.
- Hewlett, J. D. 1982. Principles of Forest Hydrology. University of Georgia, Athens, GA. 184 pp.
- Holbo, H.R. and Luvall, J.C. 1989. Modeling surface temperature distributions in forest landscapes. *Remote Sensing of Environment*, 27:11-24.

- Huband, N.D.S. and J.L. Monteith. 1985. Radiative surface temperature and energy balance of a wheat canopy. *Boundary Layer Meteorology* 36:1-17.
- Huete, A.R. and R.D. Jackson. 1988. Soil and atmosphere influences on the spectra of partial canopies. *Remote Sensing of Environment* 25:89-105.
- Hungerford, R.D., Nemani, R.R.; Running, S.W., Coughlan, J.C. 1989. MTCLIM: a mountain microclimate simulation model. Research Paper INT-414. Ogden, UT: U.S. Department of Agriculture, Forest Service, Intermountain Research Station. 52 p.
- Kustas, W.P., B.J. Choudhury, M.S. Moran, R.J. Reginato, R.D. Jackson, L.W. Gay, and H.L. Weaver. 1989. Determination of sensible heat flux over sparse canopy using thermal infrared data. *Agricultural and Forest Meteorology* 44:197-216.
- Lee, R. 1978. *Forest Microclimatology*. Columbia University Press, New York, NY. 275 p.
- Leprieur, C.E., J.M Durand, and J.L. Peyron. 1988. Influence of topography on forest reflectance using Landsat Thematic Mapper and digital terrain data. *Photogrammetric Engineering and Remote Sensing* 54(4):491-496.
- Lillesand, T.M. and R.W. Kiefer. 1987. *Remote sensing and image interpretation*. Second edition. John Wiley and Sons, New York, New York. 721. p.
- Linacre, E., 1992. *Climate data and resources*. Routledge, London, UK. 366 p.
- Levy, P. S. and S. Lemeshow. 1991. *Sampling of populations: methods and applications*. Wiley Series in Probability and Mathematical Statistics: Applied Probability and Statistics Section. John Wiley and Sons, New York, New York. 420 p.
- McGuire, M.J., Balick, L.K., Smith, J.A., and Hutchinson, B.A. 1989. Modeling directional thermal radiance from a forest canopy. *Remote Sensing of Environment* 27:169-186.
- McNaughton, K.G. and Jarvis. P.G. 1983. Predicting effects of vegetation changes on transpiration and evaporation. *In* Water deficits and plant growth. Vol. 7. Academic Press, Inc, . New York, pp.1-47.
- Moncrieff, J.B., S.B. Verma, and D.R. Cook. 1992. Intercomparison of eddy correlation carbon dioxide sensors during FIFE 1989. *Journal of Geophysical Research* 97(D17):18,725-18,730.

- Monteith, J.L, and Unsworth, M.H. 1990. Principles of environmental physics. Edward Arnold, London, England. 291 p.
- Moran, J.M., and M.D. Morgan. 1989. Meteorology, the atmosphere and the science of weather. Second edition. MacMillan Publishing Co. New York, New York. 557p.
- Moran, M.S, R.D. Jackson, L.H. Raymond, L.W. Gay, and P.N. Slater. 1989. Mapping surface energy balance components by combining landsat thematic mapper and ground-based meteorological data. Remote sensing of the environment 30:77-87.
- Nemani, R.K. and Running, S.W. 1985. Use of synoptic weather data to drive ecological models. pp 252-255. *In Proc. 17th Conference on Agriculture and Forest Meteorology*, May 21-24, Scottsdale, Arizona. 405 p.
- Nemani, R.R. and S.W. Running. 1989. Estimation of regional surface resistance to evapotranspiration from NDVI and thermal I-R AVHRR data. *Applied Meteorology*, 28(4):276-284.
- Nemani, R.R. and S.W. Running. 1989. Testing a theoretical climate-soil-leaf area hydrologic equilibrium of forests using satellite data and ecosystem simulation. *Agricultural and Forest Meteorology* 44:245-260.
- Nemani, R.R., L. Pierce,, and S.W. Running. 1993. Developing satellite-derived estimates of surface moisture status. *Journal of Applied Meteorology*, 32(3):548-557.
- Nemani, R.R., S.W. Running, L.Band, D. Peterson. 1993. Regional hydro ecological simulation system: an illustration of the integration of ecosystem models in a GIS. *In Integrating GIS and Environmental Modelling* editors M. Goodchild, B. Banks, and L. Steyert, Oxford London. 488 p.
- Norusis, M. J. 1993. SPSS/PC V5.02 Manual. SPSS Inc., Chicago, IL 60611. 116 p.
- Oke, T.R. 1987. Boundary layer climates. 2nd edition, Routledge, New York, NY. 435 p.
- Ott, L 1977. Introduction to statistical methods and data analysis. Duxbury Press, North Scituate, MA. 733 p.
- Parton, W.J. and Logan J.A. 1981. A model for diurnal variation in soil and air temperature. *Agricultural Meteorology* 23:205-216.

- Peterson, D.L., W.E. Westman, N.J. Stephenson, V.G. Ambrosia, J.A. Brass, and M.A. Spanner. 1986. Analysis of forest structure using thematic mapper simulator data. *IEEE Transactions on Geoscience and Remote Sensing*, GE-24(1):113-121.
- Peterson, D.L., Spanner, M.A., Running, S.W. and Teuber, K.B. 1987. Relationship of thematic mapper simulator data to leaf area index of temperate coniferous forests. *Remote Sensing of Environment* 22:323-341.
- Peterson, D.L. and R.H. Waring. 1994. Overview of the Oregon transect research project. *Ecological Applications* 4(2):211-225.
- Pfister, R. D., B.L. Kovalchik, S.F. Arno, and R.C. Presby. Forest habitat types of Montana. USDA Forest Service Gen. Tech. Rep. INT-34. Ogden, UT: U.S. Department of Agriculture, Forest Service, Intermountain Research Station. 174p.
- Phillips, D.L., J. Dolph, D. Marks. 1991. A comparison of geostatistical procedures for spatial analysis of precipitation in mountainous terrain. U.S. EPA report, Environmental Research Laboratory, Corvallis, OR. 38 p.
- Pielke, R.A., and W.R. Cotton, R.L. Walko, C.J. Tremback, W.A. Lyons, L.D. Grasso, M.E. Nicholls, M.D. Moran, D.A. Wesley, T.J. Lee, and J.H. Copeland. 1992. A comprehensive meteorological modeling system - RAMS. *Meteorol. Atmos. Phys.* 49:69-91.
- Pierce, L.L. and Congalton, R.G. 1988. A methodology for mapping forest latent heat flux densities using remote sensing. *Remote Sensing of Environment*, 24:405-418.
- Pierce, L.L. 1994. Scaling ecosystem models from watersheds to regions: tradeoffs between model complexity and accuracy. PhD dissertation, School of Forestry, University of Montana, Missoula, MT. 146 p.
- Price, J.C. 1983. Estimating surface temperatures from satellite thermal infrared data- a simple formulation for the atmospheric effect. *Remote sensing of Environment*, 13:353-361.
- Price, J.C. 1985. On the analysis of thermal infrared imagery: the limited utility of apparent thermal inertia. *Remote Sensing of Environment* 18:59-73.

- Reicosky, D.C., L.J. Winkelman, J.M. Baker, and D.G. Baker. 1989. Accuracy of hourly air temperatures calculated from daily minima and maxima. *Agricultural Forest Meteorology* 46:193-209.
- Running, S. W. 1984. Documentation and preliminary validation of H2OTRANS and DAYTRANS, two models for predicting transpiration and water stress in western coniferous forests. USDA Forest Service Research Paper RM-252. Rocky Mountain Forest and Range Experiment Station, Fort Collins, CO. 45 p.
- Running, S. W., R.R. Nemani, and R.D. Hungerford. 1987. Extrapolation of synoptic meteorological data in mountainous terrain and its use for simulating forest evapotranspiration and photosynthesis. *Canadian Journal of Forest Research* 17(6):472-483.
- Running, S. W. and R.R. Nemani, D.L. Peterson, L.E. Band, D.F. Potts, L.L. Pierce and M.A. Spanner. 1989. Mapping regional forest evapotranspiration and photosynthesis and coupling satellite data with ecosystem simulation. *Ecology* 70(4):1090-1101.
- Running, S. W. 1990. Estimating Terrestrial Primary Productivity by Combining Remote Sensing and Ecosystem Simulation. IN Remote Sensing of Biosphere Functioning. Springer-Verlag New York. p 65-86.
- Running, S. W. and R.R. Nemani. 1991. Regional hydrologic and carbon balance responses of forests resulting from potential climate change. *Climatic Change* 19: 349-386.
- Running, S. W. and S.T. Gower. 1991. FOREST-BGC, a general model of forest ecosystem processes for regional applications. II. Dynamic carbon allocation and nitrogen budgets. *Tree Physiology* 9:147:160.
- Running, S.W. 1991. Computer simulation of regional evapotranspiration by integrating landscape biophysical attributes with satellite data. *In Land Surface Evaporation: measurement and parameterization*. Springer Verlag, New York. pp. 359-369.
- Running, S. W., T.R. Loveland, L.L. Pierce, and E.R. Hunt Jr.. 1993. A remote sensing based vegetation classification logic for global land cover analysis. *Remote sensing of the environment* (in press).
- Schimel, D.S, T.G.F. Kittel, and W.J. Parton. 1991. Terrestrial biogeochemical cycles: global interactions with the atmosphere and hydrology. *Tellus* 43AB: 188-203.

- Slater, P.N., S.F. Biggar, R.G. Holm, R.D. Jackson, Y. Mao, M.S. J.M. Palmer, and B. Yuan. 1987. Reflectance and radiance based methods for the in-flight absolute calibration of multispectral sensors, *Remote Sensing for the Environment* 22:11-37.
- Smith, J.A., T. Lie Lin, K.J. Ranson. 1980. The lambertian assumption and Landsat data. *Photogrammetric Engineering and Remote Sensing* 46(9): 1183-1189.
- Thornton, P.E. and S.W. Running. 1994. Generating daily surfaces of temperature and precipitation over complex topography. *In Second Conference of GIS and Environmental Modeling, National Center for Geographic Analysis and Information Analysis, GIS World.* (in press).
- Tomlin, C.D. 1990. *Geographic information systems and cartographic modelling.* Prentice Hall, Englewood Cliffs, New Jersey. 249 p.
- Verma, S.B., Kim, J., and Clement, R.J. 1989. Carbon dioxide, water vapor, and sensible heat fluxes over a tallgrass prairie. *Boundary-Layer Meteorology* 46:53-67.
- Warren J.R. and D.L. Vance. 1981. Remote automatic weather station for resource and fire management agencies. *USDA Forest Service General Technical Report INT-116, Intermountain Research Station, Ogden, Utah.* 11 p.
- Wonnacott, T.A. and R.J. Wonnacott. 1977. *Introductory Statistics.* John Wiley and Sons, New York, NY. 650 p.
- Woodmanse, R.G. 1988. Ecosystem processes and global change. *In: Scales and Global Change: Spatial and Temporal Variability in Biospheric and Geospheric Processes.* Thomas Rosswall, R.G. Woodmansee, and P.G. Risser. (Ed.) SCOPE-ICSU, Wiley and Sons. 355 p.

Chapter 4

Conclusions

This diurnal and topographic validation of the MT-CLIM model found moderately good agreement between observed data and model outputs for the humidity, incident solar radiation, and site temperature variables examined. In the diurnal component of the model, incident solar was generally estimated better than humidity; this is probably at least partly due to the more explicit algorithmic treatment of radiation relative to the methods used to extrapolate humidity, given the complex physical controls on diurnal humidity flux. In the topographic component of the model, the new site temperature algorithm introduced here appeared to generate universally stronger correlations between air and surface temperatures, subject to the limitations and constraints of the observed surface temperature data.

While encouraging, this study indicates some potential areas for future improvements, both in terms of phenomena not yet treated (wind, microsite air drainage, advection) as well as variables addressed now that could be estimated better.

Meteorology is a dynamic physical phenomena tightly woven through the dimensions of time and space. Open water sailors, smokejumper pilots, and chaos theorists would probably add a dimension of mysticism to these other dimensions, acknowledging the daunting unpredictability of the weather around us. Treating mountain meteorology via

extrapolation-based computer models such as MT-CLIM or MTNTEMP thus requires a certain relaxation in expectations of precision found in crop micrometeorology work. A theoretically rigorous, first principles formulation for estimating the climatology variables treated in MT-CLIM would have to calculate not only an instantaneous on-site energy balance, but also account for local and perhaps mesoscale wind influences, as well as micro-topographic effects governing such phenomena as cold air drainage. These instantaneous controls would then have to be scaled to an appropriate time-step for the given application via sophisticated data reduction methods. Even if the increased computational costs required of such an "ideal" approach were comfortably met by higher performance hardware, the larger question of reaching an appropriate balance between model precision and the needs of ecosystem research remain. Further, the raw CPU costs represent only one aspect of the overall operational requirement; the labor, data storage and retrieval overhead required to maintain and interpret very high resolution meteorology data outputs is another impediment to the presumably "ideal" scheme outlined above. It appears that a blend of empirical, statistical, and microclimatology principles (such as done in MT-CLIM) remains among the few practical ways we currently have to produce the meteorology estimates required by multiple scale ecosystem models.

The strengths and reliability of any study comparing observed vs. predicted parameters is necessarily predicated by our confidence in the observed data. Both the diurnal and topographic studies reported here suffered somewhat from uncertainties in the

observed data. In the diurnal portion of this study, faulty relative humidity instruments maintained on the OTTER project required data to be screened temporally. In the topographic component of the study, the remotely sensed surface temperature dataset had to serve as a "soft" proxy measure only indirectly representing the underlying phenomena, and separated from it by several critical layers of data manipulation. Each of these transformations potentially introduced more experiment error. Aside from the attenuations to the thermal signal caused by atmospheric effects, T_s represents a physically complex measure subject to a variety of potentially compensatory influences: atmospheric forcing, water and radiation energy balances, and physiographic influences. Beyond these, sensor geometry, data-stream post-processing, and calibration issues also play a role. Given these unknowns, the modest degree of statistical agreement found between T_s and T_a across the topographic gradients evaluated suggests a fundamental level of robustness in the underlying relationships. In particular, the consistency in the regression slopes and stability of the trend directions across seasonal spatial gradients in the topographic study seems to reinforce this conclusion.

As modeling objectives begin to increasingly emphasize the 250 m, 500 m and 1 km grid cell resolutions supported by newer instruments such as NASA EOS MODIS, the need for modelers to potentially revise our notion of traditional physiography emerges. Global scale 1 km and 1° by 1° grid cells increasingly resemble complex statistical surfaces more than the simple and direct point measures of the past. When a MT-CLIM approach is scaled up to these resolutions, even more emphasis will need to be placed on

the implicit distributions of key variables represented now within each "point" weather station. Generation of statistical "virtual weather stations" that adequately characterize the spatial properties of mesoscale and regional scale regions will need to become more routine; progress towards this end is underway. The MT-CLIM approach favors simplicity of parameterization and lower compute costs at the expense of temporal and spatial precision. It is possible that the efficacy of these simpler approaches may ultimately be decided as much on the basis of research economics as technical precision. The challenging data volumes proposed by the upcoming NASA EOS research program and others, in concert with funding limitations, seem to argue more than ever for a balance between compute efficiency, precision, and more tractable parameterizations, in spite of continual advances in computer technology. The ultimate value of the MT-CLIM logic is probably best seen as a cooperating tool used along with and cross-validated by more theoretically rigorous energy-conservative based models such as RAMS.

Lastly, while the study objectives stated earlier do not specifically address model software implementation issues, some of these merit a brief discussion here. Historically, the trend has been to develop models like MT-CLIM in an ad-hoc fashion, using software languages to express the science in as streamlined and succinct a form as possible. The down side of the ad-hoc approach is that the (proper) emphasis on the discipline science (meteorology) is sometimes achieved at the expense of software quality, provability, and extensibility. The MTNTEMP prototype implementation used in this study represents a conscious effort to at least partly address each of these. Significant set-backs in modeling

projects have historically occurred due to investigators confusion over a) which inputs were actually used to generate a given set of outputs, b) which algorithms were actually present in the model used for a run, and c) missing internal documentation on the general goals for the run. While such issues may be dismissed by practitioners as "just common-sense data management" or seen as ill-afforded luxuries, they directly affect the basic integrity of much of our work. The science modeling software we develop can and should support these and other related concerns more explicitly than they do now.

MTNTEMP includes specific facilities to promote documentation of model runs (free form commenting of input script files) and archive (optional, transparent "packaging" of all inputs and outputs into one compressed archive volume). Emerging object oriented data modeling and software paradigms collectively represent a significant advance in how meteorology software could be implemented. In the future, advances in software implementations that support the above concerns will likely come as the result of better interdisciplinary collaboration with computer scientists working with these new paradigms.

Appendix 3.1

Statistical Summary of Study Site Variables

The main physiographic and canopy variables used to characterize the study site were elevation, slope, aspect, and percent canopy closure. Aspect was transformed to $\cos(\text{aspect})+1.0$ to force all periodic transformed aspects positive, to the range $\{0..2.0\}$.

Variable	Mean	Std Dev	Minimum	Maximum	N
ELEV	1255.10	211.68	940.0	1892.0	3364
SLOPE	13.61	7.69	.00	35.00	3364
CLOSURE	.73	.18	.01	.85	3364
ASPCOS_1	1.09	.74	.00	2.00	3364

The discrete form of these variables are summarized below:

Variable	Minimum	Maximum	N
ELEV_CL	1	6	3364
CLOSE_CL	1	5	3364
ASPEC_CL	1	8	3364
SLOPE_CL	1	4	3364

The sample specific, ratio level variables defined in the study include relative solar loading, surface temperature, site air temperature, radiation ratio, and incident shortwave solar radiation ($\text{kJ}/\text{m}^2/\text{day}$). These vary by sample and site temperature method and are reported below for the new method by sample:

Sample-Specific Continuous Variables

March Sample

Variable	Mean	Std Dev	Minimum	Maximum	N
RSOL	61.04	19.25	1	100	3364
TSURF	14.32	5.31	2.00	35.00	3364
TSITE	10.09	2.37	2.19	16.06	3364
TSYNOP	10.52	1.23	6.73	11.92	3364
RADRAT	.99	.08	.740	1.184	3364
SOLAR	20154.97	1707.89	15086.61	24130.70	3364

June Sample

Variable	Mean	Std Dev	Minimum	Maximum	N
RSOL	65.15	18.44	1	100	3364
TSURF	24.58	4.13	16.00	41.00	3364
TSITE	16.99	3.09	6.31	25.84	3364
TSYNOP	18.20	1.23	14.41	19.60	3364
RADRAT	.99	.02	.919	1.012	3364
SOLAR	33761.92	587.47	31318.65	34518.12	3364

August Sample

Variable	Mean	Std Dev	Minimum	Maximum	N
RSOL	67.98	18.93	1	100	3364
TSURF	29.96	4.69	20.00	47.00	3364
TSITE	22.58	3.75	13.51	33.19	3364
TSYNOP	23.72	1.23	19.94	25.12	3364
RADRAT	.99	.04	.854	1.071	3364
SOLAR	27975.98	1158.55	24125.29	30285.43	3364

Variable Description

RSOL	relative Solar Loading Score
TSURF	surface Temperature, deg C.
TSITE	estimated air temperature, deg C
TSYNOP	synoptic site temperature, deg C
RADRAT	flat/sloped radiation ratio
SOLAR	incident shortwave radiation
ELEV	Elevation (meters)
SLOPE	Slope (percent)
CLOSURE	Canopy Closure Percent
ASPCOS_1	cos(aspect_rad)+1.0
ELEV_CL	Elevation Class
SLOPE_CL	Slope Class
CLOSE_CL	Canopy Closure Class
ASPEC_CL	Aspect Class (45 deg arc classes)

Appendix 3.2

Example of MT-CLIM Model Input Requirements

Cascade Head, Site 1	
NASA OTTER PROJECT MTCLIM Validation	
CASC89.MTC	Input data file (temperatures in deg C)
CASC89.CLM	Output data file
S	English (Temps: F and PPT: inches, or SI (CM) Units, [E,S])
N	Dew point temperature supplied [Y or N]
1	Number of PPT stations [1 or 2]; if 2 then use 2 isohyets below
N	Use threshold radiation [Y or N]
T	Total or Average radiation [T or A]
Y	Use Yearday (Julian) in place of month & day [Y or N]
208	N. days, Integer variable, all the rest are single precision real values.
44.05	Latitude, in decimal degrees.
49.0	Site elevation (meters for si, or feet for english).
125.0	Site aspect 0 to 360 degrees (0 = north; 180 = south)
10.0	Site slope (Percent)
6.3	Site lai (all sided)
2.0	Site isohyet (precipitation)
2.0	Base isohyet station 1
0.0	Base isohyet station 2 (optional) see number of ppt stations
1.0	Site east horizon (degrees)
1.0	Site west horizon (degrees)
0.16	Site albedo (.2 = 20%)
0.60	Tranclf (Sea level atmospheric transmissivity)
0.45	Tempcf (Temperature correction for sine approx)

6.671	Environmental lapse rate (deg C cooling per 1000' m rise)
7.288	Lapse rate for maximum temperature (Degrees / 1000 m or ft)
3.644	Lapse rate for minimum temperature (Degrees / 1000 m or ft)
2.730	Dew lapse rate (Degrees / 1000 m or ft)

Appendix 3.3

Inputs Used for MTNTEMP Model Runs

The analyses for this study were based on two sets of MTNTEMP model runs. The first applied the original MT-CLIM site temperature algorithm to each of the three sample days (March 21, June 25, and August 13, 1990), and the second applied the new site temperature algorithm introduced in this paper.

The inputs for a given run are comprised of several files that work on a heirarchical "delta" basis; all keyword named-pairs in the defaults file are processed first, and then a run-specific input script file is processed, over-riding any named-pairs defined in the defaults file. The defaults file is named *mnttemp.rc* and typically contains all inputs for the run that do not vary by sample date. The inputs that do vary by sample date are contained in files named by the sample.

The first set of (3) model runs are labelled "Original Method Run", and the second set of (3) model runs are labelled "NewMethod Run". Input script files used to parameterize MTNTEMP for both sets of runs are included in this appendix.

Original Method Run: Default Inputs

```
# mnttemp.rc mnttemp rev 1.51
# Inputs Revised: 05/03/1994 @ 16:55:56
# joe glassy, NTSG
#
# The goal of this analysis is to provide a BASELINE run using the
# original site temperature estimation algorithm.
#
# This mnttemp analysis uses:
# 1) a canopy cover classification based on terrain corrected Aug Band 5
#    with cells coded 1,15,38,63,85 for .01,.15,.38,.63,.85 pct closure.
# 2) an albedo layer based on literature values matched to cover classes
# 3) 93.784m elevation, aspect, slope layers
# 4) standard RADRAT method for adjusting synoptic temperatures.
# 5) corrected lapse rates based on actual Santiam Pass, Metolius
#    comparision.
#
START_SETUP      "BASELINE run"
ECHO_TO          LOG                # {LOG,CLM,BOTH,NONE} to echo .imt
N_WX_DAYS        365                # if used should be >= PERIODS
STYLE            PIXEL              # POINT, PARTITION, or PIXEL
MODEL_BY         TIME               # Time outside loop, Space inside loops
PERIODS          1:365:1           # full period masked using TIME_MASK below
REPORT_FREQ      464                # how often...
MET_DATA         metolius.mtc
OUT_VARS         TSITE TSYNOP RELHUMD VPDHUMD TADD TSUB RADRAT SOLAR
END_SETUP

START_METEOROLOGY "Standard Meteorology and Biophysical Inputs"
TEMP_METHOD      RAD_RATIO          # original method...
RAD_TIME_RES     600                # {600} Default radia. timestep interval(sec)
RAD_METHOD       TOTAL              # in kJ/m^2/day, or AVERAGE, in W/m^2
RAD_THRESHOLD    FALSE              # | TRUE if use 70 W/m^2 threshold
CALC_HUMIDITY    RH                 # {NONE,VPD,RH} include in .clm output
```

```

CALC_RAIN          FALSE          # IF TRUE,output PPT (mm) to .clm
TRANS_COEF        0.75           # coefficient, {0 < t < 1.0}
# Hungerford et al. 1987 say real range is 0.30 --.60, settled on .45 as an
# average.
TEMP_COEF         0.45           # coefficient, {0 < t < 1.0}
TEMP_LAPSE        6.0            # deg C cooling for each 1 km rise
MAX_LAPSE         9.5            # deg C cooling for each 1 km rise
MIN_LAPSE         2.0            # deg C cooling for each 1 km rise
DEW_LAPSE         2.7            # deg C cooling for each 1 km rise
END_METEOROLOGY

# Base Weather Station Properties (latitude required here now)
START_BASE_WX     "Metolius Base Station"
ELEVATION         1027.0         # always in meters.
LATITUDE          44.41         # in dec. degrees.
ISOHYET          16.0           # dummy value, not used (in mm).
END_BASE_WX

# Site Properties stanza...
START_SITE        "Site Properties"
EAST_HORIZON      0.0           # degrees to East horizon {0..90}
WEST_HORIZON      0.0           # degrees to West horizon {0..90}
# dummy isohyet, not used...
ISOHYET           35.0          # in mm.
ELEVATION         elev.img
SLOPE             slope.img
ASPECT            aspect.img
# Closure coded: 1,15,38,63,85...
CLOSURE           closeb5.img
ALBEDO            albecano.img
END_SITE

```

Original Method Run: March Specific Inputs

```

# mar_503.imt mtntemp rev 1.50
# Inputs Revised: 05/03/1994 @ 16:55:56
# joe glassy, NTSG
#
# The goal of this analysis is to provide a BASELINE run using the
# original site temperature estimation algorithm for the March sample.
#
START_SETUP       "March TMS, May 3 run, closeb5, new albedo layer"
TIME_MASK        7             # col in .mtc where march data toggled on
OUTPUT           mar_503.dbf
END_SETUP

# Site Properties stanza, supplied via defaults...

```

Original Method Run: June Specific Inputs

```

# jun_503.imt mtntemp rev 1.50
# Inputs Revised: 05/03/1994 @ 16:55:56
# joe glassy, NTSG
#
# The goal of this analysis is to provide a BASELINE run using the
# original site temperature estimation algorithm for the June sample
#
START_SETUP       "June TMS, closeb5, new albedo layer"
TIME_MASK        8             # col in .mtc where June data toggled on
OUTPUT           jun_503.dbf
END_SETUP

# Site Properties stanza, supplied via defaults...

```

Original Method Run: August Specific Inputs

```
# aug_503.imt mtntemp rev 1.50
# Inputs Revised: 05/03/1994 @ 16:55:56
# joe glassy, NTSG
#
# The goal of this analysis is to provide a BASELINE run using the
# original site temperature estimation algorithm for the August sample.
#
START_SETUP      "August TMS, closeb5, new albedo layer"
  TIME_MASK      9          # col in .mtc where August data toggled on
  OUTPUT         aug_503.dbf
END_SETUP
# Site Properties stanza, supplied via defaults...
```

New Method: Default Inputs

```
# mtntemp.rc mtntemp revision 1.51
# Inputs Revised: 05/10/1994 @ 10:52:35
# joe glassy, NTSG
#
# Goal: This run exercises the new synop adjust algorithm using the
# optimum MAX_SYNOP_ADJUST values identified using linear optimization
# procedure in QuattroPRO/Win. All site-inspecific 'defaults' that
# do not change reside in the mtntemp.rc defaults file, while all
# parameters that do vary by TMS flight date are contained in this
# file. Flat Solar Score scaled to {0..1.0} for august is 0.7424
#
# The observed base station daily temperature ranges are:
#   Flight:      Bmax   Bmin   Diurnal Range
#   March  21:  18.0   -4.1   22.1
#   June   25:  25.6    3.8   21.8
#   August 13:  28.7   15.7   13.0
#
START_SETUP      "New Synoptic Method using optimized MAX_SYNOP_ADJUST"
  ECHO_TO        LOG          # {LOG,CLM,BOTH,NONE} to echo .imt
  N_WX_DAYS      365          # if used should be >= PERIODS
  STYLE          PIXEL        # choices: { POINT, PARTITION, or PIXEL}
  MODEL_BY       TIME
  PERIODS        1:365:1     # no. of days to model of N_WX_DAYS below
  REPORT_FREQ    464         # how often...
  MET_DATA       metolius.mtc

# Column 5: enables ALL days
# Column 6: enables (3) TMS flight days only
# Column 7: March flight day only
# Column 8: June flight day only
# Column 9: August flight day only
# TIME_MASK      7

# Output variable choices: "NONE", "TSITE", "TSYNOP", "TMIN", "TMAX",
# "RADRAT", "SOLAR", "RELHUMD", "VPDHUMD", "PPT", "TADD", "TSUB"
  OUT_VARS      TSITE TSYNOP TADD TSUB RELHUMD VPDHUMD SOLAR RADRAT
END_SETUP

START_METEOROLOGY "Standard Meteorology and Biophysical Inputs"
# Site temp adjustment methods. Choices are:
# { RAD_RATIO, CLOSURE, RELATIVE_SOLAR, CLOSURE_SOLAR, NO_ADJUSTMENT }
  TEMP_METHOD    CLOSURE_SOLAR # new method...
  RAD_TIME_RES   600           # {600} Default radia. timestep interval(sec)
  RAD_METHOD     TOTAL         # in kJ/m^2/day, or AVERAGE, in W/m^2
  RAD_THRESHOLD  FALSE        # | TRUE to use a 70 W/m^2 threshold
  CALC_HUMIDITY  RH           # {NO,VPD,RH} include in .clm output
  CALC_RAIN      FALSE        # IF TRUE,output PPT (mm) to .clm
  TRANS_COEF     0.75         # coefficient, {0 < t < 1.0}
  TEMP_COEF      0.45         # coefficient, {0 < t < 1.0}
# parameters for synopt adjust in the .imt files...
  TEMP_LAPSE     6.0          # deg C cooling for each 1 km rise
  MAX_LAPSE      9.5          # deg C cooling for each 1 km rise
  MIN_LAPSE      2.0          # deg C cooling for each 1 km rise
```

```

DEW_LAPSE          2.7          # deg C cooling for each 1 km rise
END_METEOROLOGY

```

Base Weather Station Properties

```

START_BASE_WX      "Base WX Inputs"
ELEVATION          1027.0       # always in meters.
LATITUDE           44.41       # in dec. degrees.
ISOHYET            16.0        # in mm.
END_BASE_WX

```

Site Properties stanza...

```

# Note: closeb5 is scaled so value range {1,15,38,63,85} not {1..5}
# Albedo, rel Solar load scaled to {1..100} (percent) range.

```

```

START_SITE         "Site Inputs"
EAST_HORIZON       0.0         # degrees to E. horizon {0..90}
WEST_HORIZON       0.0         # degrees to W. horizon {0..90}
ELEVATION          elev.img
SLOPE              slope.img
ASPECT             aspect.img
# Closure coded: 1,15,38,63,85...
CLOSURE            closeb5.img
ALBEDO             albecano.img
END_SITE

```

New Method: March Specific Inputs

```

# march.imt, mtntemp revision 1.51
# Inputs Revised: 05/10/1994 @ 10:50:37
# joe glassy, NTSG
#
# Goal: This run exercises the new synop adjust algorithm using the
#       optimum MAX_SYNOP_ADJUST values identified using linear optimization
#       procedure in QuattroPRO/Win. All site-inspecific 'defaults' that
#       do not change reside in the mtntemp.rc defaults file, while all
#       parameters that do vary by TMS flight date are contained in this
#       file. Flat Solar Score scaled to {0..1.0} for march is 0.64.
#
#       The observed base station daily temperature ranges are:
#       Flight:      Bmax   Bmin   Diurnal Range
# March 21:  18.0   -4.1   22.1
# June 25:   25.6    3.8   21.8
# August 13: 28.7   15.7   13.0
#
# begin the SETUP stanza...
START_SETUP        "March TMS, New Tsite Method, MAX_SYNOP_ADJUST=6.98"
OUTPUT            mar_510.dbf
# time mask columns: 7=march, 8=june, 9 = august date
TIME_MASK         7
END_SETUP

START_METEOROLOGY  "Standard Meteorology and Biophysical Inputs"
MAX_SYNOP_ADJUST  6.98         # max amplitude (deg C) to adjust synoptic
CANOPY_NEGWGT     0.70         # closures >= this cause neg canopy weight
FLAT_SOLAR        0.64         # Neutral, flat slope rel solar score {0..1}
END_METEOROLOGY

START_SITE         "March TMS sample site inputs"
SOLAR_LOAD        mar_rsol.img
END_SITE

```

New Method: June Specific Inputs

```

# june.imt, mtntemp revision 1.51
# Inputs Revised: 05/10/1994 @ 10:50:41
# joe glassy, NTSG
#
# Goal: This run exercises the new synop adjust algorithm using the
#       optimum MAX_SYNOP_ADJUST values identified using linear optimization
#       procedure in QuattroPRO/Win. All site-inspecific 'defaults' that

```

```

# do not change reside in the mtntemp.rc defaults file, while all
# parameters that do vary by TMS flight date are contained in this
# file. Flat Solar Score scaled to {0..1.0} for June is 0.7440
#
# The observed base station daily temperature ranges are:
# Flight:      Bmax   Bmin   Diurnal Range
# March  21:  18.0   -4.1   22.1
# June   25:  25.6    3.8   21.8
# August 13:  28.7   15.7   13.0
#
START_SETUP      "June TMS, New Tsite Method, MAX_SYNOP_ADJUST=10.05"
OUTPUT           jun_510.dbf
# time mask columns: 7=march, 8=june, 9 = august date
TIME_MASK       8
END_SETUP

START_METEOROLOGY "Standard Meteorology and Biophysical Inputs"
MAX_SYNOP_ADJUST 10.05      # max amplitude (deg C) to adjust synoptic
CANOPY_NEGWGT   0.70      # closures >= this cause neg canopy weight
FLAT_SOLAR      0.74      # Neutral, flat slope rel solar score {0..1}
END_METEOROLOGY

START_SITE       "June TMS sample, site inputs"
SOLAR_LOAD      jun_rsol.img
END_SITE

```

New Method: August Specific Inputs

```

# august.imt, mtntemp revision 1.51
# Inputs Revised: 05/10/1994 @ 10:50:46
# joe glassy, NTSG
#
# Goal: This run exercises the new synop adjust algorithm using the
# optimum MAX_SYNOP_ADJUST values identified using linear optimization
# procedure in QuattroPRO/Win. All site-inspecific 'defaults' that
# do not change reside in the mtntemp.rc defaults file, while all
# parameters that do vary by TMS flight date are contained in this
# file. Flat Solar Score scaled to {0..1.0} for august is 0.7424
#
START_SETUP      "August TMS, New Tsite Method, MAX_SYNOP_ADJUST=12.66"
OUTPUT           aug_510.dbf
# time mask columns: 7=march, 8=june, 9 = august date
TIME_MASK       9
END_SETUP

START_METEOROLOGY "Standard Meteorology and Biophysical Inputs"
MAX_SYNOP_ADJUST 12.66      # max amplitude (deg C) to adjust synoptic
CANOPY_NEGWGT   0.70      # closures >= this cause neg canopy weight
FLAT_SOLAR      0.74      # Neutral, flat slope rel solar score {0..1}
END_METEOROLOGY

START_SITE       "August TMS sample site inputs"
SOLAR_LOAD      aug_rsol.img
END_SITE

```

Appendix 3.4

Major Differences Between MTNTEMP and MT-CLIM Model Implementations

The MTNTEMP revision 1.51 implementation used in this study was written in the ANSI C language (ANSI Standard X3.159-1989) and consists of approximately 17,000 lines of code, while the MT-CLIM model was developed in the FORTRAN-77 language. The MTNTEMP source codes are considerably more extensive than the original MT-CLIM model codes, as they are designed on top of a prototype ecosystem science model framework and application programming interface (API) offering a wide variety of generalized services not found in the original model implementation. Separate documentation for the ecosystem science model framework and the MTNTEMP layer is in preparation.

Through initial test phases, the MTNTEMP implementation has been ported to the IBM AIX v. 3.2 operating system using IBM's xlc ANSI compiler, MSDOS 5.0, 6.2 using the Borland International v.3.1 and v. 4.0 C/C++ compilers, and the Linux v. 1.1 LGX unix-like operating system using the Free Software Foundation (FSF) gcc v. 2.5.4 ANSI C compiler.

Although the majority of meteorological algorithms are identical between these two implementations, MTNTEMP possesses the following characteristics or attributes either not found at all in the original MT-CLIM codes or implemented in a substantially different way:

- o A stanza-oriented, script file interface provides support for free-field embedded comments, and list and/or range based numeric and string inputs.
- o Either point, partition, or pixel based data organization schemes are accommodated. "Point" refers to a single abstract site, "partition" refers to a one dimensional array of sites (e.g. set of points, or spatial regions defined as a list of vector polygons), and "pixel" refers to a row-major ordered two dimensional array of spatially contiguous but functionally independent 'sites' or cells.
- o A run-time invertible time-space model loop organization. This means that the temporal dimension of the model problem may be defined as either the outer-most or inner-most level loop process, with the spatial dimension taking the complementary position.
- o Provisions for data input/output (I/O) facilities that read, write, and perform primitive spatial overlay operations on multiple, native image processing raster format files of the same logical extent. Supported formats include ERDAS v. 7.5 images, IDRISI v. 4.1 GIS raster images, PBMPlus byte level images, and "raw"

binary rasters. Each contributing raster layer in a given session may consist of any of the following primitive data types: unsigned 8 bit characters (byte level), signed or unsigned 16 or 32 bit integer (big or little endian byte ordering), and 4 byte (32 bit) IEEE single precision real.

- o Run-time selection of data fields chosen from input or output variable lists, for output image raster (for single output fields), or delimited ASCII text or xBASE (.dbf) database tables organized with one record per model point, pixel, or partition for multiple field output.
- o Run-time selection of specific algorithmic sub-components, subject to the natural (logical) dependencies between sub-components. For example, if site air temperature outputs are required but incident solar radiation is not required, the user may elect to suppress the calculation of daily incident solar radiation, saving considerable computation time.
- o Provisions for logging all session metrics for automated documentation of model runs, and the automated generation of a compressed archive of job inputs and outputs after model execution. Compressed archives are built by the user-selected external archive utility (the default compression tool is InfoZip's cross-platform (zip, unzip) suite, licensed similar to FSF software, compatible with Phil Katz's PkWare PkZip 2.04g compression utility).

Appendix 3.5

Statistical Summary of the OTTER Project Metolius weather station

1990 daily dataset for 1990

The climatology variables used in the MTNTEMP analyses include maximum and minimum temperature (T_{\max} and T_{\min} respectively), and precipitation (PPT, mm)

```
* @(#) metodesc.sps
* rev. 06/06/1994 @ 13:14:30.
* Task: Generate descriptive variables for Metolius base weather station.
* Joe glassy, NTSG .
```

```
DESCRIPTIVES /VARIABLES TMAX TMIN PPT /STATISTICS.
```

```
-----
Number of Valid Observations (Listwise) =      365.00
```

Variable	Mean	Std Dev	Minimum	Maximum	N	Label
TMAX	14.65	9.33	.00	35.00	365	
TMIN	.25	7.08	-33.70	17.10	365	
PPT	1.51	5.69	.00	69.60	365	

```
-----
EXAMINE /VARIABLES TMAX TMIN PPT /PLOT=HISTOGRAM /STATISTICS DESCRIPTIVES.
```

TMAX

```
Valid cases:      365.0   Missing cases:      .0   Percent missing:      .0
```

Mean	14.6542	Std Err	.4881	Min	.0000	Skewness	.2562
Median	13.9000	Variance	86.9656	Max	35.0000	S E Skew	.1277
5% Trim	14.4438	Std Dev	9.3255	Range	35.0000	Kurtosis	-.8728
				IQR	14.6500	S E Kurt	.2547

```
Frequency   Bin Center
```

```
38.00    1.000 *****
18.00    3.000 *****
17.00    5.000 *****
25.00    7.000 *****
30.00    9.000 *****
25.00   11.000 *****
30.00   13.000 *****
29.00   15.000 *****
24.00   17.000 *****
22.00   19.000 *****
17.00   21.000 *****
20.00   23.000 *****
16.00   25.000 *****
18.00   27.000 *****
12.00   29.000 *****
 8.00   31.000 *****
13.00   33.000 *****
 3.00   35.000 ***
```

```
Bin width :      2.000
Each star:      1 case(s)
```

TMIN

Valid cases: 365.0 Missing cases: .0 Percent missing: .0

Mean	.2485	Std Err	.3707	Min	-33.7000	Skewness	-1.2688
Median	.6000	Variance	50.1449	Max	17.1000	S E Skew	.1277
5% Trim	.7011	Std Dev	7.0813	Range	50.8000	Kurtosis	3.9329
				IQR	8.2000	S E Kurt	.2547

Frequency Bin Center

```

11.00 Extremes *****
 3.00 -15.000 ***
  .00 -13.000
 4.00 -11.000 ****
 8.00 -9.000 *****
19.00 -7.000 *****
37.00 -5.000 *****
46.00 -3.000 *****
38.00 -1.000 *****
43.00  1.000 *****
45.00  3.000 *****
38.00  5.000 *****
34.00  7.000 *****
25.00  9.000 *****
 6.00 11.000 *****
 5.00 13.000 *****
 2.00 15.000 **
 1.00 Extremes *
    
```

Bin width : 2.000
Each star: 1 case(s)

PPT

Valid cases: 365.0 Missing cases: .0 Percent missing: .0

Mean	1.5071	Std Err	.2979	Min	.0000	Skewness	8.9220
Median	.0000	Variance	32.3965	Max	69.6000	S E Skew	.1277
5% Trim	.6634	Std Dev	5.6918	Range	69.6000	Kurtosis	96.1473
				IQR	.5000	S E Kurt	.2547

Frequency Bin Center

```

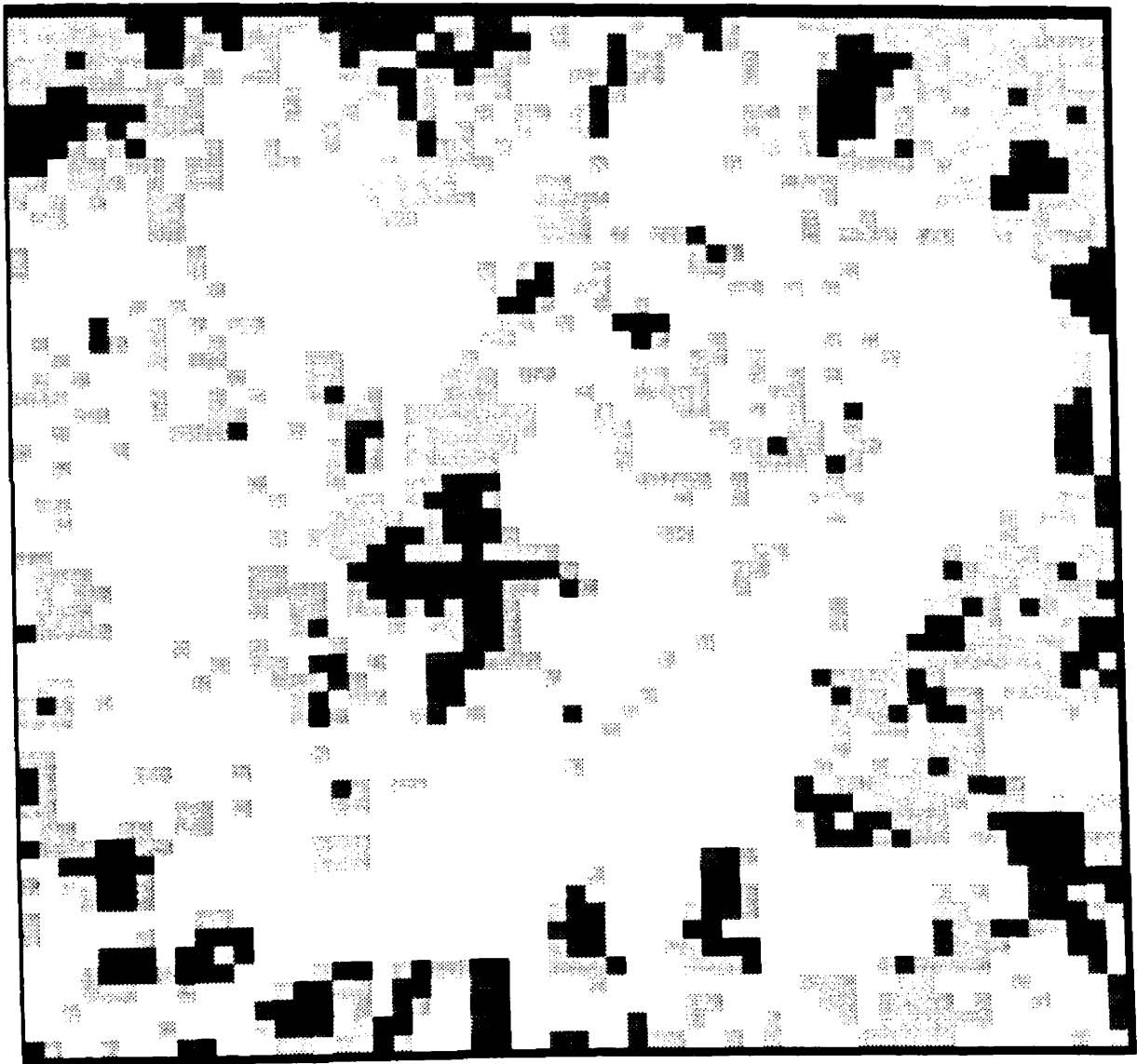
235.00 .025 *****
  .00 .075
  .00 .225
  .00 .275
 35.00 .325 *****
  .00 .375
  .00 .475
  5.00 .525 *
  .00 .725
  .00 .775
  6.00 .825 *
  .00 .875
  .00 .925
  .00 .975
  8.00 1.025 **
76.00 Extremes *****
    
```

Bin width : .050
Each star: 5 case(s)

Appendix 3.6

Percent Canopy Closure Data Layer

This 58 x 58 raster depicts the percent canopy closure data layer used for all analyses. The lightest shades represent the most closed canopies in the 5 level discrete classification (85% closure), and the darkest shades represent the most open canopies (1% closure). This classification illustrates the predominantly closed character of the 10.8 km² study site, as well as the scattered openings and scree patches.



Appendix 3.7

Annotated MTNEMP result database table structure listing

Structure for database : MARCH.DBF (same for JUNE.DBF, AUGUST.DBF)
 Number of data records : 3364
 Date of last update : 05/31/94 (Vers. 3)

Field	Field Name	Type	Width	Dec	Description
1	ELEV	Number	7.	1	: elevation (meters)
2	SLOPE	Number	6.	2	: slope (percent)
3	ASPECT	Number	6.	2	: aspect (degrees)
4	CLOSURE	Number	6.	2	: percent canopy closure
5	RSOL	Number	3.	0	: relative solar loading
6	ELEV_CL	Number	1.	0	: elevation class (1..6)
7	ASPEC_CL	Number	1.	0	: aspect class (1..8)
8	SLOPE_CL	Number	1.	0	: slope class (1..4)
9	ASPCO_CL	Number	1.	0	: transformed aspect class
10	SOLAR_CL	Number	2.	0	: incident solar rad class
11	CLOSE_CL	Number	1.	0	: canopy closure class (1..5)
12	RSOL_CL	Number	1.	0	: relative solar load class
13	CELL	Number	4.	0	: linear pixel index (1..3364)
14	TSURF	Number	6.	2	: TIR surface temperature, deg C
15	DAY	Number	4.	0	: sample year-day {80,176,225}
16	ROW	Number	4.	0	: image row index (1..58)
17	COL	Number	4.	0	: image column index (1..58)
18	TSITE	Number	6.	2	: est. site air temperature, deg C
19	TSYNOP	Number	6.	2	: synoptic air temperature, deg C
20	TEMPDIFF	Number	6.	2	: simple difference of TSITE,TSYNOP.
21	RADRAT	Number	7.	3	: Flat/Sloped radiation ratio
22	SOLAR	Number	8.	2	: incident solar radiation (kJ/day)
23	RELHUMD	Number	6.	2	: relative humidity (percent)
24	VPDHUMD	Number	8.	3	: vapor pressure deficit
25	TADD	Number	8.	2	: synoptic temp. add factor
26	TSUB	Number	8.	2	: synoptic temp. subtract factor
27	NET_ADJ	Number	6.	2	: net Synoptic temp adjustment
28	EA_ID	Number	2.	0	: elev,Aspect combined class code
29	CR_ID	Number	2.	0	: canopy closure,rel. solar code
30	AS_ID	Number	2.	0	: aspect,Slope combined class code

** Total ** 134

Bytes in Header (993) Record (134)